

NED00825

NEDO-30825  
DRF E21-0067  
84NED042  
CLASS I  
NOVEMBER 1984

CORE SPRAY SPARGER  
CRACK ANALYSIS FOR  
EDWIN I. HATCH  
NUCLEAR POWER STATION, UNIT 1

CORE SPRAY SPARGER CRACK ANALYSIS FOR EDWIN I. HATCH 1

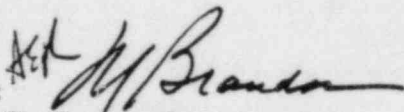
8412140218 841206  
PDR ADOCK 05000321  
Q PDR

GENERAL  ELECTRIC

NEDO-30825  
DRF E21-0067  
84NED042  
Class I  
November 1984

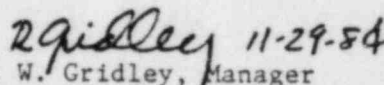
CORE SPRAY SPARGER CRACK ANALYSIS  
FOR  
EDWIN I. HATCH NUCLEAR POWER STATION  
UNIT 1

Approved:



R. J. Brandon, Manager  
Mechanical Design Engineering

Approved:



R. W. Gridley, Manager  
Fuel and Services Licensing  
Safety and Licensing Operation

---

NUCLEAR ENERGY BUSINESS OPERATIONS • GENERAL ELECTRIC COMPANY  
SAN JOSE, CALIFORNIA 95125

---

GENERAL  ELECTRIC

IMPORTANT NOTICE REGARDING  
CONTENTS OF THIS REPORT  
PLEASE READ CAREFULLY

This report was prepared by General Electric solely for Georgia Power Company (GPC) for GPC's use with the U.S. Nuclear Regulatory Commission (USNRC) for the Edwin I. Hatch Nuclear Power Station, Unit 1. The information contained in this report is believed by General Electric to be an accurate and true representation of the facts known, obtained or provided to General Electric at the time this report was prepared.

The only undertakings of the General Electric Company respecting information in this document are contained in the General Electric Company Proposal No. 416-TY626-HT1, dated October 30, 1984. The use of this information except as defined by said contract or for any purpose other than that for which it is intended, is not authorized; and with respect to any such unauthorized use, neither General Electric Company nor any of the contributors to this document makes any representation or warranty (express or implied) as to the completeness, accuracy or usefulness of the information contained in this document or that such use or such information may not infringe privately owned rights; nor do they assume any responsibility for liability of damage of any kind which may result from such use of such information.

## CONTENTS

	<u>Page</u>
1. INTRODUCTION AND SUMMARY	1-1
1.1 Structural	1-1
1.2 Lost Parts	1-1
1.3 Effect on LOCA Analysis	1-2
1.4 Conclusion	1-2
1.5 Reference	1-2
2. CORE SPRAY SPARGER STRUCTURAL INTEGRITY	2-1
2.1 Sparger Configuration	2-1
2.2 Fabrication Sequence	2-2
2.3 Installation Sequence	2-2
2.4 Performance History	2-3
2.5 Potential Sources of Stress	2-3
2.5.1 Fabrication Stresses	2-3
2.5.2 Weld Residual Stress	2-6
2.5.3 Role of Fabrication Stresses in the Observed Cracking	2-7
2.5.4 Installation Stress	2-7
2.5.5 Stresses During Normal Operation	2-9
2.5.6 Stresses During Core Spray Injection	2-10
2.6 Metallurgical Evaluation of the Core Spray Sparger Cracking	2-13
2.6.1 Background	2-13
2.6.2 Effects of Cold Work and Sensitization on SCC Behavior of Type 304 SS	2-14
2.6.3 Archive Core Spray Sparger Testing	2-15
2.6.4 Relevance to Hatch Unit 1 Core Spray Sparger Cracking	2-16
2.6.5 Probable Cause of Hatch Core Spray Sparger Cracking	2-16
2.7 Crack Arrest Assessment	2-16
2.7.1 Stresses Due to Bracket Restraint	2-17
2.7.2 Fabrication Residual Stress	2-18
2.7.3 Weld Residual Stress	2-19
2.7.4 Conclusions on Crack Arrest	2-20
2.8 Structural Integrity With 360° Throughwall Crack	2-20
2.8.1 Normal Operation	2-20
2.8.2 Core Spray Injection	2-21
2.8.3 Conclusions	2-21
2.9 References	2-21
3. LOST PARTS ANALYSIS	3-1
3.1 Introduction	3-1
3.2 Loose Piece Description	3-1
3.3 Safety Concern	3-1
3.4 Safety Evaluation	3-1
3.4.1 General Description	3-2
3.4.2 Postulated Loose Pieces	3-2
3.5 Discussion of Probability	3-6
3.5.1 Fuel Bundle	3-7
3.5.2 Control Rod Mechanism	3-10

## CONTENTS (Continued)

	<u>Page</u>
3.6 Conclusion	3-11
3.7 Reference	3-11
4. LOSS-OF-COOLANT ACCIDENT ANALYSIS WITH A CRACK IN ONE CORE SPRAY SPARGER	4-1
4.1 Introduction	4-1
4.2 Limiting Break Size and Single Failure Analysis	4-1
4.3 Phenomena Involved in the Analysis of Sparger Performance	4-3
4.4 Analysis Results	4-4
4.5 Conclusions	4-5
4.6 References	4-6

## APPENDICES

A. STRUCTURAL ANALYSIS OF THE HATCH UNIT 1 CORE SPRAY SPARGER	A-1
B. FLOW VELOCITY CALCULATIONS	B-1

## TABLES

<u>Table</u>	<u>Title</u>	<u>Page</u>
3-1	Probability of Fuel Bundle Blockage	3-12
3-2	Summary of Results of the Probability Study of Fuel Bundle Flow Blockage	3-13
4-1	Key Phenomena Related to Core Spray Cooling Performance	4-7

## ILLUSTRATIONS

<u>Figure</u>	<u>Title</u>	<u>Page</u>
1-1a	Plan View of Cracked Core Spray Sparger	1-3
1-1b	Elevation View of Cracked Core Spray Sparger	1-3
2-1	Core Spray Sparger - Elevation View	2-23
2-2	Core Spray Sparger - Plan View	2-24
2-3	Sparger to Shroud Attachment Method	2-25
2-4	Sparger Nozzles	2-26
2-5	Sparger Support Method	2-27
2-6	Pipe Bending Method	2-28
2-7	Sequence of Events Leading to the Residual Stress Distribution	2-29
2-8	Bilinear Stress-Strain Curves for Type-304 Stainless Steel	2-30
2-9	Stress and Strain Distribution in the Pipe Under Applied Moment	2-31
2-10	Moment Versus Outer Fiber Strain	2-32
2-11	Resultant Residual Stress Distribution After Fabrication	2-33
2-12	4-in. Pipe Inside Longitudinal Residual Stress Measurements Taken Both Sides 0.1 in. from Weld Fusion Line	2-34
2-13	Postulated Installation Stresses	2-35
2-14	Modified Strauss Test Results for Deformed and Undeformed 304 Stainless Steel	2-36
2-15	SCC of Cold Worked Plus Sensitized Type-304 Stainless Steel at 288°C	2-37
2-16	Compliance Change, Cracked Pipe	2-38
2-17	Assumed Stress Distribution on the Crack Face	2-39
3-1	Reactor Vessel	3-14
3-2	Steam Separator	3-15

## ILLUSTRATIONS (Continued)

<u>Figure</u>	<u>Title</u>	<u>Page</u>
3-3	Largest Piece That Can Fit Through the Turning Vane (End View)	3-16
3-4	Orificed Fuel Support	3-17
3-5	Fuel Assemblies and Control Rod Module	3-18
3-6	Loose Piece Potential Upward Flow Path	3-19
4-1	Hatch Unit 1 DBA (Limiting LOCA) Analysis	4-8



## 1. INTRODUCTION AND SUMMARY

During the inspection of the Hatch Unit 1 core spray spargers in accordance with IE Bulletin 80-13 (Reference 1-1), a crack indication was visually observed on the lower sparger in the heat-affected zone of the sparger to T-box weld. Based on the inspection results it is assumed that this crack is at least 180° (but less than 360°) in length with a maximum width of 10 mils. The crack location is shown in Figure 1-1.

This report presents the technical basis to establish continued structural integrity of the lower core spray sparger for all normal and injection conditions. The results presented herein are applicable whether the sparger is clamped or not. A discussion of the possible consequences of potential loose pieces from a cracked sparger is also presented. Finally, the effect of a postulated Loss of Coolant Accident (LOCA) with a cracked core spray sparger is discussed.

### 1.1 STRUCTURAL

A structural analysis is presented in Section 2, which describes the potential sources of stress in the spargers resulting from fabrication, installation, normal operation, and operation during a postulated LOCA. It is concluded that the structural integrity of the sparger will be maintained for all conditions of operation with or without a clamp installed. In addition, potential causes of cracking are discussed, and it is concluded that the most likely cause is Stress Corrosion Cracking (SCC) due to weld sensitization during fabrication with increased susceptibility from cold working.

### 1.2 LOST PARTS

Because continued sparger structural integrity has been demonstrated, lost parts (loose pieces) are not expected. Further, if the sparger is clamped, loose pieces are even more unlikely. However, a lost parts analysis has been performed and is presented in Section 3. It is concluded that the probability of unacceptable flow blockage of a fuel assembly or for unacceptable control rod interference is essentially zero. The potential for corrosion or other chemical reaction with reactor materials is essentially zero.

because the sparger material is designed for in-vessel use. It is also shown that loose pieces are not expected to cause damage to the other reactor pressure vessel internals.

### 1.3 EFFECT ON LOCA ANALYSIS

Section 4 presents the results of LOCA analyses assuming one cracked core spray sparger. The results show that the current reload analysis calculations are still valid because coolant injection to the upper plenum is maintained.

### 1.4 CONCLUSION

A detailed evaluation of the Hatch Unit 1 core spray sparger crack has been performed. This evaluation included structural, lost parts and LOCA analyses to determine the impact on plant operation of the cracked sparger. It is concluded that Hatch Unit 1 can safely operate in this condition and that no operational changes or restrictions are required. The results apply whether or not a clamp is installed.

### 1.5 REFERENCE

- 1.1 USNRC IE Bulletin No. 80-13, Cracking in Core Spray Spargers, May 12, 1980.

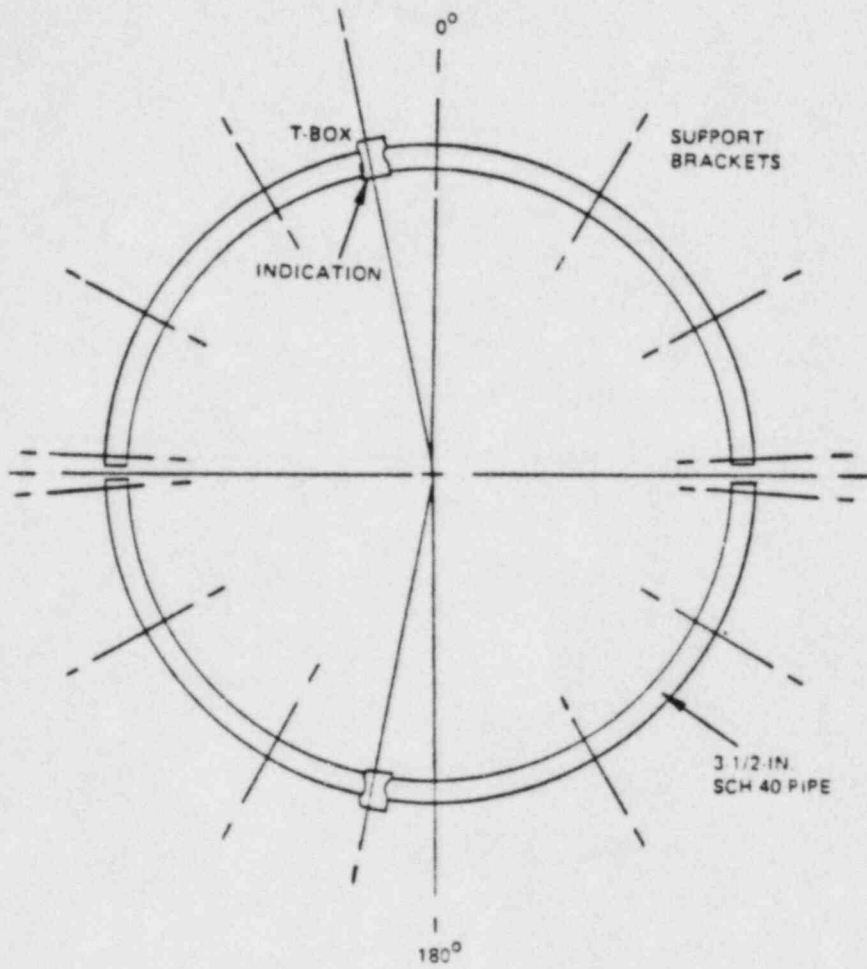


Figure 1-1a. Plan View of Cracked Core Spray Sparger

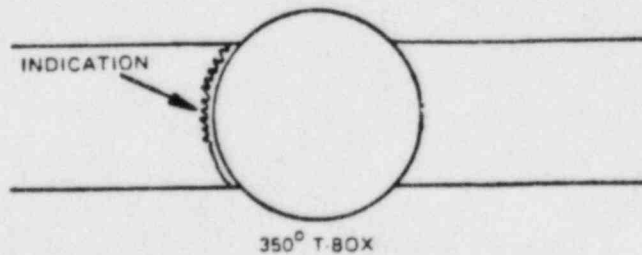


Figure 1-1b. Elevation View of Cracked Core Spray Sparger

## 2. CORE SPRAY SPARGER STRUCTURAL INTEGRITY

### 2.1 SPARGER CONFIGURATION

The core spray sparger configuration is shown in Figures 2-1 through 2-5. The spargers are mounted in the upper shroud, as shown in Figure 2-1. Vertical spacing is 10-1/4 inches between header pipe centerlines. The upper sparger has bottom-mounted nozzles and the lower sparger has top-mounted elbows. The plan view (Figure 2-2) shows that the spargers are asymmetric. The shorter header pipe has an arc length of 80°, and the longer header pipe has an arc length of 100°. The T-boxes for the spargers are located  $\pm 10^\circ$  from the vessel 0° and 180° azimuths.

Figure 2-3 shows the attachment of the T-box to the shroud. The T-box is a 5-in. Schedule 40 section of pipe with an end plate toward the vessel centerline. The 5-in. pipe extends through the shroud wall and is butt-welded to external piping. The T-box pipe is attached to the shroud by the seal ring with the attachment welds to the 5-in. pipe and the exterior surface of the shroud wall. This arrangement (as opposed to direct attachment) eliminates high thermally induced stresses during core spray injection of cold water into the reactor at operating temperature.

The sparger flow nozzles are depicted in Figure 2-4. The Hatch Unit 1 upper and lower core spray sparger headers use 1-in. shielded VNC nozzles alternating with SPRACO 3101 nozzles.

The 100° header pipe and the 80° header pipe are each supported at three locations. Figure 2-5 shows the support arrangement at locations between the T-box and end supports. The brackets are 1/2-in. thick and are welded to the shroud. The pipe-to-bracket mating surfaces are not welded to allow circumferential relative motion between the header pipe and the shroud during a core spray injection of cold water into a system at reactor operating temperature. The header pipe is 3-1/2 in. Schedule 40 Type-304 stainless steel.

The spray nozzle assemblies are composed of street elbows, 90° elbows, orifices, tees and the close nipples (used to connect the elbows and orifice the elbows) which are all Type-304 stainless steel (refer to Figure 2-4).

## 2.2 FABRICATION SEQUENCE

Fabrication records show that the Hatch Unit 1 spargers were fabricated as follows:

1. The pipe was bent using a four-roll bending process as shown in Figure 2-6. The rollers have 2 in. radius grooves, and rollers 3 and 4 are adjustable to accommodate the pipe size and to bend the pipe to the required radius. In this case, the design radius is  $R = 91.25$  inches. The maximum strain in the pipe is calculated to be 2.2%.
2. After the pipe is bent to the proper radius, it is placed in the shroud to verify that the pipe fits the shroud as-built conditions. During this fit-up process, the T-box 5-in. pipe is marked for drilling the header pipe holes.
3. After removing the pipe from the shroud, the headers are welded to the T-box.
4. The holes for each nozzle are drilled in the header pipes.
5. Stainless steel orifices are bevel welded at each nozzle opening.
6. The elbows are screwed into the assembly and roughly aimed.

## 2.3 INSTALLATION SEQUENCE

The sparger is installed in the shroud in the following manner:

1. The brackets are welded to the shroud, thereby positioning and holding the spargers. The T-box is attached to the shroud by

welding the seal ring to the T-box and the shroud. It is assumed that, because of interference between sparger ends, one or more of the spargers would be cold sprung during installation. This operation was not addressed in the fabrication records.

2. The next operation was to aim the nozzle as required by the sparger drawing.
3. The elbows were then tack welded to assure that the threaded connections remain intact.

#### 2.4 PERFORMANCE HISTORY

Hatch Unit 1 first went critical in September 1974. There have been no inadvertent core spray injections. Georgia Power Company does not flush the Hatch Unit 1 core spray spargers during refueling outages.

#### 2.5 POTENTIAL SOURCES OF STRESS

The stresses in the core spray sparger can be due to several reasons. The following section describes the stresses caused by: fabrication, installation, normal plant operation, and operation of the core spray system during postulated loss-of-coolant accidents.

##### 2.5.1 Fabrication Stresses

Residual stresses are developed when an initially straight pipe is subjected to a moment sufficient to cause yielding and later unloaded, as would occur during the fabrication of the core spray spargers. The fabrication operation is idealized in Figure 2-7. The steps involved in the calculation of the residual stresses are:

1. Determine the moment-curvature curve for the pipe assuming simple beam theory.
2. Calculate the applied moment,  $M_t$ , corresponding to the final unloaded radius of curvature. Determine the stress distribution associated with this moment.
3. Calculate the elastic stress distribution corresponding to the applied moment ( $-M_t$ ) to describe the unloading.
4. Determine the residual stress in the pipe which is the algebraic sum of the elastic-plastic stresses due to  $M_t$  and the elastic stresses due to ( $-M_t$ ).

In calculating the moment-curvature curve for the pipe, thin shell theory was applied and a representative bilinear stress-strain curve (Figure 2-8) was used.

As shown in Figure 2-9, the strain varies linearly through the section, while the stress follows the bilinear curve for angles greater than  $\theta$ .

The applied moment ( $M_t$ ) is given by:

$$M_t = 2 \int_0^{\frac{\pi}{2}} (E \epsilon_o \sin \phi) (a \sin \phi) (2a t d\phi) \\ + 2 \int_{\theta}^{\pi/2} \{ (\epsilon_o \sin \phi - \epsilon_y) E_t + E \epsilon_y \} (a \sin \phi) (2a t d\phi) \quad (2-1)$$

where

$\epsilon_o = a/\rho =$  outside strain

$a =$  radius of pipe

$R$  = radius of curvature

$\epsilon_y, \sigma_y$  = yield strain

$E, E_t$  = elastic and plastic modulus, respectively

The first term in Equation 2-1 is the contribution from the elastic part of the stress distribution, and the second term corresponds to the plastic portion of the stress distribution.

After integration and rearrangement, Equation 2-1 becomes:

$$M_t = M_o \left[ \frac{(1 - E_t/E)}{\pi} \left\{ \frac{(2\theta - \sin 2\theta)}{\sin \theta} + 4 \cos \theta \right\} + \frac{E_t}{E \sin \theta} \right]$$

and  $\sin \theta = \epsilon_y / \epsilon_o \frac{\epsilon_y R}{a}$

$M_o$  = moment corresponding to the first onset of yielding on the outside surface =  $\sigma_y \pi a^2 t$ .

Clearly, for fully elastic behavior,  $\theta = \pi/2$ , and  $M_t = M_o$ .

Figure 2-10 shows the variation of the applied moment with the outside fiber strain and also the bend radius  $R$ . As shown in the figure, in order to get a final radius of 91.25 inches, the outer fiber strain during bending is 2.37%. The corresponding moment is  $1.43 \sigma_y \pi a^2 t$ .

The residual stress distribution can now be determined by combining the elastic stress corresponding to  $(-M_t)$  and the elastic-plastic stress during bending. Figure 2-11 shows the resulting stress distribution.

Figure 2-11 shows that the pipe is subjected to high residual stresses (approaching the yield stress), and that the stress distribution varies around the circumference of the pipe. In particular, it shows tensile stresses on the surface facing the centerline of the vessel. It should be



noted that the actual stresses could be higher due to local yielding at locations where Hertzian contact stress (between the roller and the pipe) occurs during bending. Since this would be most likely to occur on the surface of the sparger facing the center of curvature, higher stresses could be expected at this location.

The residual stress shown here was calculated for room temperature conditions. However, for reactor operating temperatures  $\approx 550^{\circ}\text{F}$ , the residual stresses are expected to relax to approximately the yield stress at that temperature (18.8 ksi at  $550^{\circ}\text{F}$ ).

### 2.5.2 Weld Residual Stress

High tensile stress is a major contributor to SCC. Residual stress due to welding is a primary component of the overall stress state at a weld location. Residual stress measurements of small diameter piping show that weld residual stress is typically between 30 and 40 ksi. Measurements have also shown that the weld residual stress varies with azimuthal location. Figure 2-12 (Reference 2-1) shows the azimuthal variation of residual axial stress on the inside surface of a 4-inch pipe. The residual stress on the outside surface of the pipe is comparable in magnitude but opposite in sign to that on the inside surface.

The weld residual stress produced at the T-box sparger weld could be higher than that for butt welded-straight pipe. The higher residual stress would occur in the sparger due to the added stiffness of the tee-box compared to that of a straight pipe.

In addition to high weld residual stress, welding at the T-box sparger junction causes sensitization of the material adjacent to the weld. Also, grinding and other mechanical working of the weld HAZ region before and after welding could lead to local cold working. Both the sensitization and cold work have a significant effect on stress corrosion cracking in Type-304 stainless steel components.

### 2.5.3 Role of Fabrication Stresses in the Observed Cracking

The conclusions from the evaluation of fabrication stresses presented in this section are summarized below:

1. Stresses due to fabrication and welding could be significant and would exist throughout plant operation.
2. A possible synergistic combination of adverse metallurgical conditions (e.g., sensitization, cold work) and high residual stresses may explain the observed cracking.
3. Since the stresses change sign (become compressive) around the circumference, a crack that initiates in the tensile region can be expected to arrest in the compressive regions.

### 2.5.4 Installation Stress

Stresses sufficient and necessary to cause initiation and propagation of cracks by stress corrosion cracking (SCC) can be identified by postulating certain installation variables. Figure 2-13 shows two cases which can be postulated.

In Case 1, it is postulated that differential weld shrinkage occurred during welding of the header pipes to the T-box. The outer bracket would provide a force to cause the header to contact the shroud wall. For simplicity, the arm is assumed to have an arc length of 90°. A 1/8-in. differential weld shrinkage is assumed. The deflection resulting at the header end would be approximately:

$$\frac{1/8}{4.0} = \frac{\Delta}{91.25} ; \Delta = 2.85 \text{ inch.}$$

Then, from Reference 2-2, Table 13.4, Case 1:

$$\Delta = \frac{WR^3}{4EI} (2\phi - \sin 2\phi) , \text{ where } \phi = 90^\circ F.$$

Solving  $W = 647$  lb, assuming:

$$R = 91.25 \text{ in.}$$

$$E = 28.3 \times 10^6 \text{ ksi}$$

$$I = 4.79 \text{ in.}^4$$

Since  $M = WR$

$$\sigma = \frac{WRC}{I} = \frac{647 \times 91.25 \times 2.0}{4.79}$$

$$\sigma = 24700 \text{ psi}$$

$$\sigma \approx 25000 \text{ psi (elastic)}$$

For Case 2, it is assumed that  $R$  is incorrectly fabricated to a radius of 90.25 inches. It is further assumed that the vessel brackets cause a uniform moment on the pipe, thus increasing the radius to 91.25 inches.

The initial inner length is  $\pi/2 \times 88.25 = 138.62$ . After forming, the inner length is  $\pi/2 \times 89.25 = 140.19$ :

$$\text{Strain} = \epsilon = \frac{\Delta l_{\text{inner}}}{l_{\text{inner}}} = \frac{140.19 - 138.62}{138.62} = 0.011$$

$$= 1.1\%$$

Using a stress-strain curve for Type-304 stainless steel, the resulting secondary stress is found to be 37,000 psi for 1.1% strain.

For the postulated conditions, these two examples show that high deflection limited tensile stress can occur during installation. This stress has not been confirmed. In addition, the welding process produces residual stress in the pipe near the weld. The magnitude and sign of the stress varies with distance from the weld and depend on pipe size and welding speed. This stress is likely to vary circumferentially. Maximum

tensile residual stress in the range of 18 ksi to 40 ksi have been measured in weld pipe tests (Reference 2-1).

Installation stress considered in conjunction with the material consideration discussed later (Section 2.6) may explain the cracks that have been observed. It should be emphasized that the installation stress postulated above is all deflection-limited secondary stress that will relax to the elevated temperature yield strength of the material during normal plant operation.

#### 2.5.5 Stresses During Normal Operation

All identified stresses during normal operation were found to be negligible. Loadings that were considered include impingement loads (i.e., flow past the spargers), seismic, pressure, thermal mismatch, stagnant line top-to-bottom temperature gradients, stagnant line throughwall temperature gradients and weight. Stress calculations are given in Appendix A.

It should be noted that, during normal plant operation, there is no core spray flow. The sparger  $\Delta P = 0$  and  $\Delta T = 0$ . Impingement loads are 1.0 lbf/in. on the header arm, resulting in negligible stress. Weight of the spargers and water is only 1.37 lbf/in., again resulting in negligible stress. Stagnant line temperature gradient calculations are not provided since the maximum  $\Delta T$  for top-to-bottom gradients and for through wall gradients were found to be less than 8°F, which would result in insignificant stress. It should be noted, however, that the  $\Delta T$  for core spray injection is addressed in Section 2.5.6.

It is concluded that the normal operating loadings do not result in stresses that could explain the crack observed in the Hatch Unit 1 core spray sparger.

### 2.5.6 Stresses During Core Spray Injection

Stresses during core spray injection are the design stresses for the spargers. Design loadings include all those discussed in Section 2.5.5 plus those that occur because the system is no longer a passive system. The pressure differential in the sparger at rated flow is approximately 28 psid. The resulting hoop stress in the pipe is about 230 psi. Impingement load stress is less during spray injection than during normal operation. Thermal stress due to the throughwall temperature gradient are high and are given by:

$$\sigma_T = \frac{E \cdot \alpha \cdot \Delta T}{2(1 - \nu)}$$

This stress is not a concern for one or a few cycles. The radius of the sparger shrinks when the sparger is cooled, resulting in a secondary bending stress of approximately 3100 psi. The axial stress in the pipe due to  $\Delta P$  and bracket friction is low--less than 220 psi. Flow through the nozzles results in stress in the nozzle-to-pipe weld which is low--less than 500 psi. Weight stress is negligible. Water hammer is not expected because the pipe is essentially an open pipe, and the nozzle opening areas are approximately equal to the pipe internal area, even for the short leg. However, water hammer is addressed in the following section.

#### 2.5.6.1 Water Hammer Loads

Water hammer loads as discussed herein are those hydraulic loads associated with injection of core spray water into a core spray system. The system piping downstream of the check valve in primary containment is assumed empty (or filled with steam) because of the draining of water from the spargers and/or the flashing of water to steam during depressurization prior to core spray injection.

For the purpose of maximizing injection loads on the core spray spargers, it is assumed that reactor pressure is essentially atmospheric (as for a large LOCA), enabling system flow to increase to runout controlled only by the injection valve opening characteristics. Upon valve opening, the

head (H) is available to accelerate the flow, but as the velocity increases, the acceleration head is reduced by friction and local losses. If  $L_e$  is the equivalent length of the pipe system, the final velocity  $V_f$  is given by application of the energy equation:

$$H = f \frac{L_e}{D} \frac{V_f^2}{2g}$$

The maximum velocity attainable is limited to that at system runout flow (6000 gpm), which produces a velocity of 54 ft/sec in the sparger (at the entrance to the long sparger arm to be more concise; the velocity at the ends is zero).

This is conservative because the velocity of the water first entering the sparger will be less than runout velocity because of the relatively slow opening characteristics of the injection valve. The injected water fills the pipe line between the injection valve and the sparger at a time prior to full valve opening and therefore, before the final runout velocity is attained.

Assuming the maximum velocity attainable, the resulting momentum load in the sparger is:

$$P_m = \frac{V^2}{144 gv} = \frac{(54)^2}{144(32.2)(0.160)} = 39.3 \text{ psi}$$

or

$$F_m = P_m A_p = 39.3 (9.89) = 389 \text{ lb.}$$

where

$P_m$  = momentum pressure (psi);

$F_m$  = momentum load (lb);

$V$  = velocity (ft/sec);

$g$  = gravitational acceleration (32.2 ft/sec<sup>2</sup>);

$v$  = specific volume (0.0160 ft<sup>3</sup>/lb) (~50°F water); and

$A_p$  = pipe flow area (9.89 in.<sup>2</sup>) (3-1/2-in. Schedule 40 pipe).

If the end plates at the ends of the spargers were removed, it is obvious there would be no impact load. Even if the ends were cupped and the sparger nozzles were plugged, there would be no water impact load because the trapped gas in the line acts as a surge tank.

The actual end condition of the spargers is somewhere in between these two extremes. It is much closer to the open end condition, except that there are several "ends" instead of one end, and they are located along the length of the sparger arms.

The exit flow area of the sparger nozzles is computed as follows:

	<u>Number</u>	<u>Area (in.<sup>2</sup>)</u>	<u>Total Area (in.<sup>2</sup>)</u>
1-in. VNC Nozzle	27	1.018	27.5
3101 Nozzle	25	0.307	7.7
Total Open Flow Area Per Sparger =			35.2

The exit flow area of the nozzles and elbows is 78% greater than the flow area of the two sparger arms ( $2 \times 9.89 = 19.78$  in.<sup>2</sup>).

An estimate of pressures induced in the sparger at the end of the filling time of the spargers and piping can be made by considering a sparger with only one open elbow located at the end of each arm. Steam would be pushed ahead of the oncoming front of water, exiting the sparger through the assumed single nozzle. The developed differential pressure to expel the steam would be approximately 7 psid. Adding all sparger elbows and nozzles to this logic clearly demonstrates that the sparger indeed behaves like an

open-ended pipe, and conventional water hammer loads of any significant magnitude would not be present. Injection conditions at higher reactor pressure would clearly be bounded by the runout case presented here.

## 2.6 METALLURGICAL EVALUATION OF THE CORE SPRAY SPARGER CRACKING

The purpose of this section is to present the metallurgical evaluation of the cracking in the Hatch Unit 1 core spray sparger. Extensive field experience and laboratory data have confirmed the role of cold work and weld sensitization in stress corrosion cracking (SCC) of stainless steel components. A brief summary of data relevant to core spray sparger cracking is presented below.

### 2.6.1 Background

Field cracking has been discovered in non-solution heat treated Type 304 stainless steel core spray spargers in six BWR plants. Cracking occurred both in and away from weld sensitized regions following 64 to 136 months of service. It has been postulated that failure in non-sensitized regions is due to stress corrosion cracking (SCC) accelerated by localized cold work typically remaining in non-solution heat treated core spray spargers. Cracking in weld sensitized zones was most likely a result of the combination of cold work and sensitization effects.

The metallurgical basis for the anticipated increased susceptibility to cracking in core spray spargers due to localized cold working is supported by an extensive data base. Constant extension rate technique (CERT) and constant load stress corrosion tests (Reference 2-3) performed on an archive core spray sparger arm manufactured using fabrication procedures similar to those used for Hatch Unit 1 showed accelerated SCC in cold worked regions. In addition, the effects of cold work and subsequent sensitization on stress corrosion cracking of stainless steels have been well documented in both laboratory and field applications.



### 2.6.2 Effects of Cold Work and Sensitization on SCC Behavior of Type 304 SS

Numerous studies (Reference 2-4) have shown that the presence of cold work accelerates stress corrosion cracking in non-sensitized Type 304 stainless steels. However, the combination of cold working followed by sensitization can result in a synergistic deleterious effect on SCC behavior. Since Hatch Unit 1 core spray sparger cracking occurred near the T-box weld where both cold work and sensitization were likely, this discussion focuses on their combined effect on SCC of Type 304 SS components.

The presence of cold work in stainless steels results in changes in microstructure which affect both mechanical and chemical material properties. Increased hardness, ultimate tensile strength, and yield strength along with decreased ductility accompany increasing amounts of cold work. Microstructural phase transformations from austenitic face-centered cubic (fcc) to body-centered tetragonal (bct) martensite often occur in severely cold worked Type 304 stainless steels. The increased internal energy associated with cold worked metal leads to a general increase in chemical reactivity of the material.

Increased internal energy from cold work alone enhances the kinetics of sensitization in the temperature range where sensitization of austenitic stainless steels normally occurs. The presence of cold work induced martensite has an even greater effect on sensitization. Since both chromium and carbon diffuse more rapidly in bct martensite than in fcc austenite, precipitation kinetics are more rapid and can occur at lower temperatures in the martensitic phase. Chromium depletion will also occur at a more rapid rate. The effects of cold work on sensitization are schematically illustrated in Figure 2-14 which shows a comparison of time-temperature-sensitization (T-T-S) curves for Type 304 SS in both deformed (cold worked) and undeformed conditions.

The combination of cold work and sensitization results in accelerated SCC in BWR type environments. A comparison of Type 304 stainless steel SCC susceptibility for furnace sensitized and cold worked plus sensitized material conditions is shown in Figure 2-15 from Reference 2-5. Specifically it shows that SCC can occur at stresses well below the yield stress under the combination of cold work and sensitization. The increased susceptibility to SCC due to the presence of cold work with sensitization was expected since SCC is a consequence of sensitization, and sensitization kinetics are accelerated by the presence of cold work.

### 2.5.3 Archive Core Spray Sparger Testing

Testing was performed on an archive core spray sparger arm that was intended for installation in a BWR plant, but was scrapped because flatness requirements were not met. The sparger arm was retrieved for testing purposes since the material condition was otherwise typical of non-solution heat treated Type 304 SS core spray spargers installed in BWR's such as Hatch Unit 1.

The outer diameter of the archive sparger exhibited axially oriented cold worked scuff bands presumably created by bending fixtures used to guide the sparger arm during cold forming operations. Metallography and hardness readings showed local regions of high cold working up to Rc 40 (>50% cold work) extended to 8-10 mils deep in scarred areas. Ferrite scope measurements indicated transformation to a magnetic phase such as martensite had occurred in regions with localized cold work.

CERT and constant load stress corrosion test specimens were machined from various locations around the archive sparger arm circumference. The original outer diameter surface was preserved for exposure to the 8 ppm  $O_2$ /288°C water test environment. CERT results showed specimens from heavily scuffed cold worked regions failed due to transgranular stress corrosion cracking (TGSCC) three times faster than specimens machined from the same sparger arm in unscarred regions. Constant load stress corrosion test specimens from heavily scarred areas exhibited TGSCC with failure times of 64 and 325 hours. Similar specimens machined from unscuffed regions showed

no failure until after 2600 to 3500 hours when intergranular stress corrosion cracking (IGSCC) mechanisms at the creviced tab area became dominant.

The results of CERT and constant load tests performed on the archive sparger arm confirm that localized cold work on non-solution heat treated Type 304 SS spargers may be sufficient to cause increased SCC susceptibility.

#### 2.6.4 Relevance to Hatch Unit 1 Core Spray Sparger Cracking

The cracking in the Hatch Unit 1 core spray sparger was discovered after 80 months of service. The cracked area was limited to the region adjacent to the T-box to bottom sparger arm weld. The time to cracking initiation and the location of cracking was consistent with experience at other BWR's.

Fabrication procedures followed when the Hatch Unit 1 sparger was manufactured were similar to those used for the archive core spray sparger arm discussed in Section 2.6.3. Hence, the presence of severely cold worked regions on the outer diameter surface of the Hatch Unit 1 sparger arm would be anticipated. Welding of the sparger arm to the T-box would probably be sufficient to sensitize the 0.045 wt % carbon sparger arm without previously cold worked regions. However, the presence of localized cold work with some cold work induced martensite would have increased the degree of sensitization.

#### 2.6.5 Probable Cause of Hatch Core Spray Sparger Cracking

The most probable cause for the premature cracking of the Hatch Unit 1 core spray sparger T-box to bottom sparger weld was stress corrosion cracking. The susceptibility of this particular joint was likely increased due to the presence of cold work enhanced sensitization.

### 2.7 CRACK ARREST ASSESSMENT

In assessing the possibility of crack arrest the following sources of stress are considered:

1. Stress due to pressure, mechanical loads and thermal gradients:  
These stresses have been shown to be negligible and therefore do not affect crack growth.

2. Stress due to bracket restraint: Stress due to bracket restraint is considered a secondary stress. This stress would relax as initial crack propagation occurs.
3. Residual stress due to fabrication: The stress intensity factor will decrease for a crack propagating circumferentially from a tensile region into a compressive region. This results in slower crack growth and eventual crack arrest.
4. Residual stress due to welding: Weld residual stress at the T-box - sparger welds would influence crack propagation. These stresses are likely to vary circumferentially and also relax as the cracks become larger.
5. Vibration induced stress: Vibration due to flow during core spray operation and flow past the sparger during normal plant operation, is considered negligible.

In considering crack arrest, the stress due to bracket restraint and residual stress due to fabrication and welding are significant and are evaluated in detail.

#### 2.7.1 Stresses Due to Bracket Restraint

Stresses due to bracket restraint are governed by the applied displacement and the compliance of the pipe. Since the displacement is fixed, the compliance change with crack growth could lead to crack arrest. This is comparable to crack arrest in a bolt-loaded wedge-opening-loading (WOL) specimen in stress corrosion tests. Figure 2-16 shows the variation of compliance with crack length for a pipe subjected to bending. The compliance was determined using the relationship between the strain energy release rate  $G$  and the compliance change per unit area of crack extension  $dc/dA$  (Reference 2-6). For the cracks in the sparger,  $L/d$  is expected to be in the range of  $0 < L/D < 40$ . Figure 2-16 shows that, when more than 30% of the pipe is cracked, the compliance of the pipe increases by a factor of 10. Therefore, for the given initial displacement, the stress in the sparger and the applied stress

intensity factor would decrease by a factor of 10 when more than 30% of the pipe circumference is cracked. Clearly, when the crack length exceeds this value, the restraint stresses become negligible and crack arrest is expected.

### 2.7.2 Fabrication Residual Stress

The residual stresses due to fabrication vary around the circumference, and a precise calculation of the stress intensity is not possible. Nevertheless, a conservative representation of the stress is used to calculate the stress intensity factor. The assumptions made are as follows:

1. The crack in the sparger is modeled as a through wall crack in an infinite plate.
2. It is assumed that the tensile stress ( $\sigma$ ) is uniform and is applied on the crack face over a length ( $2b$ ). (Later this will be conservatively taken as 25% of the circumference.)
3. The remaining portion of the crack is assumed to be subjected to a compressive stress, which is half the tensile stress (Figure 2-17).
4. The crack length ( $2a$ ) for which the combined stress intensity factor reduces to zero is calculated.

The stress intensity factor due to the tensile stress can be shown to be:

$$K_I^{\text{tension}} = \frac{2\sigma a}{\sqrt{\pi a}} \sin^{-1} \left( \frac{b}{a} \right)$$

The stress intensity factor due to the compressive stress  $\sigma/2$  is given by:

$$K_I^{\text{compression}} = \frac{-2(\sigma/2) a}{\sqrt{\pi a}} \left\{ \frac{\pi}{2} - \sin^{-1} \left( \frac{b}{a} \right) \right\}$$

Setting  $K_I^{\text{tens}} + K_I^{\text{comp}} = 0$ , we get

$$\sin^{-1} \left( \frac{b}{a} \right) = \frac{1}{2} \left\{ \frac{\pi}{2} - \sin^{-1} \left( \frac{b}{a} \right) \right\}$$

$$\text{or, } \sin^{-1} \left( \frac{b}{a} \right) = \frac{\pi}{6}$$

$$\text{or, } b = 0.5a$$

If we assume  $2b = 25\%$  of the circumference is under tension  $\sigma_y$  and the remaining portion of the crack is under compressive stress (equal to half the tensile stress), the applied stress intensity factor becomes zero when the crack length is equal to 50% of the circumference. Thus, even under extremely conservative assumptions, crack arrest is expected.

### 2.7.3 Weld Residual Stress

As stated in Section 2.5.2, weld residual stress due to the T-box-sparger weld is a primary contributor to the overall stress state at the cracked section. Circumferential growth of cracks requires the weld residual stress to be tensile along most of the pipe circumference. However, residual stress measurements show that the weld residual stress varies with azimuthal location as shown in Figure 2-12. A crack initiating in a tensile stress region (between  $45^\circ$  and  $225^\circ$ , Figure 2-12) could grow beyond the tensile region, but would soon arrest due to the compressive stress.

Therefore, cracking at the T-box-sparger weld can be expected due to the sensitized material and high tensile residual stress (along with stress from other sources, Section 2-5). However, arrest of these cracks will occur due to the azimuthal variation of the weld residual stress.

The conclusions reached in Section 2.7.1 regarding crack arrest can also be applied to the weld residual stress.

#### 2.7.4 Conclusions on Crack Arrest

Based on the above material, the following conclusions may be drawn:

1. Since the applied loading is predominantly displacement controlled, the stress can be expected to relax as the crack grows. Crack arrest is therefore expected.
2. The residual stress due to fabrication varies from tension to compression along the circumference of the weld. As the cracks propagate into regions of compressive stress, the K value reduces to zero. Even for extremely conservative assumptions, crack arrest can be shown for a 50% circumferential crack.
3. The residual stress due to welding varies from tension to compression along the circumference of the weld. As the cracks propagate into compressive stress regions stress intensity values decrease.
4. The above conclusions are valid as long as there is no stress cycling due to vibration (e.g., flow-induced vibration).

#### 2.8 STRUCTURAL INTEGRITY WITH 360° THROUGHWALL CRACK

Even though GE believes that a 360° throughwall crack is improbable, a structural analysis was performed (see Appendix A) which conservatively assumed that the existing crack propagated 360° throughwall. Loads which were considered included all loads applicable to the intact sparger (see Section 2.5). The analysis ignored the effect of a clamp (or assumed a clamp was not installed).

##### 2.8.1 Normal Operation

Bending stress in the broken sparger arm due to impingement is low -- 868 lb/in<sup>2</sup>. During the postulated seismic event, bending stress is calculated to be 2380 lb/in<sup>2</sup>. All other operating loads result in negligible stresses.

### 2.8.2 Core Spray Injection

Stresses on the broken sparger during core spray injection are bounded by the stresses given for the intact sparger (Section 2.5.5). Normal stress will therefore be less than  $3320 \text{ lb/in}^2$  in the sparger pipe. In the nozzle-to-pipe weld, the maximum normal and shear stresses are  $4270 \text{ lb/in}^2$  and  $4400 \text{ lb/in}^2$ , respectively. In the welded brackets, bounding normal and shear stresses are  $5980 \text{ lb/in}^2$  and  $752 \text{ lb/in}^2$ , respectively.

### 2.8.3 Flow Induced Vibration

Flow induced vibration is not a concern for the broken sparger case. The ratio of natural frequency of the broken sparger arm to the vortex shedding frequency is greater than 6, which exceeds the GE design basis by more than a factor of 2.

### 2.8.4 Conclusions

Stresses during normal operation and during core spray injection were found to be well below allowables. The natural frequency of the assumed broken sparger remains high enough so that flow induced vibration is not a concern. It is concluded that the sparger will lose no pieces and will remain attached to the shroud wall under the conservative assumption that the existing crack propagates  $360^\circ$  throughwall.

### 2.9 REFERENCES

- 2-1. H. H. Klepfer, et al, "Investigation of Cause of Cracking in Austenitic Stainless Steel Piping," NEDO-21000-1, July 1978.
- 2-2. Hopkins, Design Analysis of Shafts and Beams, McGraw-Hill Book Company.
- 2-3. S. E. Carter, "Core Spray Sparger SCC Susceptibility Testing Program," PME&T Transmittal No. 80-509-84.



- 2-4. B. M. Gordon, "Effect of Cold Work on the Stress Corrosion Cracking of Austenitic Stainless Steels in the BWR Environment," PMT Transmittal No. 84-178-014 Rev. 1, October 1984.
  
- 2-5. C. L. Briant, "The Effect of Deformation Induced Martensite on the Sensitization of Austenitic Stainless Steels," 1980 American Society for Metals.
  
- 2-6. E. Kiss, J. D. Heald, D. A. Hale, "Low Cycle Fatigue of Prototype Piping," GEAP-10135, January 1970.

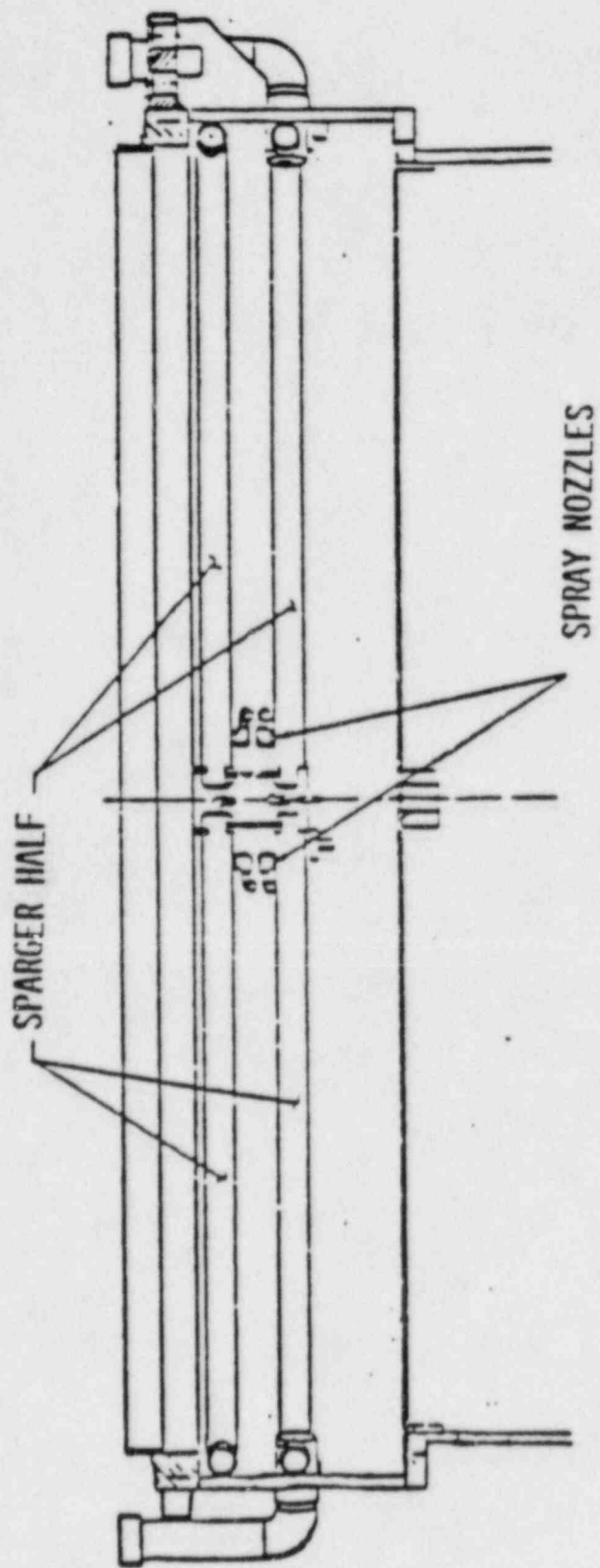


Figure 2-1. Core Spray Sparger - Elevation View

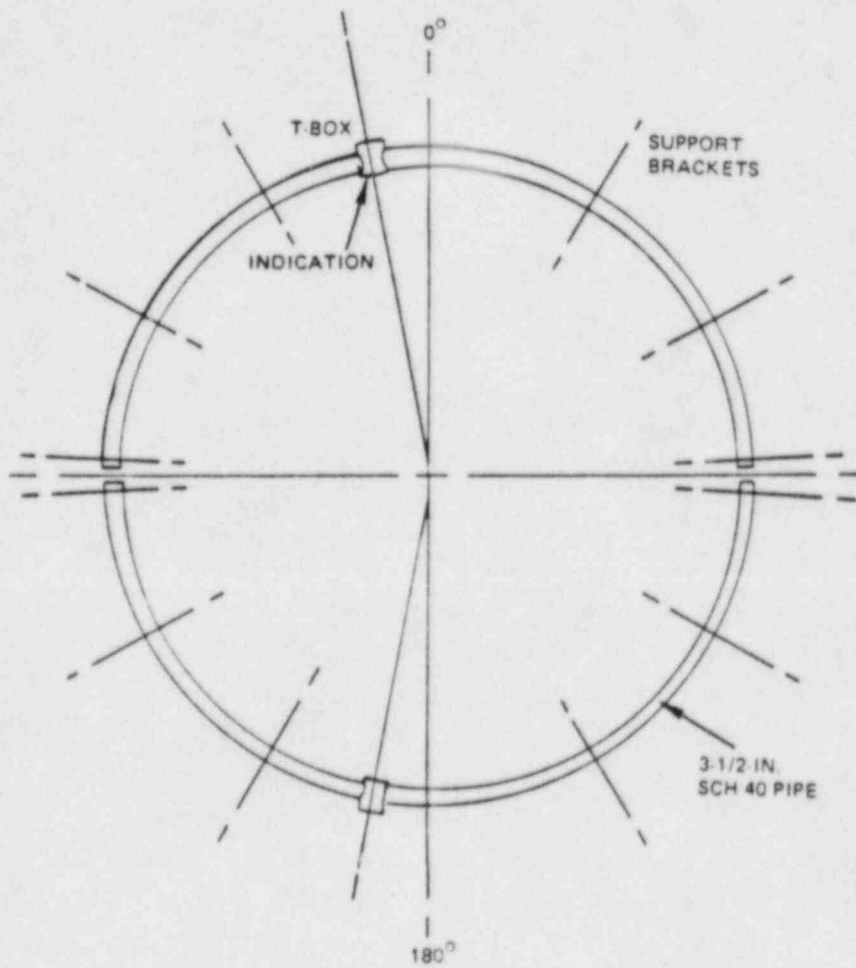


Figure 2-2. Core Spray Sparger - Plan View

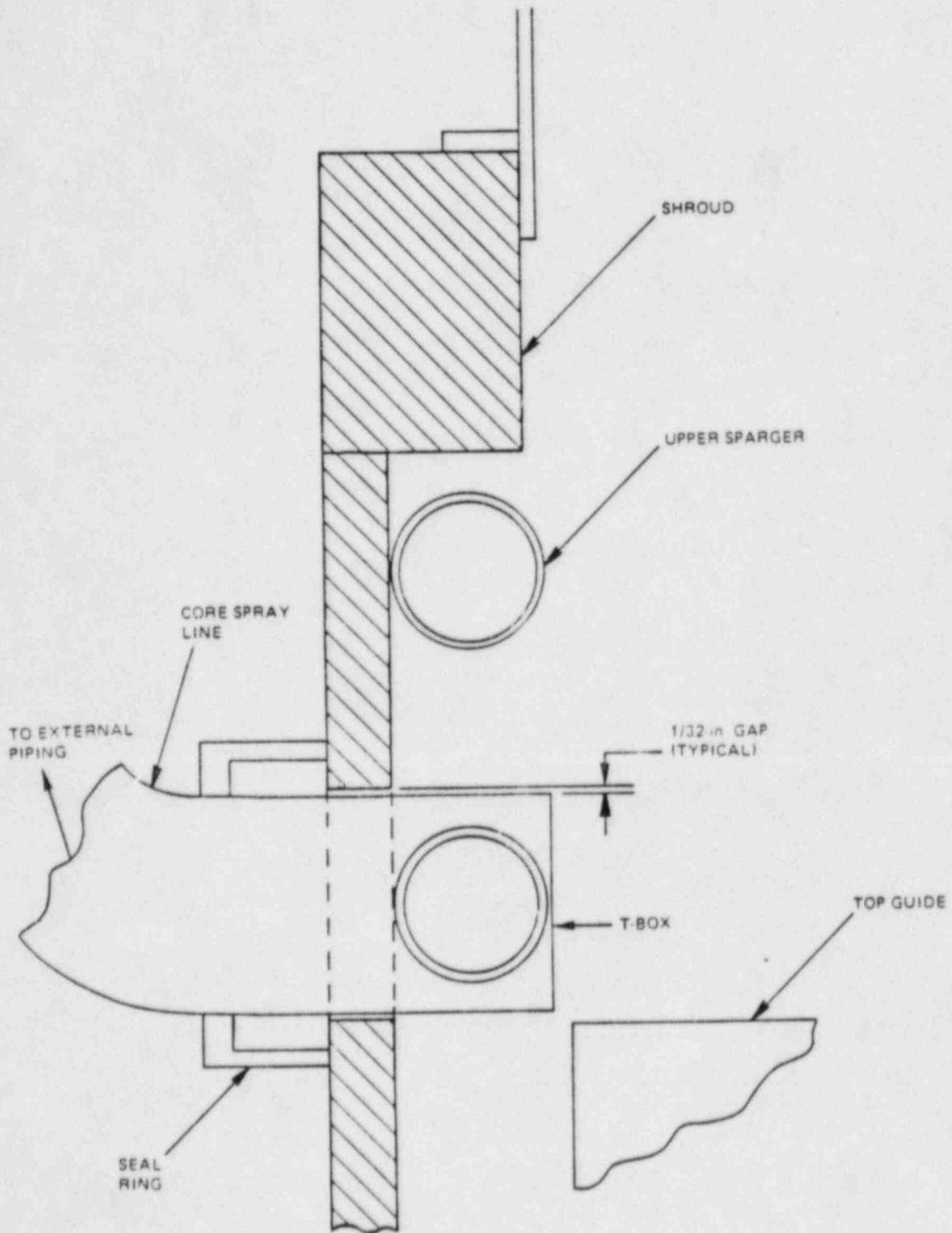


Figure 2-3. Sparger to Shroud Attachment Method

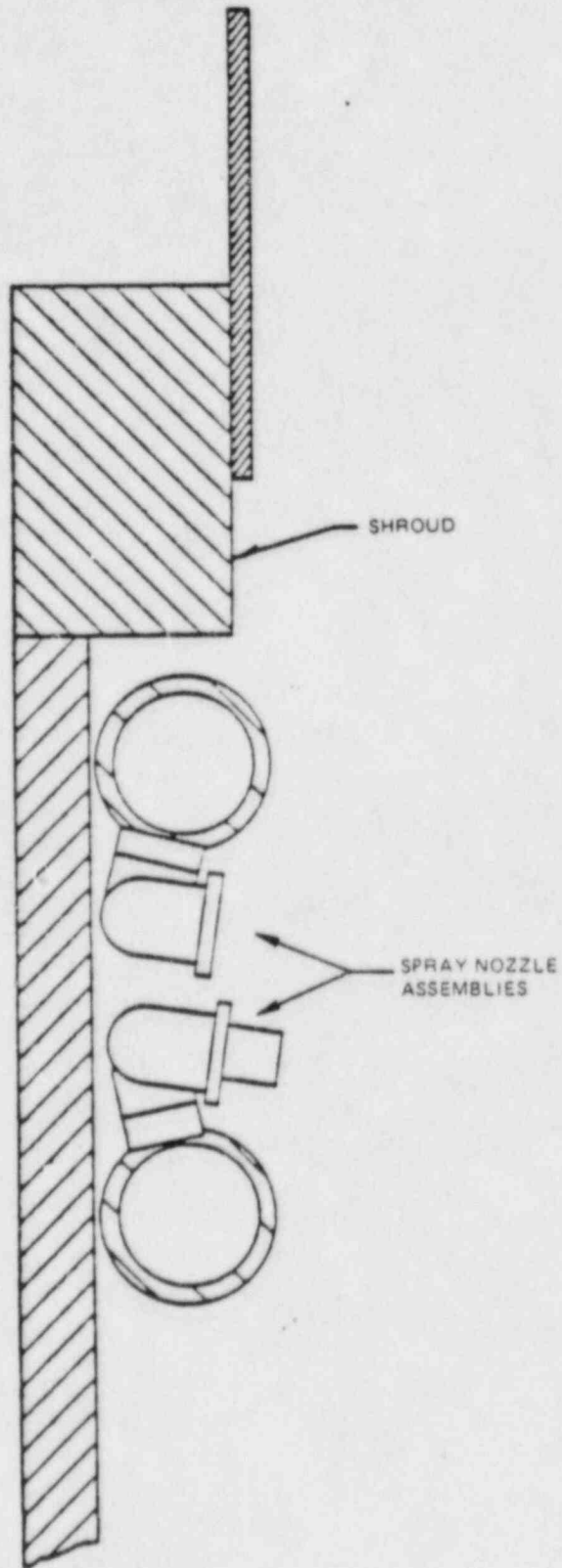


Figure 2-4. Sparger Nozzles

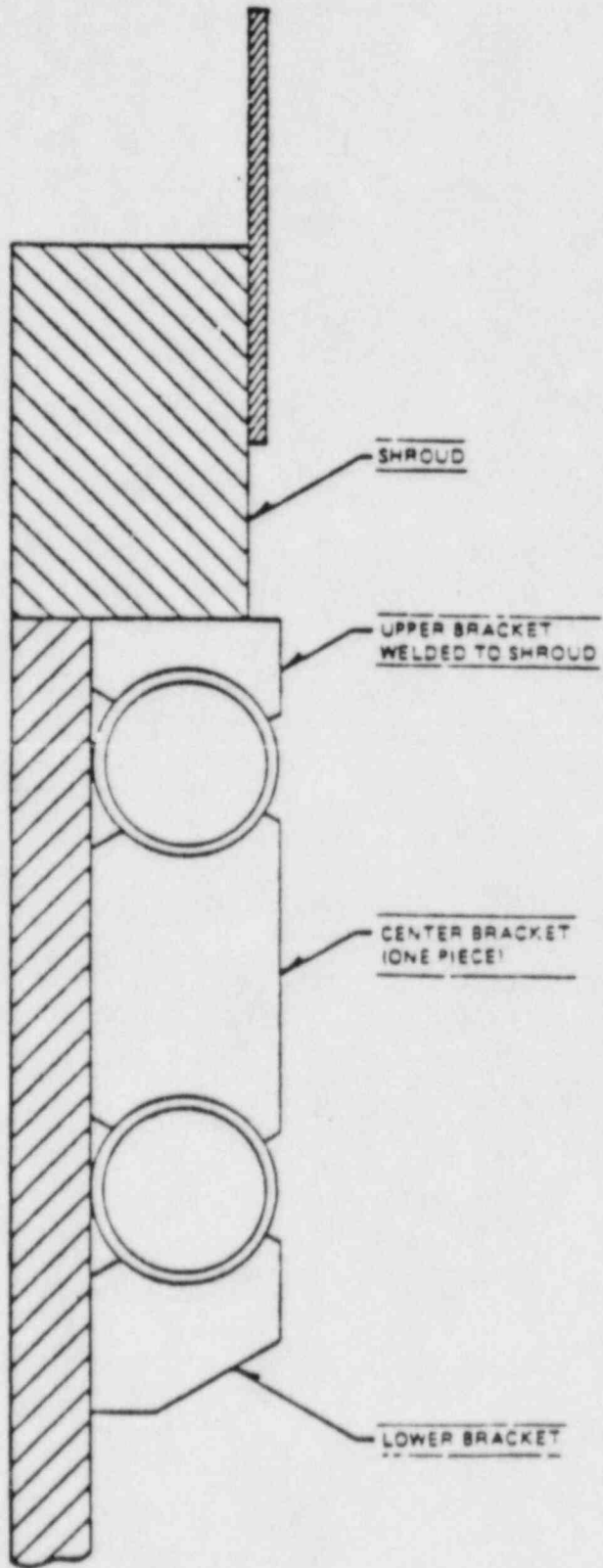


Figure 2-5. Sparger Support Method

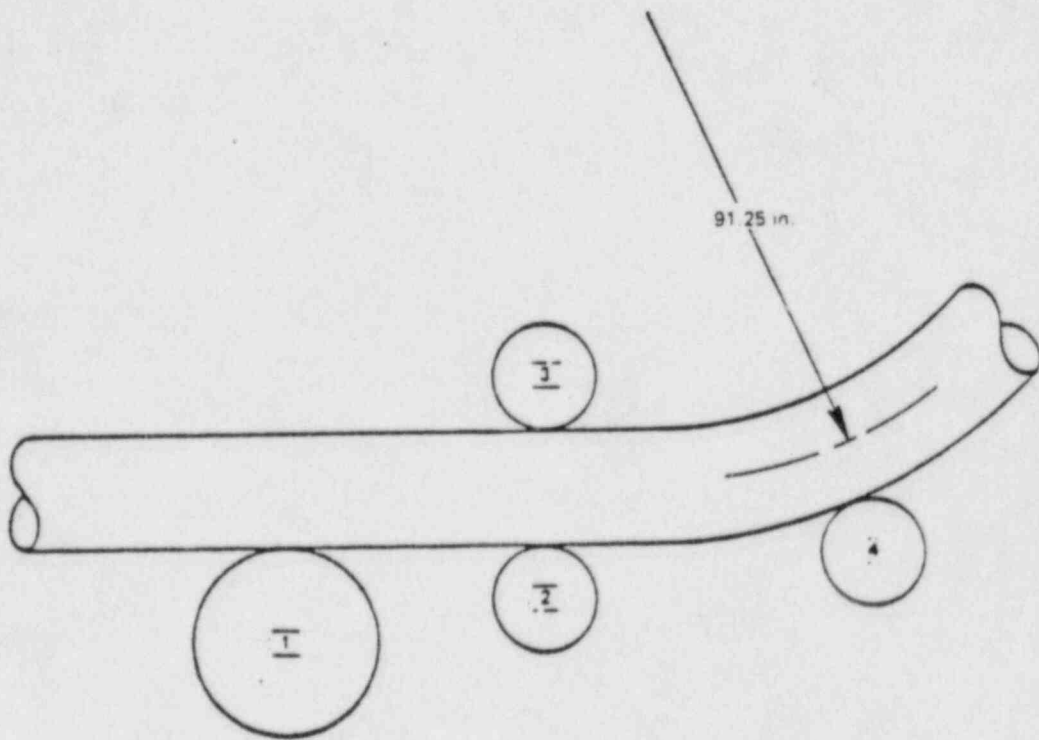
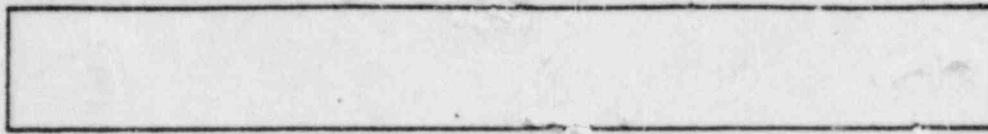
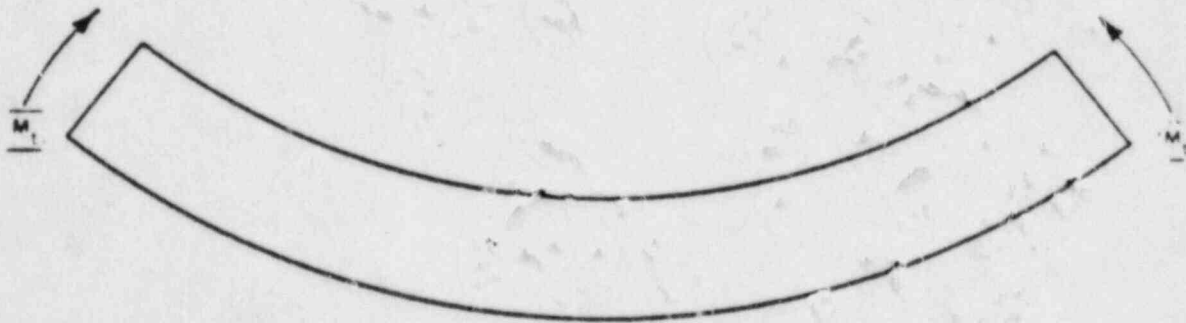


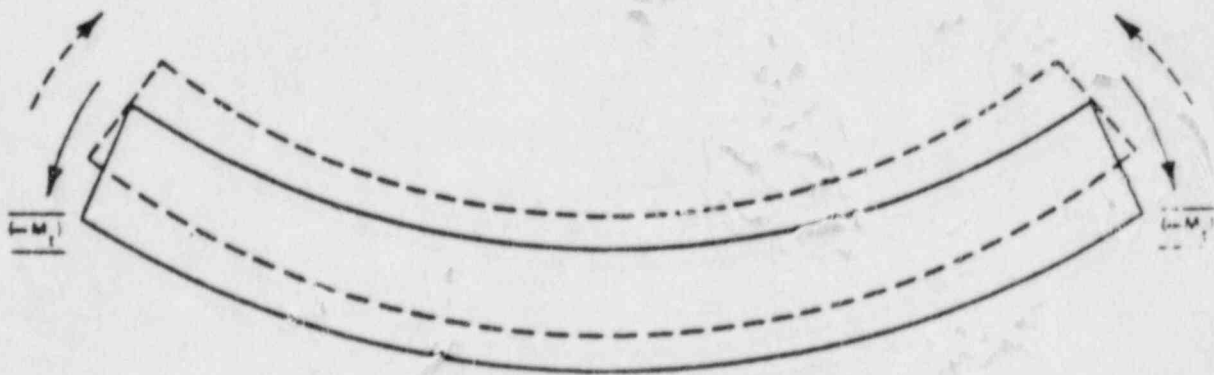
Figure 2-6. Pipe Bending Method



INITIAL CONFIGURATION



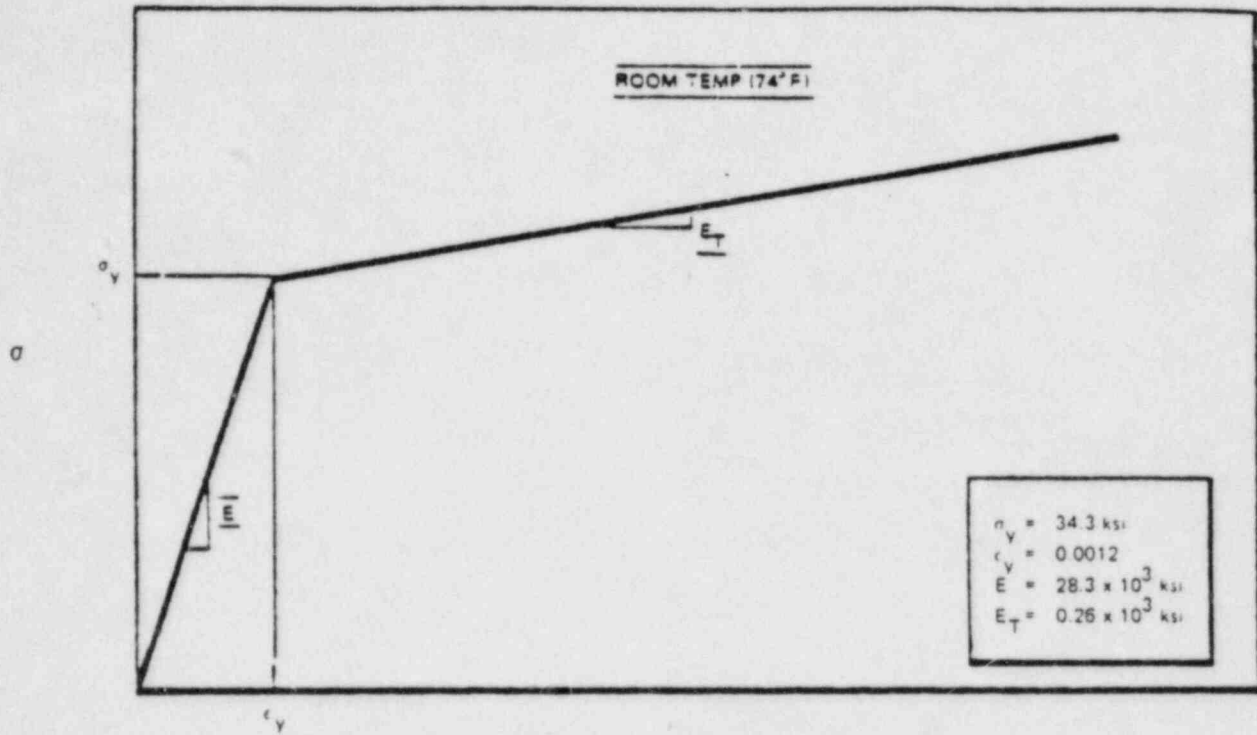
LOAD APPLICATION DURING FABRICATION



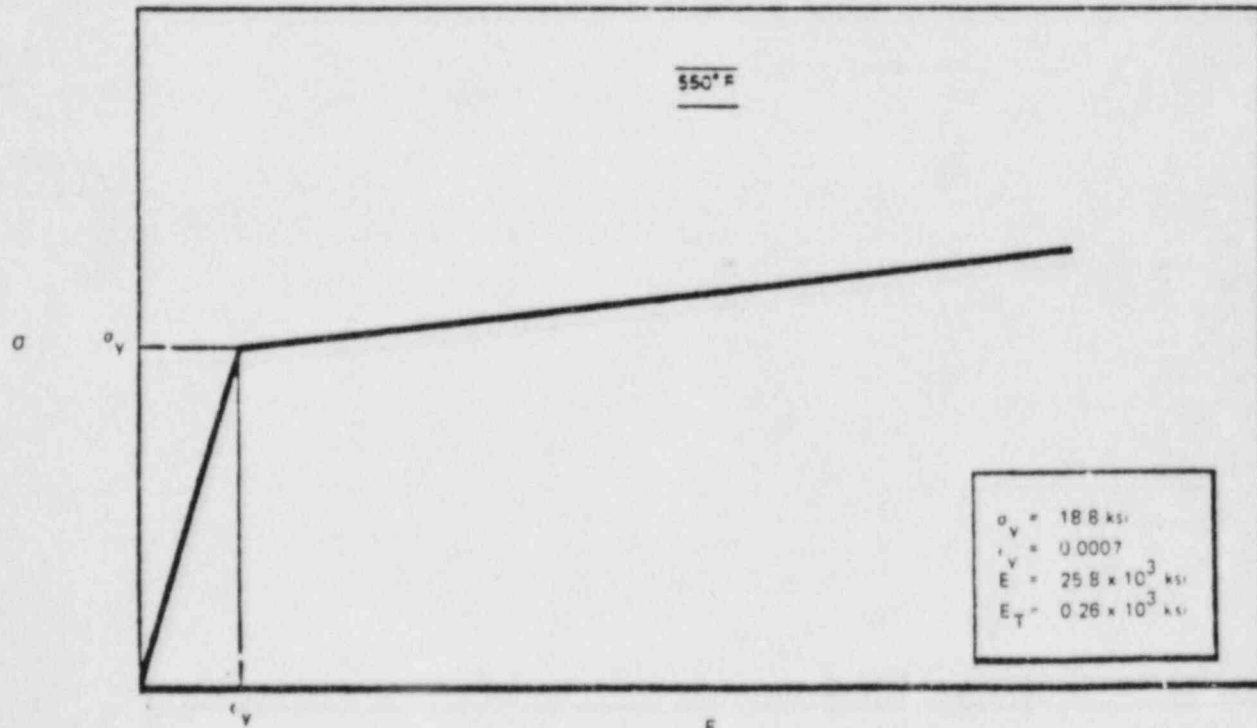
FINAL DEFORMED SHAPE AFTER LOAD REMOVAL

Figure 2-7. Sequence of Events Leading to the Residual Stress Distribution





E  
(a)



E  
(b)

Figure 2-8. Bilinear Stress-Strain Curves for Type-304 Stainless Steel

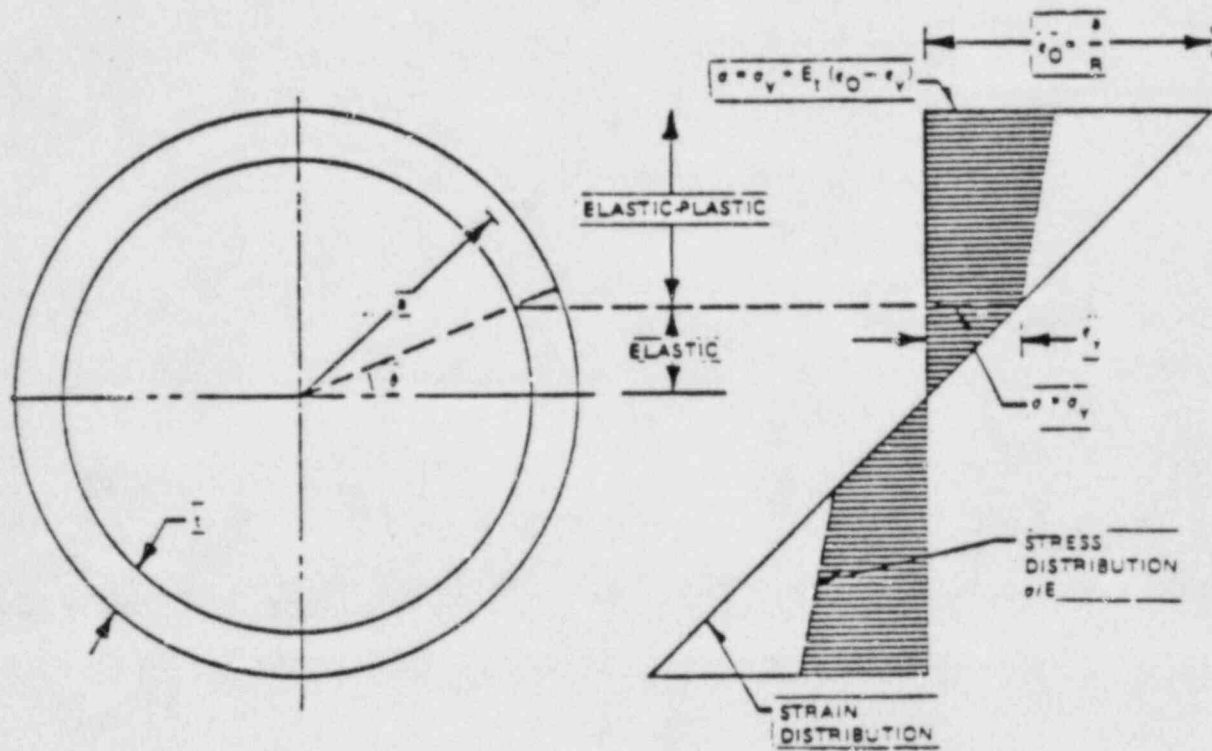


Figure 2-9. Stress and Strain Distribution in the Pipe Under Applied Moment

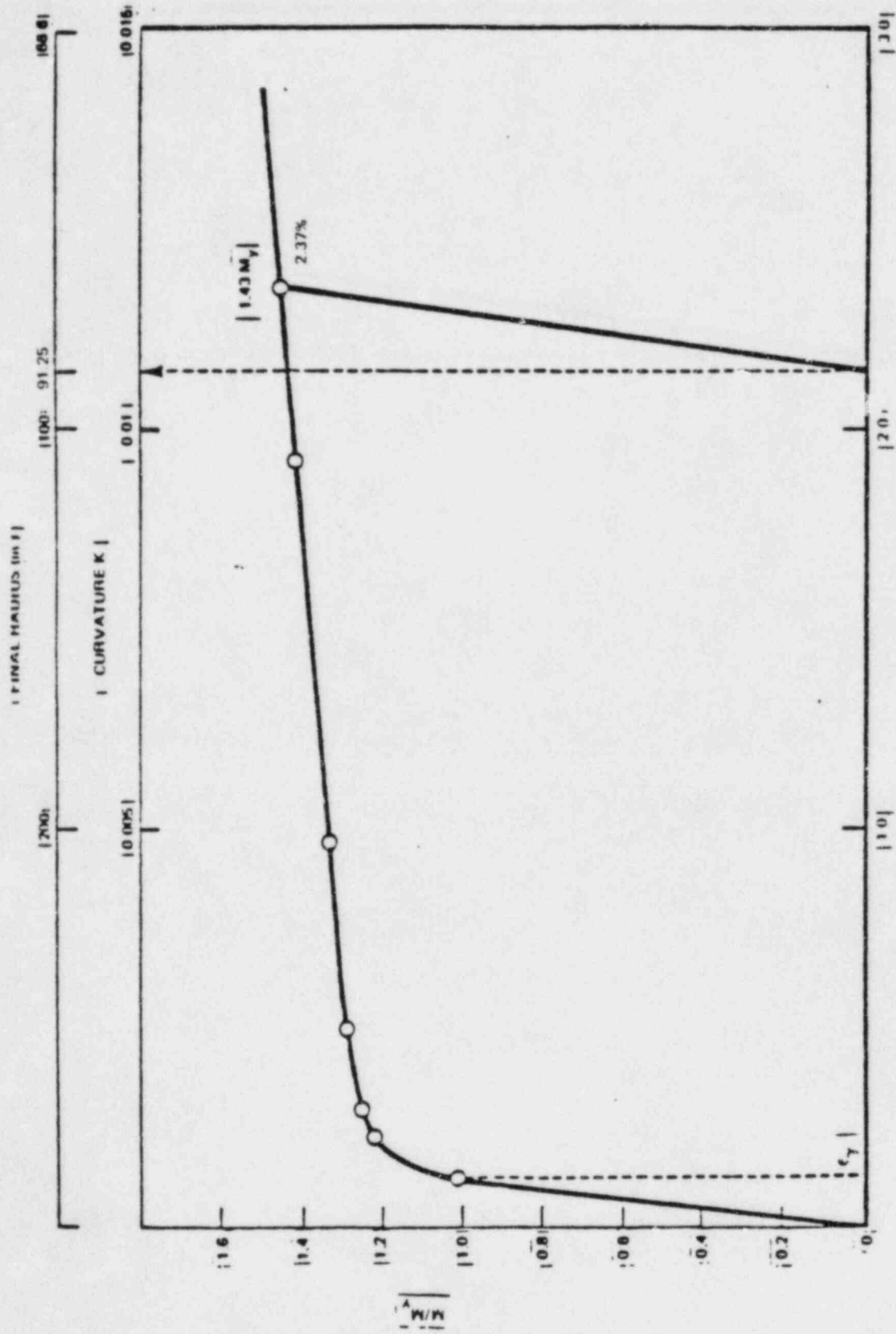


Figure 2-10. Moment Versus Outer Fiber Strain

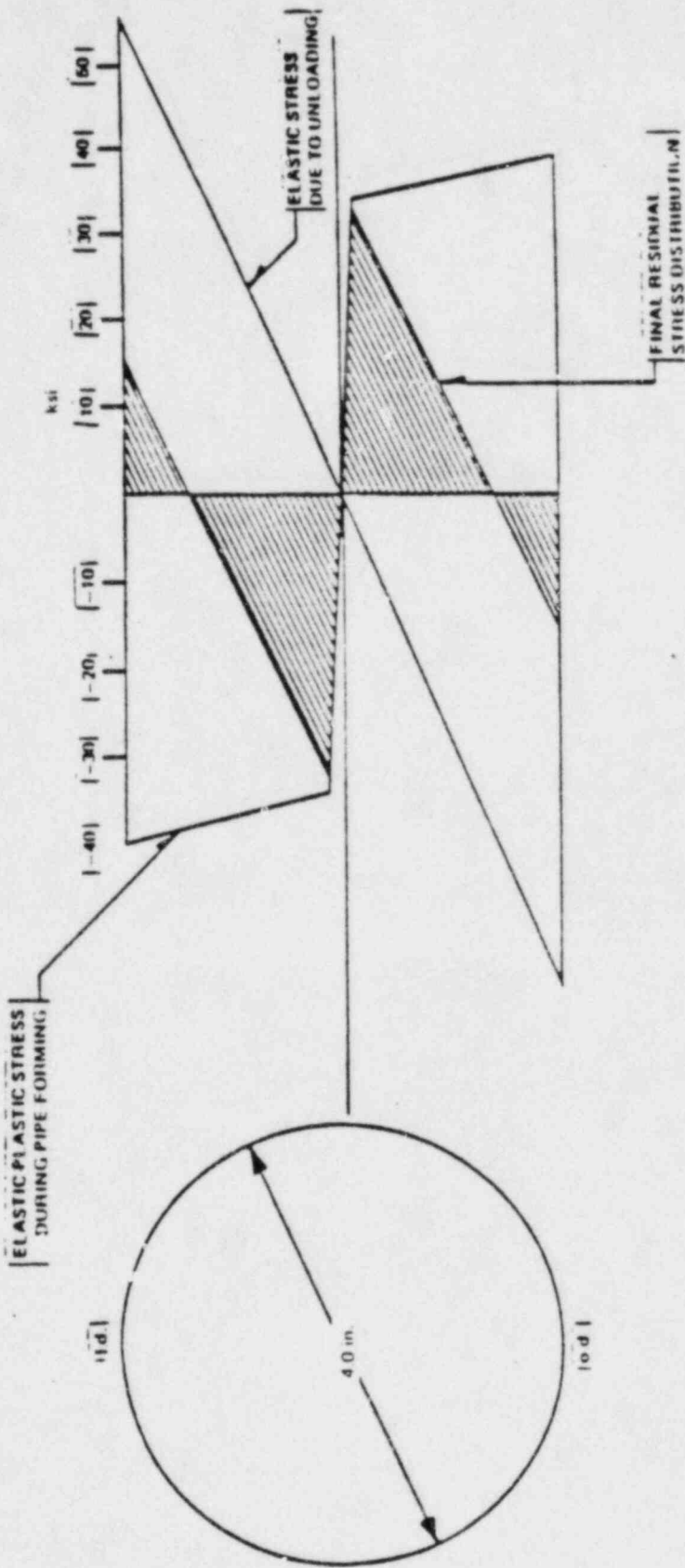


Figure 2-11. Resultant Residual Stress Distribution After Fabrication

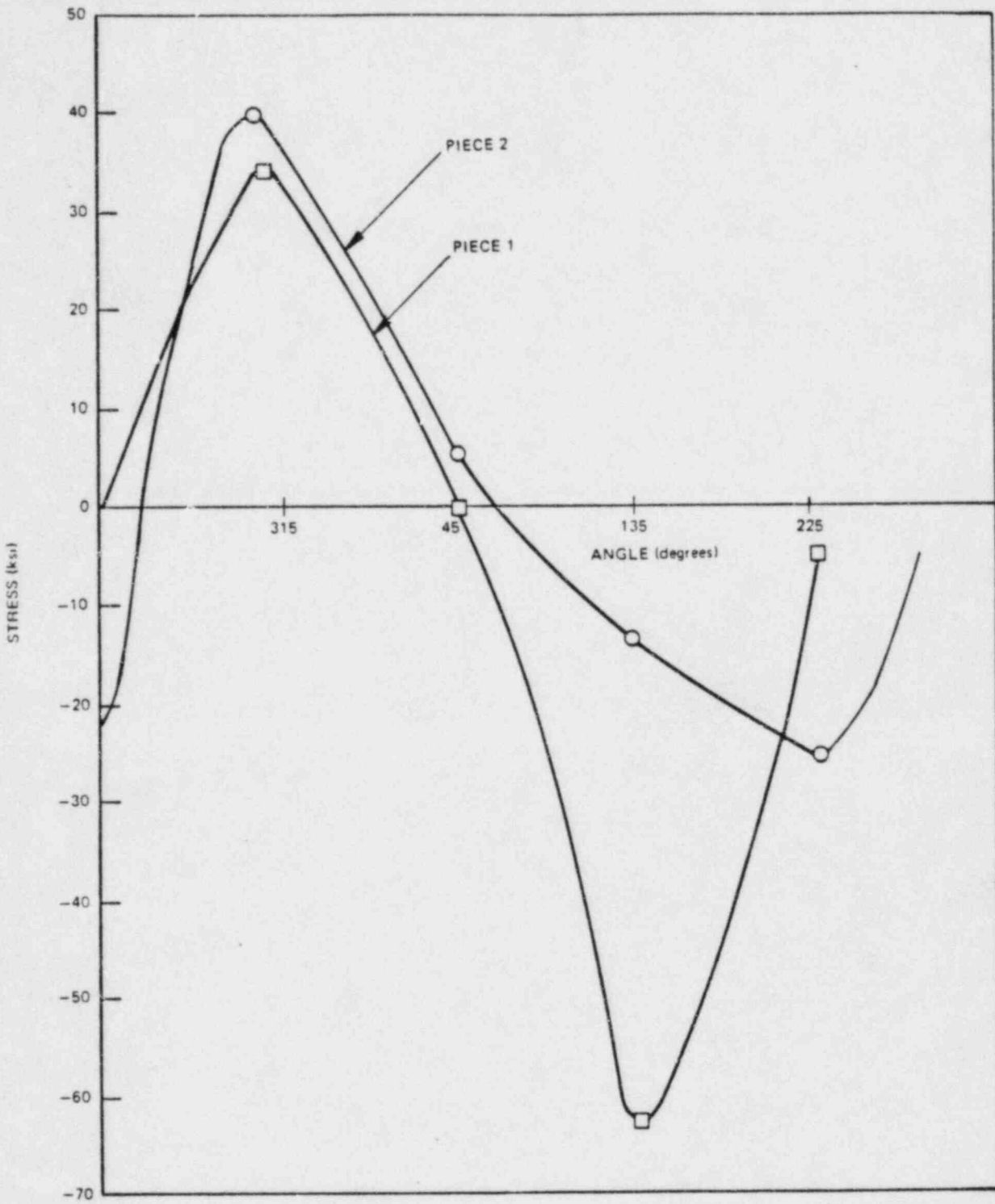
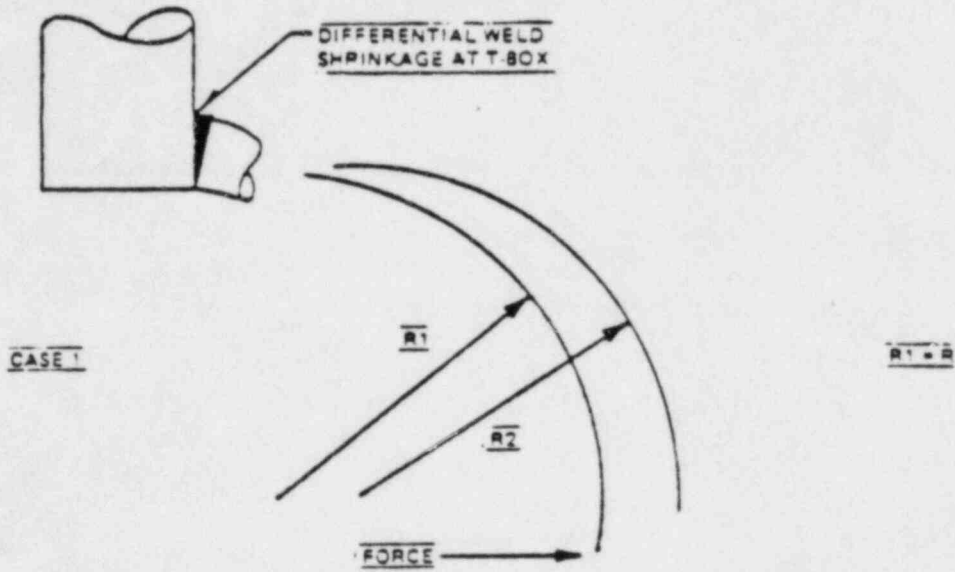


Figure 2-12. 4-in. Pipe Inside Longitudinal Residual Stress Measurements Taken Both Sides 0.1 in. from Weld Fusion Line

INSTALLATION-RADIAL MISMATCH



FOR SHRINK = 1/8 in.  
 $\sigma$  AT T-BOX = 25 ksi (ELASTIC)

ASSUME  $R_1 = 90.25$   
 $R_2 = 91.25$   
 UNIFORM FORMING  
 $\epsilon = 1.1\%$   
 $\sigma = 38$  ksi (FROM  $\sigma$ - $\epsilon$  CURVE)

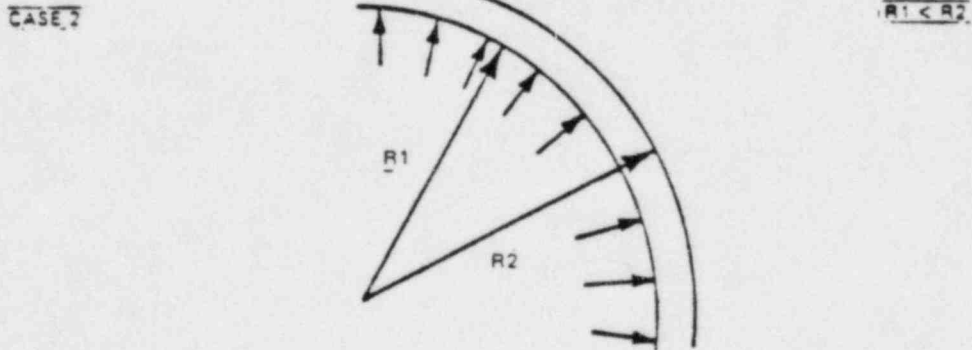


Figure 2-13. Postulated Installation Stresses

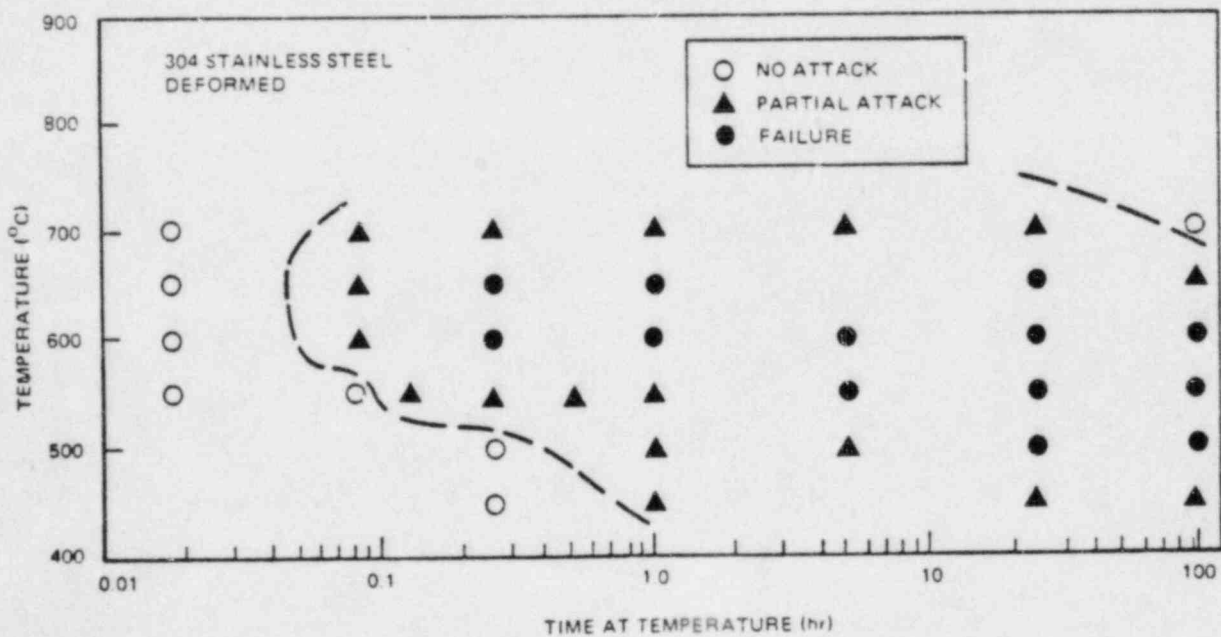
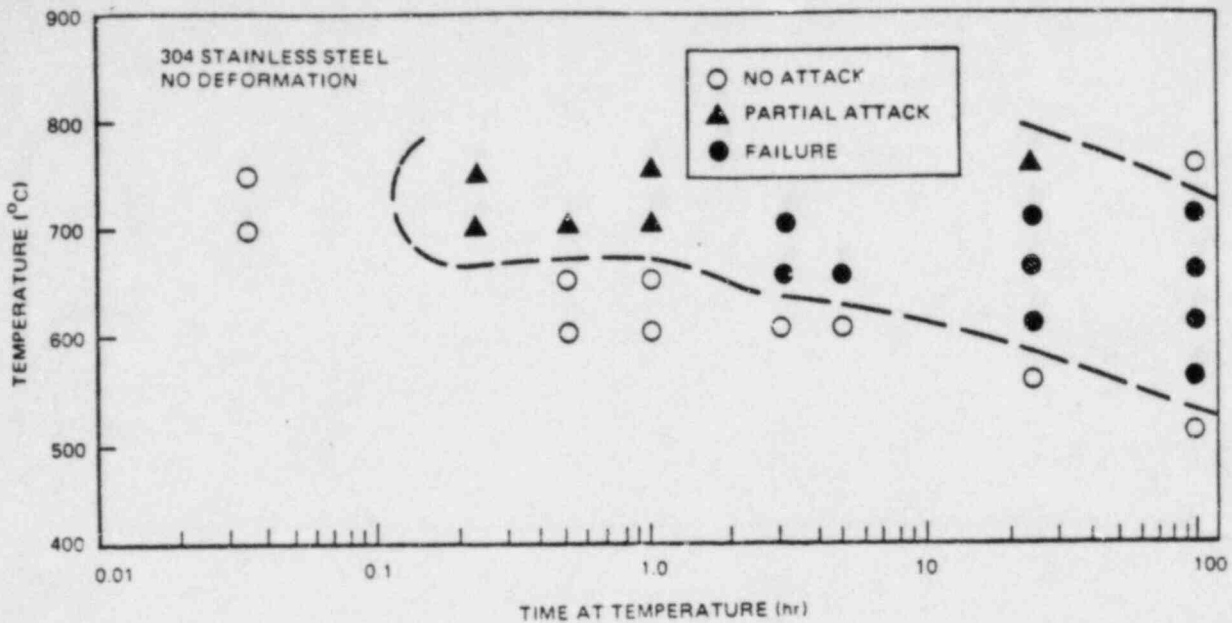


Figure 2-14. Modified Strauss Test Results for Deformed and Undeformed 304 Stainless Steel. (Each point corresponds with a time and temperature of heat treating. Each symbol denotes the response in the test. The dashed lines separate the time-temperature combinations which produce sensitization from those that do not.)

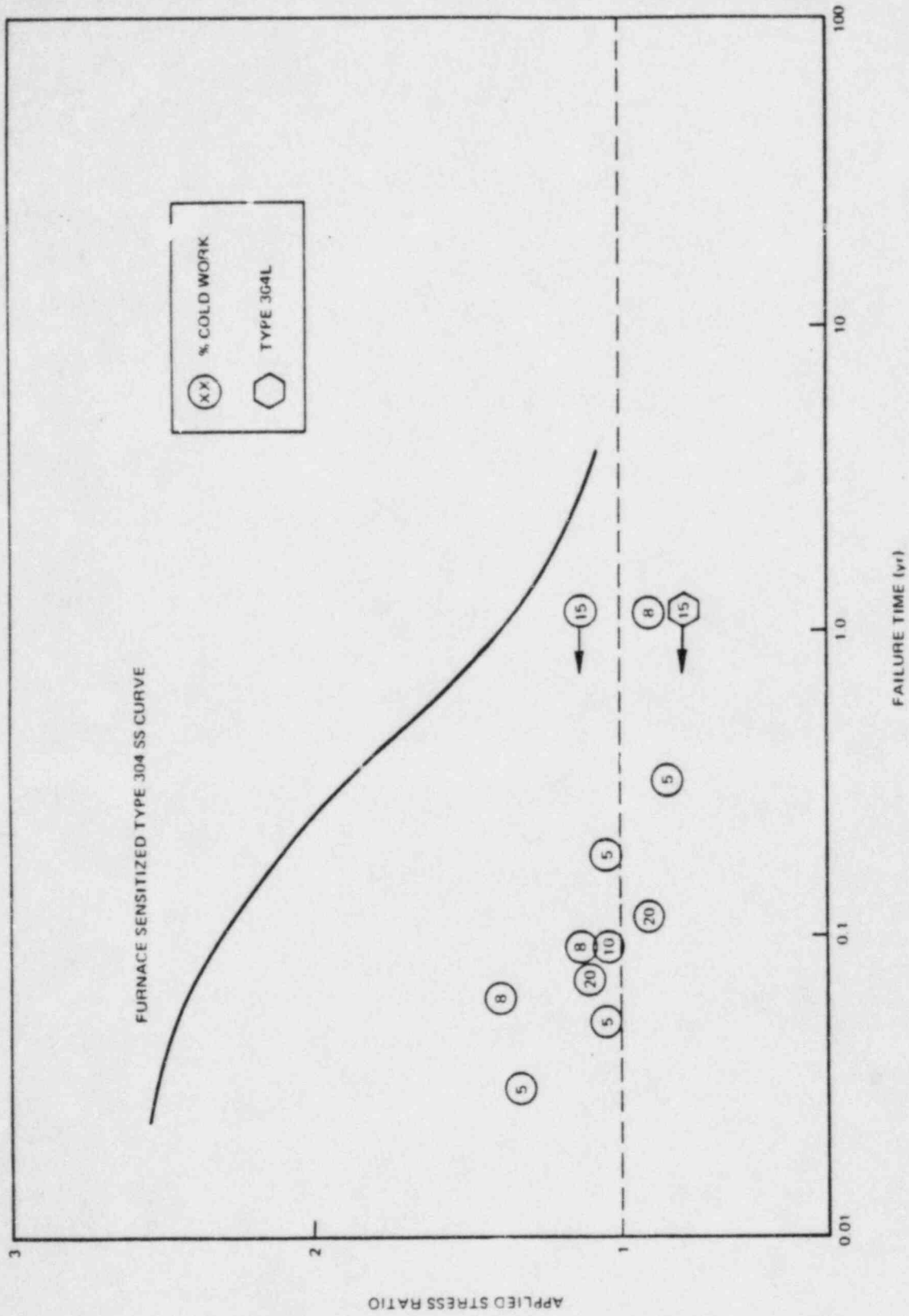


Figure 2-15. SCC of Cold Worked Plus Sensitized Type-304 Stainless Steel at 288°C



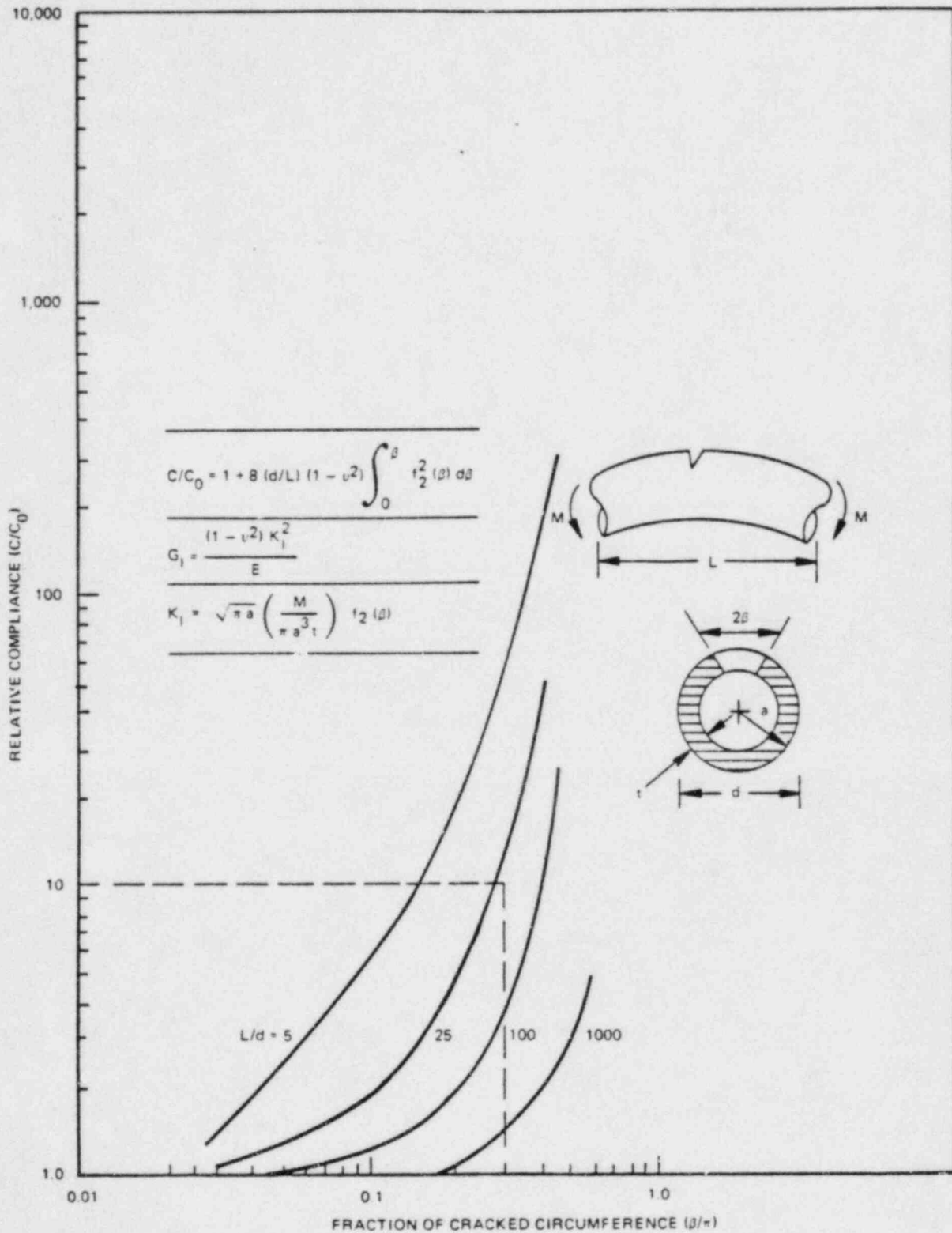


Figure 2-16. Compliance Change, Cracked Pipe

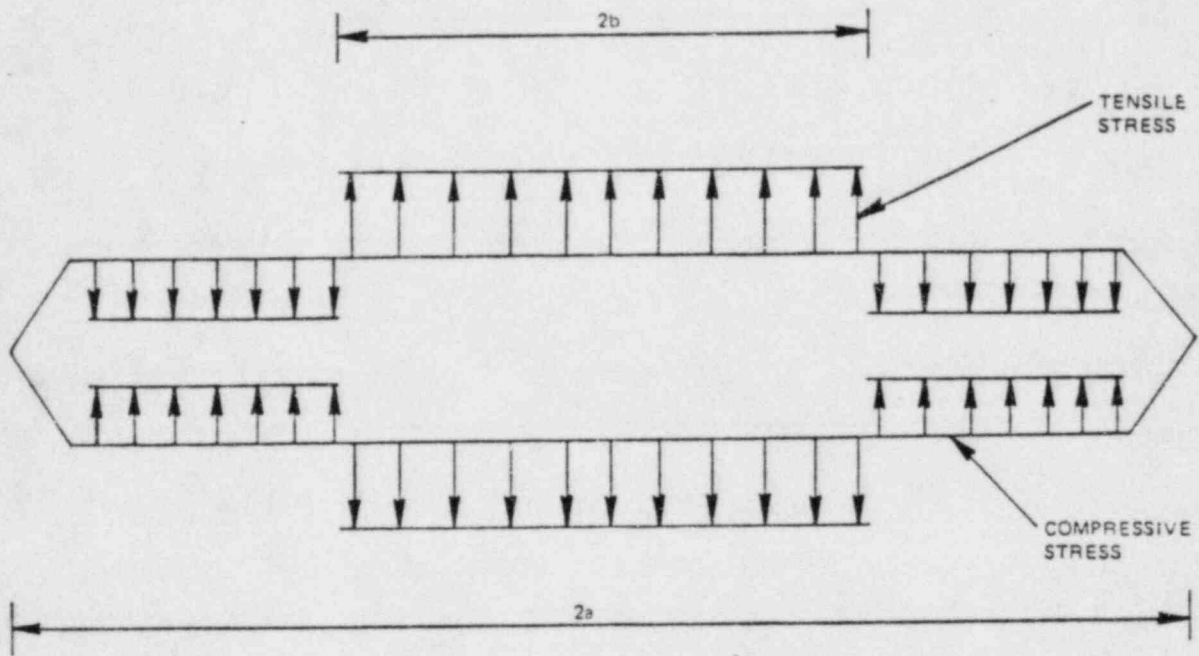


Figure 2-17. Assumed Stress Distribution on the Crack Face

### 3. LOST PARTS ANALYSIS

#### 3.1 INTRODUCTION

Based on the structural analysis given in Section 2, it is expected that the Hatch Unit 1 core spray sparger with the crack indication will not break and result in loose pieces in the reactor. Further, if the sparger is clamped loose parts are even more unlikely. However, an evaluation of the possible consequences of a potential loose piece is presented in this section.

#### 3.2 LOOSE PIECE DESCRIPTION

Since a piece has not been lost, it cannot be uniquely described. Three different types of loose pieces are postulated in Subsection 3.4.2: (1) a section of sparger pipe; (2) an outlet nozzle; and (3) a small piece of the sparger. The entire sparger is fabricated of Type-304 stainless steel.

#### 3.3 SAFETY CONCERN

The following safety concerns are addressed in this safety analysis:

1. Potential for corrosion or other chemical reaction to reactor materials.
2. Potential for fuel bundle flow blockage and subsequent fuel damage.
3. Potential for interference with control rod operation.
4. Potential for damage to other reactor internals.

#### 3.4 SAFETY EVALUATION

The above safety concerns for the postulated loose pieces are addressed in this section. The effect of these concerns on safe reactor operation is also addressed.

### 3.4.1 General Description

The core spray spargers are attached to the inside of the core shroud (Figure 3-1) in the upper plenum. For a piece of the sparger to reach and potentially block the inlet of a fuel assembly, it would have to be carried out of the upper plenum and pass down into the lower plenum. To accomplish this, it would have to be carried by the fluid flow in the upper plenum up through the steam separators then outward to the downcomer annulus, then through the jet pump nozzle into the lower plenum, then make a 180° turn and be carried upward to the fuel assembly inlet orifices. A part of the sparger cannot reach the fuel assembly inlet orifices by falling down inside the core shroud because the core support plate and the loaded core will prevent this. For a part of the core spray sparger to reach a control rod it must first traverse the upper plenum from the outer region of the shroud toward the center, then either fall through the restrictive passage between two fuel channels, or fall through an opening between the outside of the peripheral bundles and the core shroud, both of which are unlikely. (A conservative estimate of this probability is  $10^{-4}$  - see Subsection 3.5.2).

Since all parts of the core spray sparger are designed for in-reactor service, there is no possibility that any loose part will cause any corrosion or other chemical reaction with any reactor material.

### 3.4.2 Postulated Loose Pieces

#### 3.4.2.1 Sparger Pipe

The sparger pipe is 3-1/2-in. Schedule 40 pipe and is attached to the core shroud at seven locations (T-box plus six brackets). The maximum span between supports is about 62 inches. In order to generate a loose piece of pipe, a minimum of two throughwall cracks would have to propagate 360° around the sparger. The weight of the largest pipe segment would be approximately 80 lb. Because of the slow propagation rate of potential cracks, and based on previous experience with cracks in core spray spargers, it is judged that pieces will not break off and become loose. However, for purposes of

evaluating the probability for loose pieces potentially causing core damage, a conservative estimate of this probability has been chosen as  $10^{-3}$  (see Subsection 3.5).

A pipe segment could come to rest in any of three locations: (1) the top surface of the top guide outboard of the fuel assemblies; (2) the top surface of the fuel assembly; or (3) the bottom of the core bypass region on the core support plate. In all three of these locations, the flow velocity is low and insufficient to lift a segment of the pipe. The flow velocity in the upper plenum region is less than 4 ft/sec; in the bypass region near the core support plate it is less than 1 ft/sec (see Appendix B). Therefore, any piece will remain at one of these locations and is not expected to lift or rattle around. Further, an 80-lb piece of pipe which falls from the core spray sparger will not harm the core support plate, top guide or fuel assemblies, since these components are conservatively designed for much larger loads.

Since the pipe cannot be lifted by the flow and since the pipe cannot fit through either the steam separator or the jet pump, it will not cause any flow blockage at the fuel inlet orifice. Since the pipe is too large to fit between fuel channels, it will not cause any interference with control rod operations.

#### 3.4.2.2 Spray Nozzle

Each spray nozzle consists of two 1-in. elbows fabricated of Type-304 stainless steel, which are welded to the sparger. In order to generate a loose nozzle, a throughwall crack would have to propagate  $360^{\circ}$  around the nozzle. The weight of each nozzle assembly is approximately 1-3/4 lb. A loose nozzle would most likely come to rest on the top surface of the core support plate or on the top surface of the fuel top guide. The flow velocities in these regions are insufficient to lift the nozzle; thus, it will remain at one of the above mentioned locations.

Since the nozzle cannot be lifted by the flow and since the nozzle cannot fit through the steam separator, it will not cause any flow blockage at the fuel assembly inlet orifices. The nozzle is too large to fit between two fuel channels; thus, it cannot cause any control rod interferences.

### 3.4.2.3 Small Pieces

In order to generate small pieces of the sparger, both longitudinal and circumferential throughwall cracking must occur. A small piece could be lifted by the flow if it maintained an orientation with its maximum projected area perpendicular to the flow. Due to flow turbulence and nonsymmetry of the loose piece, the piece will tend to rotate so that the minimum projected area will be perpendicular to the flow. With this orientation and based on the velocities in the upper and lower plena, all parts in the upper plenum with a length of greater than approximately 0.4 in. and in the lower plenum with a length of greater than approximately 1.4 in. will sink (Reference 3-1). Thus, most pieces will not be carried by the flow toward the steam separator. However, in the unlikely event that a piece reaches the steam separator, it would have to pass through the steam separator turning vane (Figure 3-2). There are eight curved vanes with the outlet of each vane overlapping the inlet of the adjacent vane. The longest straight piece that can fit through the turning vane is approximately 6 inches long and it must be oriented with the long dimension in the vertical direction. The largest piece that can fit through the turning vane is shown in Figure 3-3 and is approximately 6 x 2 x 2 inches. The flow velocities are insufficient to carry this maximum sized piece through the turning vane.

After passing through the turning vane, the fluid momentum is further reduced as the water is removed. At the separator exit, the fluid is almost entirely steam. A typical water content is 1 weight %. Thus, it is very unlikely that any piece could be carried out of the separator by the steam. If any piece were carried through the separator by the steam, then it could be carried into the downcomer annulus, through the jet pump and enter the lower plenum. A piece that entered the lower plenum would probably be driven by the jet pump flow to the bottom of the reactor pressure vessel where it would be expected to remain. However, a small piece  $\leq 0.4$  in. could be carried by the flow up to the flow inlet orifices. The orifice size varies from approximately 1.25 to 2.22 inches in diameter.

It is extremely unlikely for a piece larger than the 1.25-in. orifice and essentially impossible for a piece larger than the 2.22 in. orifice to be

carried through the steam separator. The outside diameter of the sparger is 4 inches, while the fuel inlet orifices are slightly recessed relative to the surface of the control rod guide tubes (Figure 3-4), which have an outside diameter of 10-3/4 inches. Due to the different radii of curvature, flow would be able to enter the fuel assemblies. Thus, unacceptable flow blockage as defined by Reference 3-1 would require that more than one loose piece be carried to the same inlet orifice. This is based on the size of the piece(s) that, in a highly unlikely circumstance, have the potential of reaching the vessel lower plenum. The probability of unacceptable flow blockage of any fuel orifice is judged to be insignificant. (This requires multiple pieces at the same orifice. The probability of several pieces blocking a significant portion of the bundle inlet to cause significant fuel damage is judged to be essentially zero - see Table 3-1).

The flow velocities near the sparger are lower than those above the fuel assemblies. Thus, it is unlikely that a small piece would be carried over the fuel assemblies. If the piece were carried over the fuel assemblies and then rotated so that the flow could no longer carry it, the piece would fall on top of a fuel assembly or between fuel assemblies.

Figure 3-5 shows a typical unit cell of four fuel assemblies and one control rod. The control rod moves in the gap between the fuel channels. There is a possibility that a piece small enough to fit in the channel wall-control blade gap could sink and pass through the cavity between the control blade and the fuel support casting and migrate into the control rod guide tube. Should this happen the piece will most likely come to rest on top of the velocity limiter where it is expected to remain and move only with the movement of the velocity limiter as the control rod is inserted or withdrawn. If the piece is small enough to pass through the velocity limiter and the guide tube wall it will most likely sink and come to rest at the bottom of the guide tube. Due to the hardware geometry of the control blade drive mechanism it is highly unlikely that any piece would be small enough to migrate into the control blade drive system. Thus, any potential small piece which migrates to the control rod guide tube is not expected to pose any concern for potential interference with control rod operation.

A piece of precisely the right size could be in contact with the control rod and one or two fuel channels. Such a piece might be detected during the normal control rod exercising. The rods are inserted one notch and withdrawn one notch each week. It is also possible, though unlikely, that a piece might settle between two fuel channels above the control rod and thus not be detected by normal control rod operations. If the rod were to be inserted, the control rod mechanism has enough force to lift one fuel assembly. If the fuel assembly were lifted 1 or 2 inches, it would be able to move horizontally at both the bottom and the top, thus almost certainly relieving any interference caused by the piece. The rod would then insert and the fuel assembly would settle back into place. Thus, it is not credible that any control rod will fail to insert.

One of the licensing bases of the reactor is that the highest worth control rods can be fully stuck out and the reactor can be safely shut down. Thus unacceptable control rod interference would require multiple precisely sized pieces interfering simultaneously with control rods that are in close proximity to each other. The probability of this is judged to be insignificant (Subsection 3.5.2).

### 3.5 DISCUSSION OF PROBABILITY

This section provides the basis which supports the conclusions discussed above that the probability of loose parts from the core spray sparger causing a safety concern are negligible.

Based on operating history of BWRs with cracks in the core spray sparger in the last several years, and based on the structural evaluation of the core spray sparger cracks, no loose parts have been found, and the generation of a loose part is believed to be incredible, i.e., the probability to have a loose part of any size as the result of a crack is believed to be zero. However, for the purpose of this study, a bounding probability for having a loose piece break off of the sparger is assumed to be  $10^{-3}$ .



### 3.5.1 Fuel Bundle

For a core spray sparger loose piece to reach a fuel bundle and potentially cause some safety concerns it would have to be carried out of the upper plenum and pass through the downcomer, jet pumps, down into the lower plenum and then into the core region (either block a fuel bundle or interfere with the operation of the control rod). However, the probability for a piece to be carried out of the upper plenum, through the steam separator, and outward to the downcomer annulus is limited by the minimum projected area (perpendicular to the flow) that can be lifted by the fluid flow and the size of piece that can physically fit through the turning vane of the separator (Subsection 3.4.2.3). Likewise, if a piece were to have been carried to the lower plenum, the probability of a piece to potentially be carried to the core is also limited by the minimum projected area that can be lifted by the fluid flow in the lower plenum.

As discussed in Subsection 3.4.2.3, it is physically possible for a piece approximately 6 x 2 x 2 inches to fit through a separator; however, the fluid velocities in the upper plenum are not sufficient to carry this size piece out and hence it would remain there in the upper plenum. The maximum size piece that can be carried out of the upper plenum is limited to approximately 0.4 x 0.4 x 0.4 inches as discussed in Subsection 3.4.2.3. If this piece were to be carried to the lower plenum, which is unlikely, it could be lifted toward the core because the vertical fluid velocity in the lower plenum is high enough to lift this size piece. Therefore, pieces of this size or smaller are used to evaluate the potential of their reaching the core region from the lower plenum. Hence, the loose piece is conservatively assumed to be a small piece of 0.4 x 0.4 x 0.4 inch or less (the thickness of the core spray sparger pipe is only 0.23 inch). These pieces are based on the assumption that the part would tend to orient itself with the minimum dimension normal to the flow stream.

Figure 3-6 is a diagram of the path that a potential loose part from the sparger would follow if it were carried out of the upper plenum into the lower plenum and core. For each flow path a probability is assigned and the

cumulative probability is also shown (in brackets). As discussed above the probability for a part to break off in the upper plenum is conservatively estimated to be  $P_1 = 10^{-3}$ . Since it is postulated that a piece of this size is small enough to be carried by the upper plenum fluid velocity it is assumed that it will leave the upper plenum, i.e.,  $P_2 = 1.0$ . Once out of the upper plenum it is assumed that the piece travels with the liquid flow out of the separator and is carried down the downcomer, i.e.,  $P_3 = 1.0$ . There, the piece is likely to come to rest at the jet pump support plate at the bottom of the shroud and remain there ( $P_6$ ). However, because of the potential for the piece to be injected into the jet pump flow ( $P_4$ ), or to be sucked into the recirculation line ( $P_7$ ) and driven into the jet pump ( $P_8$ ), it is conservatively estimated that this probability is the sum of the probability for these flow paths, hence  $P_9 = P_8 + P_4 = 0.75 \times 10^{-3}$ . These probabilities, i.e.,  $P_4$  and  $P_7$ , are based on the projected flow areas and biased by the flow velocity ratios in the jet pumps and annulus downcomer for  $P_4$  and by the recirculation suction line and downcomer for  $P_7$ . Once in the jet pump it is assumed that the part will be carried by the flow stream toward the core, hence  $P_{10} = 1.0$ .

To enter the core region from the lower plenum, the part must first pass through the fuel bundle inlet orifices ( $P_{11}$ ) (there are three different sized bundle orifices). Once past the orifice, the part must pass through the lower tie plate ( $P_{12}$ ) and into the fuel bundle ( $P_{13}$ ).

The path from the lower plenum through a fuel bundle to the upper plenum is restricted by the following flow areas:

1. inlet orifices, sizes between 1.25 and 2.22 inches, flow area between 1.24 and 3.9 square inches;
2. lower fuel bundle tie plate, made up of 49 irregular-shaped holes with a total flow area approximately 11 square inches;
3. fuel bundle with 64 rods inside a square channel with a free flow area of approximately 15 square inches;

4. seven grid spacers along the bundle with a free flow area of approximately 13 square inches; and
5. upper tie plate similar to the lower tie plate.

For a part to enter a fuel bundle it would physically have to pass through the lower tie plate which would further limit its size to less than approximately 0.25 inch. A part of this size would either pass completely through the bundle, beginning the cycle over again, or be trapped within the fuel bundle possibly at one of the grid spacers. If it remained trapped at a spacer for a sufficiently long period of time there is a potential for fretting wear. Extensive fretting may ultimately lead to local fuel rod perforation and possibly some small release of fission products. This is not a safety problem because it is extremely unlikely and many such failures would be required to produce a significant offgas release. In addition, off-gas radiation monitors are designed to detect fission product release and limit off-site dose to within 10CFR100 limits.

For BWR fuel, the smallest and most restrictive flow path is at the fuel bundle inlet flow orifice. The percentage of blocked orifice area must be greater than 75% before a boiling transition condition would be approached for the most limiting, peak power fuel bundle (Reference 3-1). These bundles have the largest orifices. However, for a conservative estimate the potential for flow blockage for the smallest-sized orifice is evaluated. To block 75% of the area of the smallest orifice, at least five of the loose pieces must somehow migrate to the same fuel bundle inlet orifice. Five pieces that pass through the inlet orifices and remain trapped within the bundle would block considerably less flow area and hence would be less restrictive. It is extremely unlikely to have more than one loose piece, and the probability of more than one piece to migrate to the same fuel bundle is also negligible. However, for evaluating this potential it is assumed that the probability for one loose piece to enter a particular fuel bundle is the cumulative probability for a piece from the upper plenum to reach the lower plenum. We call this  $P$  and later it is set equal to the cumulative probability at  $P_{10}$ . There are 560 fuel bundles in the Hatch 1 core, each with inlet orifices. The probability of having  $n$  loose pieces is  $P_1^n$ . The probability of having  $n$  loose pieces from the lower plenum simultaneously, partially blocking one given fuel bundle is substantially lower. Therefore, the probability of  $n$  pieces at a given fuel bundle is

$$P_n = (1/560)^{n-1}, \text{ where } n > 1.$$

Therefore, the probability for blockage of given bundle is the product

$$P_{10}^n \cdot (1/560)^{n-1}$$

To block 75% of the minimum inlet orifices (which control the lowest powered fuel bundles) would require at least five small pieces somehow arriving and becoming wedged at the inlet orifice simultaneously. To estimate this probability, take  $n = 5$  in the above expression to block 75% of the smallest inlet orifice. As can be seen the probability of one piece entering the lower plenum is  $7.5 \times 10^{-4}$ . When this is used in the above expression for  $P_{10}$  and for 75% blockage  $n = 5$ , the resulting probabilities are incredibly small.

For BWR fuel, the inlet orifice can withstand nearly complete (>98%) flow blockage before severe fuel damage within one bundle will occur (Reference 3-1). This would require over 7 pieces simultaneously blocking the smallest orifice and would result in an incredibly small probability.

The probability for  $n$  pieces being carried from the upper plenum to the lower plenum and going to the same orifice is shown in Table 3-1.

Table 3-2 summarizes the estimated probabilities and the potential consequences related to fuel damage associated with a piece or number of pieces either entering a fuel bundle or potentially blocking a bundle. As shown in this table the potential consequences do not pose any safety concerns and further are of extremely low (incredible) probabilities.

### 3.5.2 Control Rod Mechanism

The probability of forming a small loose piece (small enough to fall down from the sparger to the bypass region) is assumed to be  $10^{-3}$  as previously discussed. Small pieces could be lifted by the flow velocities in the upper plenum and during a hot shutdown condition of the reactor could drop or fall back and possibly pass through the flow area from the upper plenum to the

bypass (approximately 18.5 ft<sup>2</sup> total). The total flow area in the upper plenum above the fuel bundles is approximately 182 ft<sup>2</sup>. Therefore the probability of such a piece (after being formed) to fall into the bypass region is 18.5/182  $\approx$  0.1. The total probability of the piece forming and reaching the bypass is  $0.1 \times 10^{-3} = 1 \times 10^{-4}$ .

As indicated in Section 3.4.2.3 multiple small pieces are required to cause unacceptable control rod interference. The probability of multiple pieces (i.e., n pieces) reaching a specific control rod guide tube is:

$$P(n) = (10^{-4})^n / (\text{no. guide tubes})^{n-1}.$$

$$\text{If } n = 2, P(2) = (10^{-4})^2 / 137 \approx 7 \times 10^{-11}.$$

Therefore the probability of multiple pieces reaching a guide tube (control rod drive) and causing unacceptable interference is negligible.

### 3.6 CONCLUSION

The core spray sparger at Hatch Unit 1 is expected to remain intact; therefore, it is highly unlikely that pieces of the sparger will break off. Nevertheless, from the above evaluation it is concluded that the probability for unacceptable corrosion or other chemical reaction due to loose pieces from the sparger is zero. The potential for unacceptable flow blockage or other damage to a fuel assembly is essentially zero. The potential for unacceptable control rod interference is essentially zero. Therefore, it is concluded that there is no safety concern posed by the lost parts issue.

### 3.7 REFERENCE

- 3-1. "Consequences of a Postulated Flow Blockage Incident in a Boiling Water Reactor," General Electric Company, October 1977 (NEDO-10174, Rev. 1).

Table 3-1  
PROBABILITY OF FUEL BUNDLE BLOCKAGE

$n$	$(1/560)^{n-1}$	$P_n$
2	$2 \times 10^{-3}$	$1 \times 10^{-9}$
3	$3 \times 10^{-6}$	$1 \times 10^{-15}$
>3	$<10^{-8}$	$<<10^{-15}$

$n$  = Total number of pieces generated

$P_n$  = Probability that there is at least one orifice which is blocked by two or more pieces up to a total of  $n$

Table 3-2

SUMMARY OF RESULTS OF THE PROBABILITY STUDY OF FUEL  
BUNDLE FLOW BLOCKAGE

<u>No. Pieces or Percent Flow Blockage</u>	<u>Probability</u>	<u>Consequences</u>
1 piece	$7.5 \times 10^{-4}$	May become trapped within a bundle and after extended period could lead to local fuel rod perforation and subsequent fission product release in RPV
<5 pieces	$<10^{-15}$	Same as above
5 pieces 75% blockage	$<<10^{-15}$	Same as above with possibility of local boiling transition and several perforated rods.
7 pieces 98% blockage	$<<<10^{-15}$	Same as above with possibility of local fuel melting within one bundle

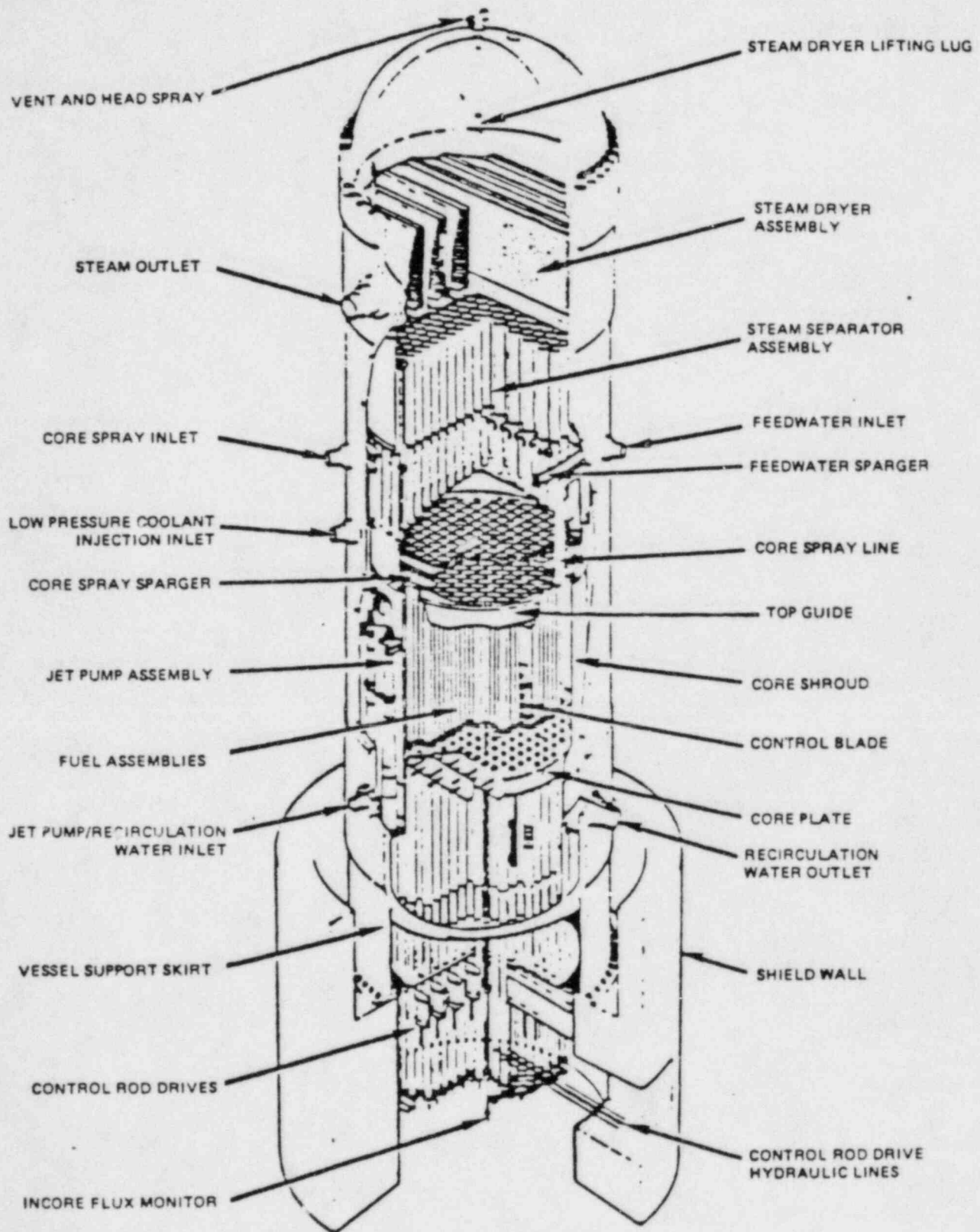


Figure 3-1. Reactor Vessel



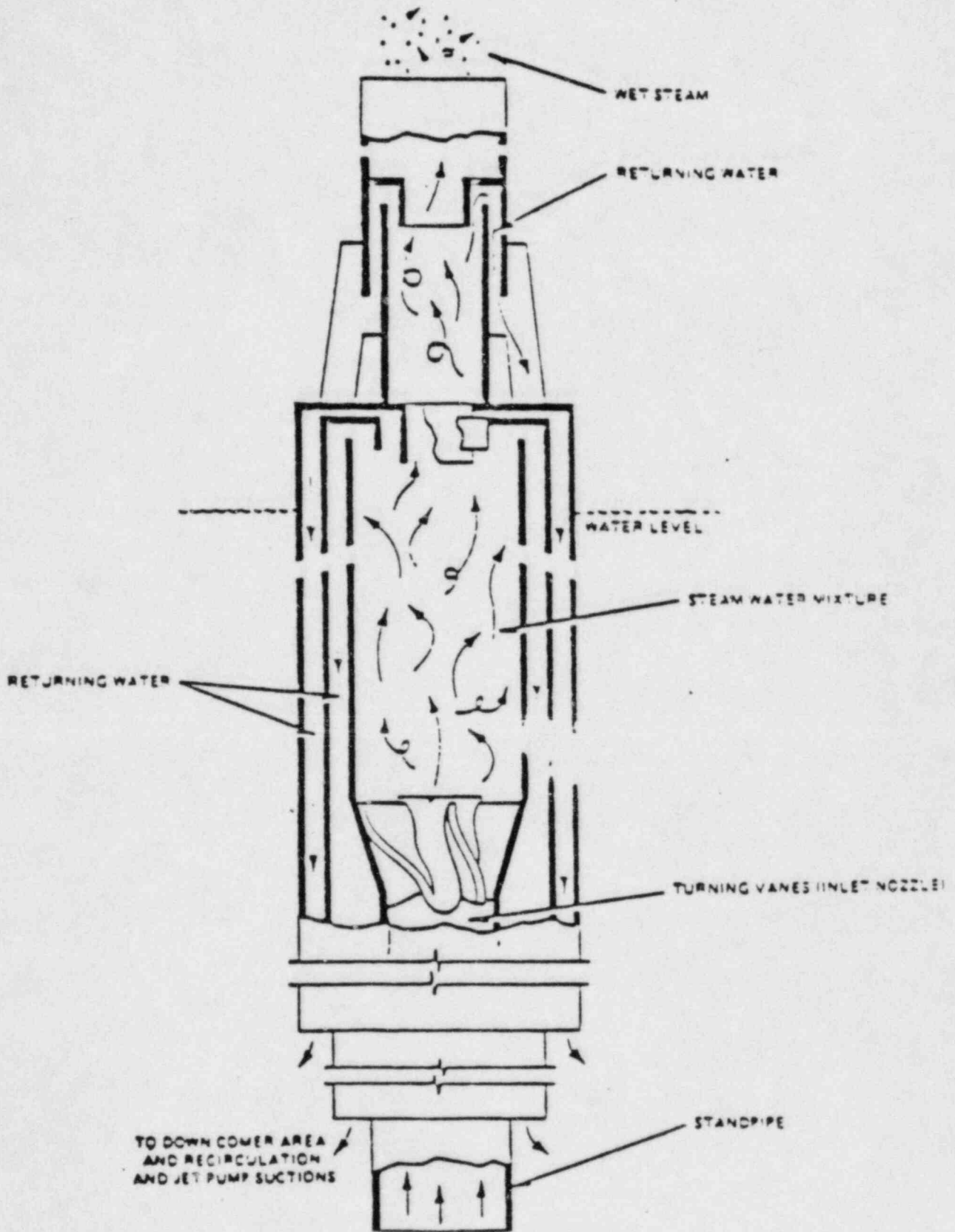


Figure 3-2. Steam Separator

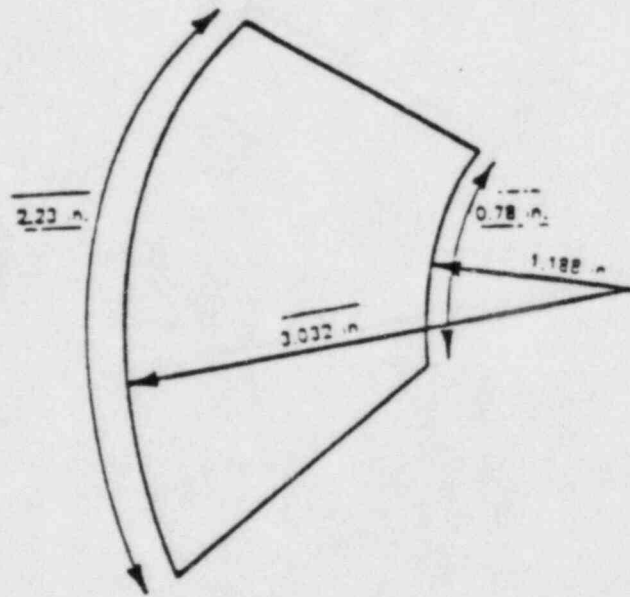


Figure 3-3. Largest Piece That Can Fit Through the Turning Vane (End View)

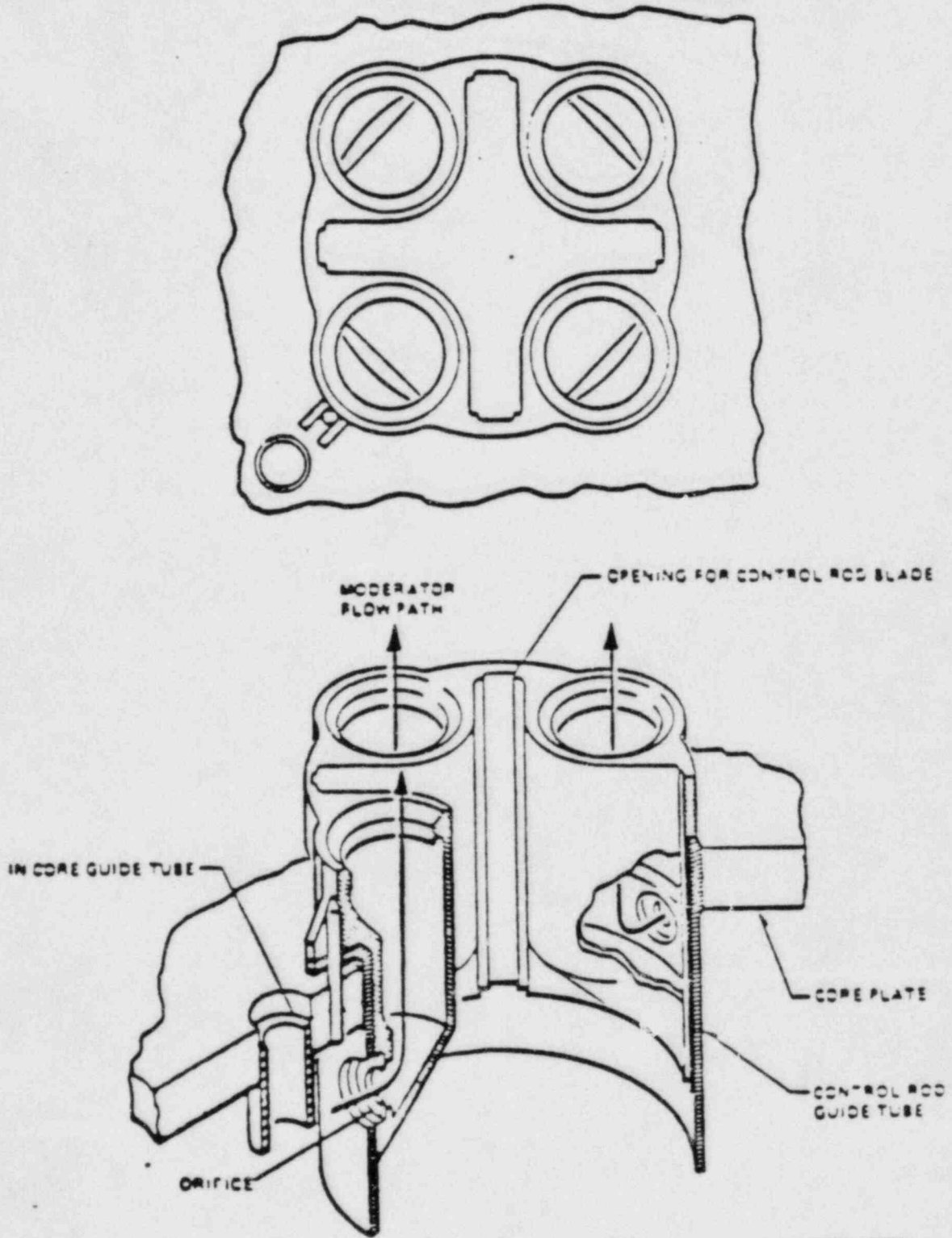
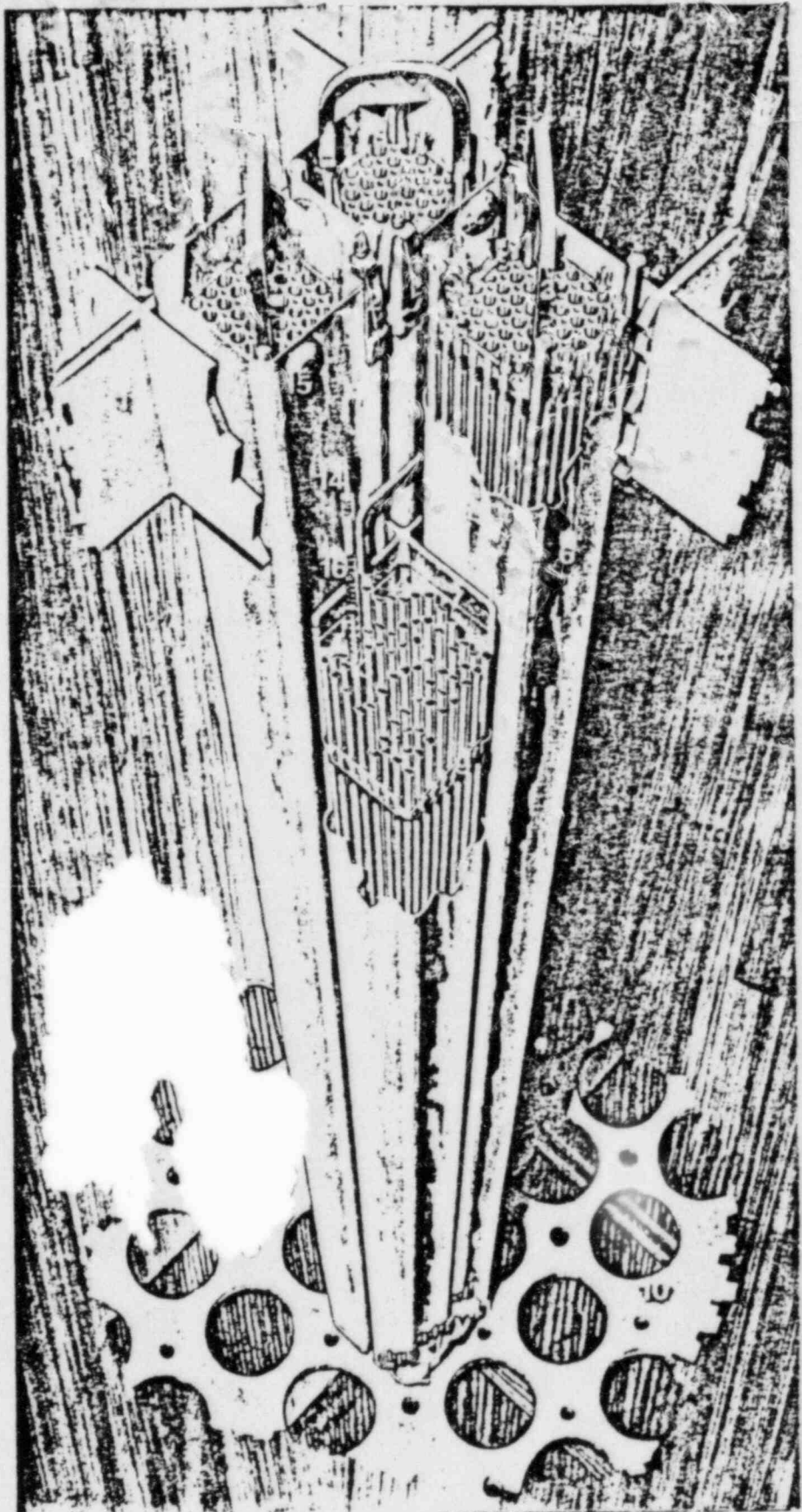


Figure 3-4. Orificed Fuel Support

# FUEL ASSEMBLIES & CONTROL ROD MODULE

- 1.TOP FUEL GUIDE
- 2.CHANNEL FASTENER
- 3.UPPER TIE PLATE
- 4.EXPANSION SPRING
- 5.LOCKING TAB
- 6.CHANNEL
- 7.CONTROL ROD
- 8.FUEL ROD
- 9.SPACER
- 10.CORE PLATE ASSEMBLY
- 11.LOWER TIE PLATE
- 12.FUEL SUPPORT PIECE
- 13.FUEL PELLETS
- 14.END PLUG
- 15.CHANNEL SPACER
- 16.PLENUM SPRING



GENERAL  ELECTRIC

Figure 3-5. Fuel Assemblies and Control Rod Module

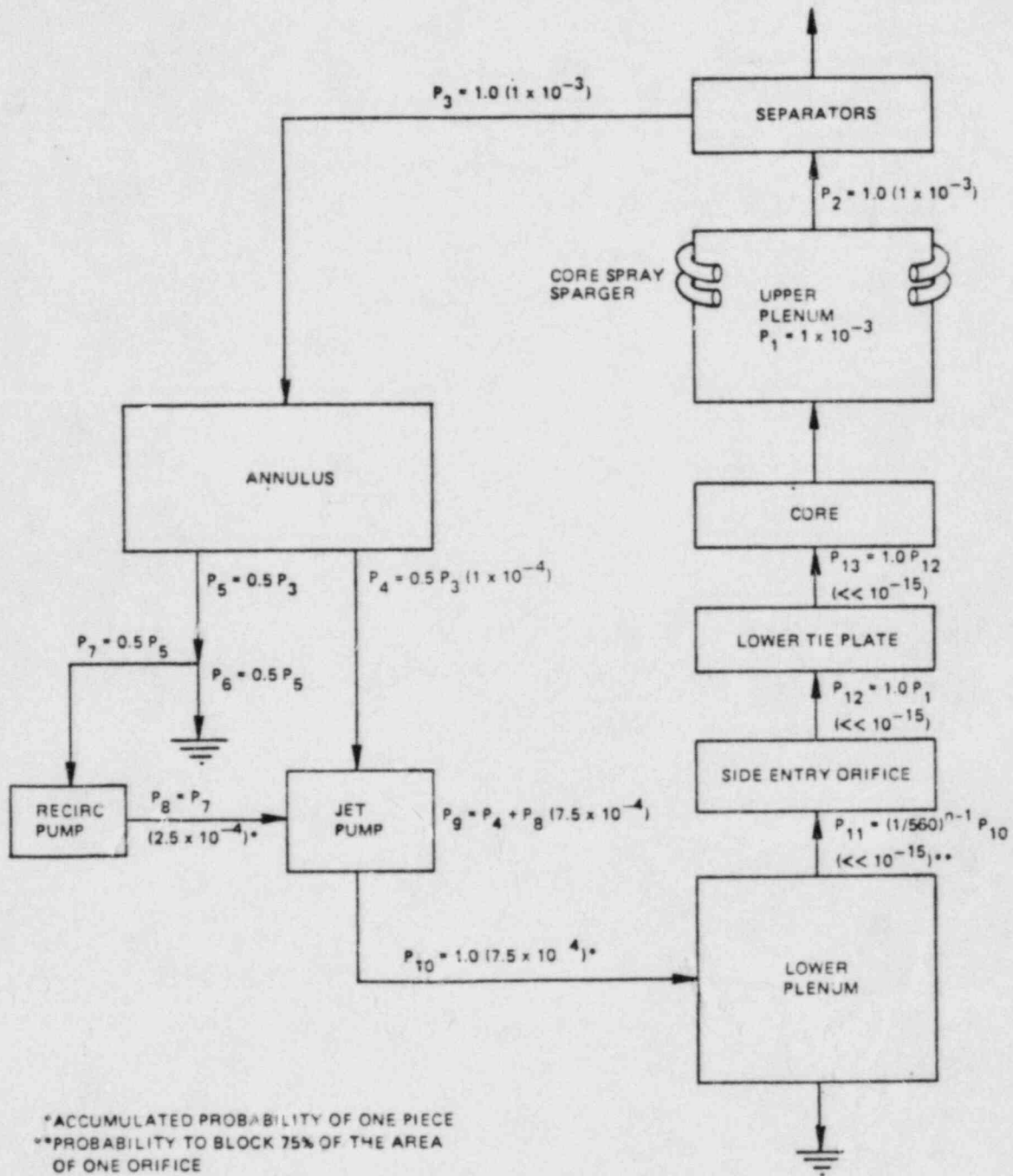


Figure 3-6. Loose Piece Potential Upward Flow Path

#### 4. LOSS-OF-COOLANT ACCIDENT ANALYSIS WITH A CRACK IN ONE CORE SPRAY SPARGER

##### 4.1 INTRODUCTION

A crack indication has been found in the core spray sparger at the Hatch Unit 1 plant, located in the lower sparger. The structural integrity of the sparger is not degraded by the crack as shown in Section 2. The intended cooling function of the spray system is not adversely affected by the presence of the crack for the reasons given below. Therefore, no change in Emergency Core Cooling System (ECCS) performance analysis or Maximum Average Planar Linear Heat Generation Rate (MAPLHGR) limits is required.

This section describes the methods used to evaluate the MAPLHGR requirements to meet 10CFR50.46 for the Hatch Unit 1 operating cycle 8 with an assumed crack in the core spray sparger. The potential effect of spray distribution on the choice of the limiting break size and single failure that must be analyzed is discussed in Section 4.2. The phenomena involved and the inputs to the approved 10CFR50 Appendix K computer codes are discussed in Section 4.3, the results of analyses performed are given in Section 4.4, and the conclusions are presented in Section 4.5.

##### 4.2 LIMITING BREAK SIZE AND SINGLE FAILURE ANALYSIS

For the Hatch Unit 1 plant, there are no single failures for any break location (other than a core spray line break) that can result in less than one core spray system injecting water into the upper plenum above the reactor core. For a core spray line break, there are always at least three low pressure ECCS pumps injecting water into the reactor vessel, thereby ensuring that this break is not a limiting event. For medium and large break sizes (which depressurize relatively quickly), the most limiting failures are those that result in the least number of ECCS pumps remaining operable (i.e., injecting water into the reactor vessel).

Independent of the core spray heat transfer, the only two single failure candidates that are potentially limiting for medium to large recirculation pipe break sizes are:

- A. Diesel Generator Failure: 1 core spray (LPCS) + 1 Low Pressure Coolant Injection (LPCI) + HPCI + the ADS operable;
- B. LPCI Injection Valve Failure: 2 core spray (LPCS) + HPCI + the ADS operable.

Since the High Pressure Coolant Injection (HPCI) is steam turbine powered, it is not a significant contributor to mitigating medium to large breaks which depressurize rapidly. Also, since the function of the Automatic Depressurization System (ADS) is to depressurize the reactor as a backup to the HPCI, it contributes little toward mitigating medium and large break LOCAs. Therefore, failure candidates A and B are limiting and each result in a dependence on only two ECCS pumps.

The plant specific LOCA analysis based on the SAFE and REFLOOD codes (Reference 4-3), indicates that failure candidate B (LPCI Injection valve failure) is limiting by a large margin because of the conservative modeling of counter current flow limiting (CCFL) at the fuel assembly upper tie plates. The calculation limits the coolant delivery or downflow from the core spray systems to the fuel bundles and further delays core reflooding by neglecting the water held back in the upper plenum.

Both single failure candidates (A and B) were re-examined for large breaks to determine whether there would be a change in the limiting break. The limiting single failure, break size, and location were found not to change. This is because the calculated core uncover and recovery times and the reactor depressurization rates are insensitive to changes in spray cooling heat transfer due to the conservative treatment of CCFL (see Section 4.3).

For smaller break sizes, the limiting single failure is the high pressure ECCS (HPCI) since the transient is a relatively slow depressurization event that is dominated by the time required to either reflood the reactor with the high

pressure system or the time to depressurize the reactor so that the low pressure systems become effective. Furthermore, the effects of CCFL in limiting coolant delivery to the core are not as large at higher reactor pressures. The small break LOCA transient is, therefore, insensitive to spray distribution because reflooding occurs very rapidly once any one or two of the six low pressure ECCS pumps begin injecting coolant into the reactor vessel.

Therefore, only medium and large break LOCA calculations have any potential for dependence on spray distribution, and detailed LOCA calculations need only be performed for large limiting break sizes with the current limiting single failure.

#### 4.3 PHENOMENA INVOLVED IN THE ANALYSIS OF SPARGER PERFORMANCE

The key phenomena involved in evaluating core cooling performance resulting from the injection of spray through the core spray sparger in the BWR are listed in Table 4-1. The analytical assumptions regarding these phenomena which are important to understanding system performance and the predicted core cooling are also tabulated.

The models used in the standard reload analysis include these phenomena, but the input assumptions that are used in these analyses (SAFE and REFLOOD codes) are overly conservative. The extent of this conservatism is evident from Table 4-1 in light of the realistic phenomena observed and tabulated. The bases for the first three of these realistic inputs are derived from recently completed, jointly sponsored, large scale BWR safety research programs between NRC, EPRI and GE (Reference 4-1). It should be noted that these phenomena are realistically modeled in the newly NRC approved BWR LOCA/ECCS model, SAFER (Reference 4-4).

The relevant phenomena do not depend on the distribution of the injected spray through the nozzles but on the injection of coolant into the upper plenum (Reference 4-1). The NRC staff has evaluated the issues related to the adequacy of the core spray systems in the BWR and their ability to distribute spray water to the core (Reference 4-2). This evaluation was in response to



Concerns that the core spray systems may not distribute any spray to certain regions of the core when injected into an upper plenum steam environment. The staff testimony (Reference 4-2) concluded that the spray distribution adequacy is not a safety concern because the coolant injected into the upper plenum will either disperse uniformly in a pool of water above the core or will flow to the lower plenum producing rapid reflooding. Therefore, the current reload calculations using the plant specific LOCA analysis basis is applicable and conservative despite the presence of any crack(s) in the core spray sparger.

#### 4.4 ANALYSIS RESULTS

The current reload analysis for the limiting LOCA with the most limiting fuel type and exposure combination results in a calculated PCT of approximately 2200°F.

Figure 4-1 shows the heat transfer assumed as a function of time (Curve 1) compared with the realistic heat transfer (Curve 2). A bounding calculation (Curve 3) of the limiting LOCA with approved Appendix K reload models but with CCFL breakdown input based on observed large scale tests, and no convective core cooling prior to reflooding, results in a maximum PCT of less than 1380°F at a MAPLHGR of 12.1 KW/ft. This result demonstrates that the current reload calculation is conservative by more than 820°F. No credit for steam cooling or the improved decay heat correlation which would further reduce the PCT are included in this calculation.

A comparison of the current reload analysis with the conservatively calculated PCT using CCFL breakdown is shown in Curve 4 at the bottom of Figure 4-1. It is clear from this figure that the overly conservative treatment of CCFL results in the unrealistically slow core reflooding time and high calculated PCT in the reload analysis.

## 4.5 CONCLUSIONS

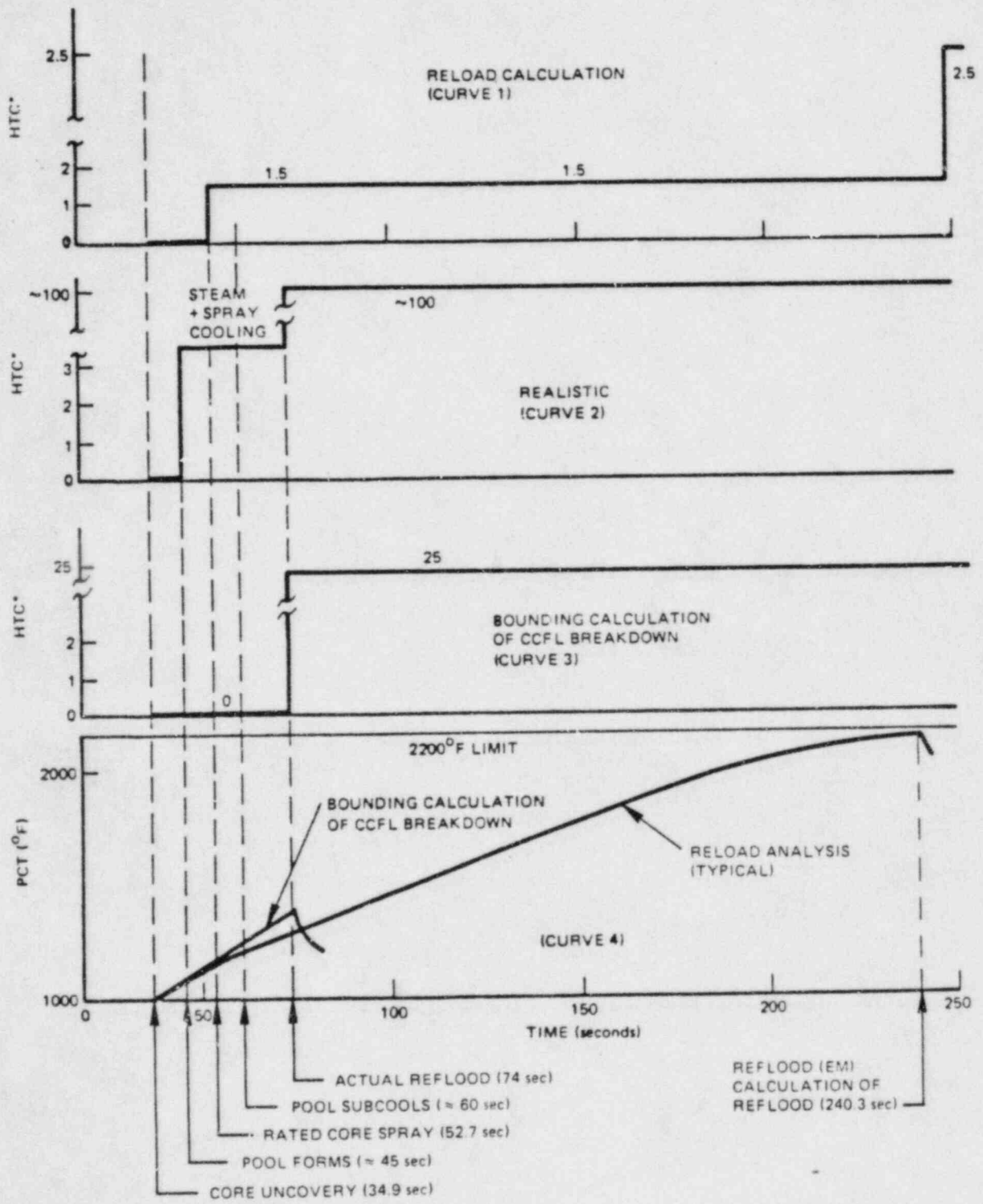
An analysis utilizing the approved Appendix K reload evaluation models has been performed for Hatch Unit 1 to bound the effects of a potential crack in the core spray sparger. The results of this analysis demonstrate that with CCFL breakdown (derived from a conservative interpretation of recent large scale tests) the calculated PCT is at least 820°F less than the current reload calculation. Without CCFL breakdown the upper plenum inventory (pool of water) ensures adequate coolant delivery to the core. Therefore, the current reload (or any subsequent reload) calculation is applicable and conservative.

## 4.6 REFERENCES

- 4-1. BWR Refill-Reflood Program Final Report, L.L. Myers, General Electric Co., NUREG/CR-3223, EPRI NP-3093, GEAP-30257, July 1983.
- 4-2. Transcript of Testimony before the Atomic Safety and Licensing Board For Long Island Lighting Co., May 28, 1982 - Docket No. 50-322-OL. NRC Staff Testimony of Summer B. Sun on ECCS Core Spray.
- 4-3. "Loss-of-Coolant Accident Analysis Report for Edwin I. Hatch Nuclear Plant Unit 1", NEDO-24086, December 1977.
- 4-4. Safety Evaluation Report for SAFER/GESTR-LOCA, C. O. Thomas (NRC) to J. F. Quirk (GE), June 1, 1984.

Table 4-1  
KEY PHENOMENA RELATED TO CORE SPRAY COOLING PERFORMANCE

Phenomena	Analytical Assumptions Used in the Current Reload Analysis	Realistic Assumptions
Upper Plenum Inventory	Conservatively assumed to not interact or contribute to core reflood during LOCA transient	Pool of water present throughout transient assures coolant delivery to all fuel bundles (supported by Large Scale Tests)
Counter Current Flow Limiting	Saturated water in upper plenum above core	Some subcooling and less CCFL occurs. A residual pool of water remains during and after core reflooding. (supported by Large Scale Tests)
	No CCFL breakdown	Breakdown of CCFL shortly after spray initiation causes rapid reflooding (supported by Large Scale Tests)
Core heat transfer	Limited spray cooling after blowdown (Appendix K credit only)	Steam cooling contribution as much as 10 times greater than Appendix K spray cooling
Decay Heat	1971 ANS + 20% specified by Appendix K	1979 ANS (GE has submitted a technical basis as a part of the Standard Plant docket which is based on the 1979 ANS decay heat correlation)



\*HTC = HEAT TRANSFER COEFFICIENT (Btu/hr-sq ft °F)

Figure 4-1. Hatch Unit 1 DBA (Limiting LOCA) Analysis

Appendix A

STRUCTURAL ANALYSIS OF THE HATCH UNIT 1 CORE SPRAY SPARGER

SUMMARY

This appendix contains structural analyses that support Sections 2.5.3, 2.5.4, 2.6, 2.7 and 2.8 of this report.

Section A.1 contains the calculation of loads during normal plant operation and during the core spray injection event for input into Section A.2, A.3 and A.4 of this Appendix.

Section A.2 contains flow-induced vibration and natural frequency calculations that show that flow-induced vibration is not a problem for the intact sparger condition and for an assumed broken sparger condition.

Section A.3 contains the structural analysis of the core spray sparger in an intact condition. The stresses were found to be low during all identified loading conditions.

Section A.4 contains the structural analysis of the core spray sparger which conservatively assumes a 360° throughwall crack in the longer sparger arm at the T-box. The analysis ignores the effect of a clamp (or assumes no clamp is installed).

The stresses were found to be low during all identified loading conditions.

Section A.5 contains heat transfer calculations to determine the maximum (bounding) temperature differential between the sparger pipe arms and the shroud wall.

Because the calculated stresses were well below the allowables, it was deemed unnecessary to calculate principle stresses and stress intensities. The material properties are given below for comparison purposes.

- Material - 304 SS
- Temperature - 550°F
- Material Properties (ASME Section III)

$$S_m = 16.9 \text{ ksi (upset allowable)}$$

$$S_y = 18.8 \text{ ksi}$$

$$S_u = 57.3 \text{ ksi}$$

$$E = 25.75 \times 10^6 \text{ lb/in.}^2$$

The structural analysis results of the intact sparger and the broken sparger are summarized below.

SUMMARY OF STRESSES FOR INTACT SPARGER

	Seismic Bending Stress (lb/in. <sup>2</sup> )	Impingement Bending Stress (lb/in. <sup>2</sup> )	Thermal Mismatch Normal Stress (lb/in. <sup>2</sup> )
Sparger Pipe	476	174	3319
	Normal Stress (lb/in. <sup>2</sup> )	Shear Stress (lb/in. <sup>2</sup> )	
Nozzle (Weld)	369	101	
Lower Bracket (Plate)	3845	954	
Lower Bracket (Weld)	3067	617	
Middle Bracket (Plate)	1422	31 (avg)	
Middle Bracket (Weld)	654	44 (avg)	

SUMMARY OF STRESSES FOR BROKEN SPARGER

	Seismic Bending Stress (lb/in. <sup>2</sup> )	Impingement Bending Stress (lb/in. <sup>2</sup> )	Thermal Mismatch Normal Stress (lb/in. <sup>2</sup> )
Sparger Pipe	2380	868	3316

	Normal Stress (lb/in. <sup>2</sup> )	Shear Stress (lb/in. <sup>2</sup> )
Nozzle (Weld)	4267	4396
Lower Bracket (Plate)	3031	752
Lower Bracket (Weld)	5974	534
Middle Bracket (Plate)	5210	158 (avg)
Middle Bracket (Weld)	1800	224 (avg)

A.1 DESIGN LOADS

This section contains the calculation of loads on the core spray sparger during normal plant operation and during the core spray injection event. The loads are used in Section A.2 for natural frequency calculations and in Sections A.3 and A.4 for calculating stresses in the intact sparger condition and the assumed broken sparger condition respectively.

A.1.1 Weight of Sparger

3 1/2" sch. 40 pipe

$$\begin{aligned}
 W_{\text{pipe}} &= \frac{\pi}{4} (d_o^2 - d_i^2) \rho_{\text{stainless steel}} \quad \rho_{\text{ss}} = 488 \text{ lb/ft}^3 \\
 &= \frac{\pi}{4} \left( \left( \frac{4.0}{12} \right)^2 - \left( \frac{3.548}{12} \right)^2 \right) (488) = 9.1 \text{ lb/ft}
 \end{aligned}$$

$$W_{\text{water}} = \frac{\pi}{4} \left( \frac{3.548}{12} \right)^2 62.2 = 4.3 \text{ lb/ft}$$

$$W_{\text{nozzles}} = 3 \text{ lb/ft}$$

$$W = 9.1 + 4.3 + 3 = 16.4 \text{ lb/ft}$$

$$= \frac{16.4}{12} = \underline{1.37} \text{ lb/in.}$$

A.1.2 Impingement Loads (90° Deflection of Flow)

$$F = PA = \frac{\rho V^2 DL}{g}$$

$$\frac{F}{L} = \frac{\rho V^2 D}{g}$$

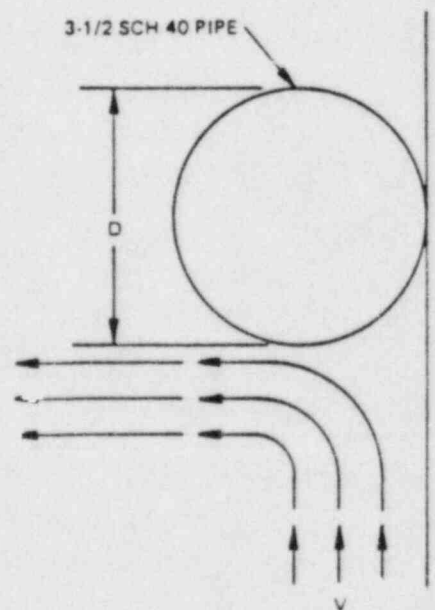
$$\rho = 45.87 \text{ lb/ft}^3 \text{ @ } 550^\circ\text{F}$$

$$D = \frac{4.0}{12} \text{ ft} \quad V = 5 \text{ ft/sec}$$

(conservative value -  
more realistic value  
is ~3.5 ft/sec)

$$\frac{F}{L} = \frac{45.87 (5)^2 (4.0/12)}{32.2}$$

$$\frac{F}{L} = 11.87 \text{ lb/ft} = \underline{1.0} \text{ lb/in.}$$



A.1.3 Impingement and Seismic Load

Impingement Only

$$W_i = -1.0 \text{ lb/in. (upward)}$$

(Sect A.1.1)

Seismic Only - Assume 1g (conservative)

$$W_s = W \pm (1.0) W \quad W = 1.37 \text{ lb/in.}$$

(Sect A.1.2)

$$W_s = 1.37 - 1(1.37) = \underline{0} \text{ lb/in. (upward)}$$

$$W_s = 1.37 + 1(1.37) = \underline{2.74} \text{ lb/in. (downward)}$$



Impingement & Seismic

$$W_T = -1.0 - 0.0 = \underline{-1.0} \text{ lb/in. (upward)}$$

$$W_T = -1.0 + 2.24 = \underline{1.74} \text{ lb/in. (downward)}$$

Seismic loading (absolute value) is more severe than seismic plus impingement loading.

A.1.4 Pressure/Flow Loads

Maximum Flow = 6000 gpm (Rated Flow = 4625 gpm) (Section A.5.3)

$$Q = 6000 \text{ gal/min} \times \frac{1 \text{ min}}{60 \text{ sec}} \times \frac{\text{ft}^3}{7.48 \text{ gal.}}$$

$$= 13.37 \text{ ft}^3/\text{sec}$$

- Maximum pressure in sparger arm

$$\Delta P_{\text{measured}} = 28 \text{ psig @ 4491 gpm}$$

$$\Delta P_{\text{max}} = 28 \left( \frac{6000}{4491} \right)^2 = \underline{50.0} \text{ psig}$$

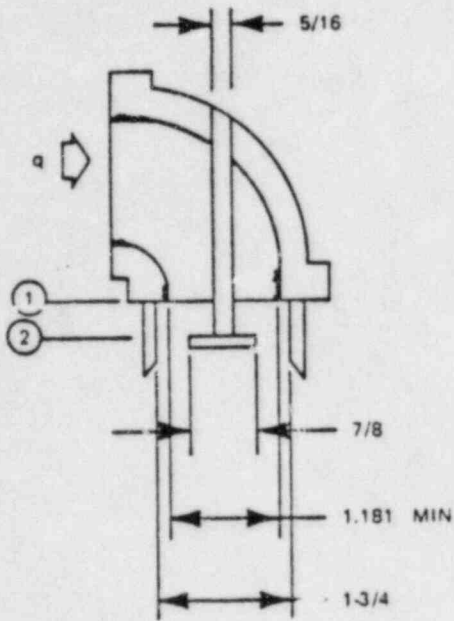
- Pressure load on sparger segment

$$F = \Delta P A \quad A = \frac{\pi}{4} d_i^2 = \frac{\pi}{4} (3.548)^2 = 9.89 \text{ in.}^2$$

$$F_{\text{max}} = 50.0 (9.89) = \underline{495 \text{ lb}}$$

- Maximum nozzle flow

The one inch VNC nozzle has the highest flow and will produce the greatest nozzle thrust.



$$A_1 = \frac{\pi}{4} (1.181^2 - 0.313^2) = 1.018 \text{ in.}^2 \text{ (min.)}$$

$$A_2 = \frac{\pi}{4} (1.75 - 0.875^2) = 1.804 \text{ in.}^2$$

$$\rho = 62.2 \text{ lb/ft}^3 @ 80^\circ\text{F}$$

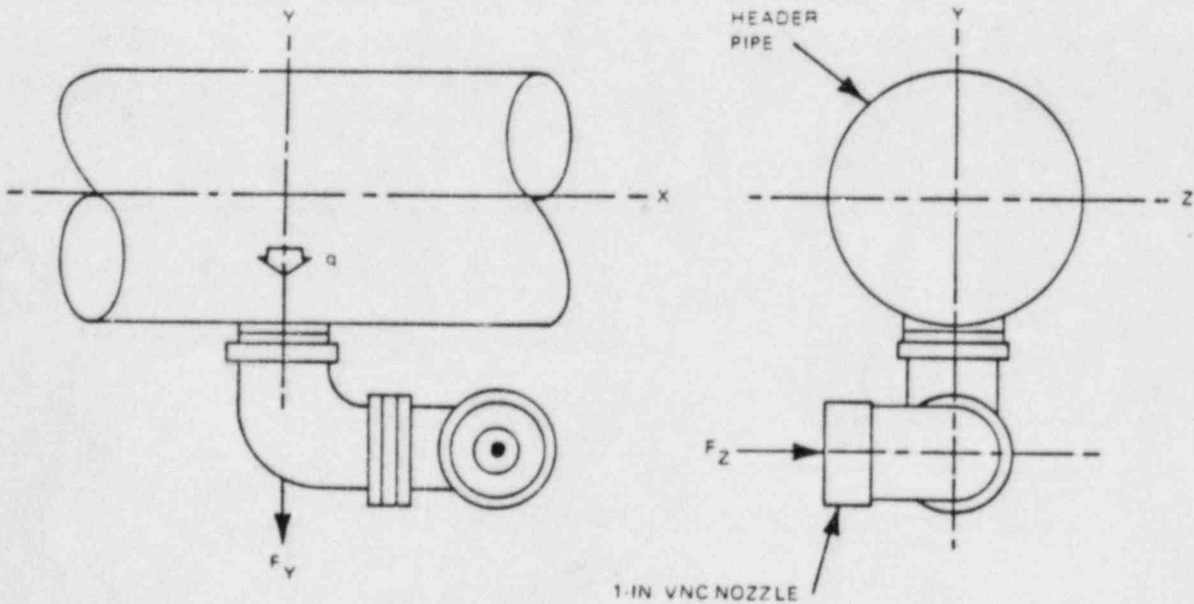
$$q_{\text{max}} = 64 \text{ gpm @ } 4491 \text{ gpm}$$

$$q_{\text{max}} = 64 \left( \frac{6000}{4491} \right) = 85.5 \text{ gpm}$$

$$W_{\text{max}} = \frac{85.5(62.2)}{60(7.48)} = 11.85 \text{ lb/sec}$$

$$V_{\text{max}} = \frac{W_{\text{max}}}{\rho A} = \frac{11.85(144)}{62.2(1.018)} = \underline{26.95} \text{ ft/sec @ exit from nozzle}$$

A.1.5 Nozzle Thrust Loads



$$F_y = \Delta P A + \frac{\rho V^2 A}{g}$$

$$\Delta P = 28 \text{ @ } 4491 \text{ gpm test flow}$$

$$\Delta P = 28 (6000/4491)^2 = 50.0 \text{ psi @ mount}$$

$$A = \frac{\pi}{4} d^2$$

where

$$d = 1.181 \text{ in (minor diameter of 1" straight internal threads)}$$

$$A = \frac{\pi}{4} (1.181)^2 = 1.095 \text{ in}^2$$

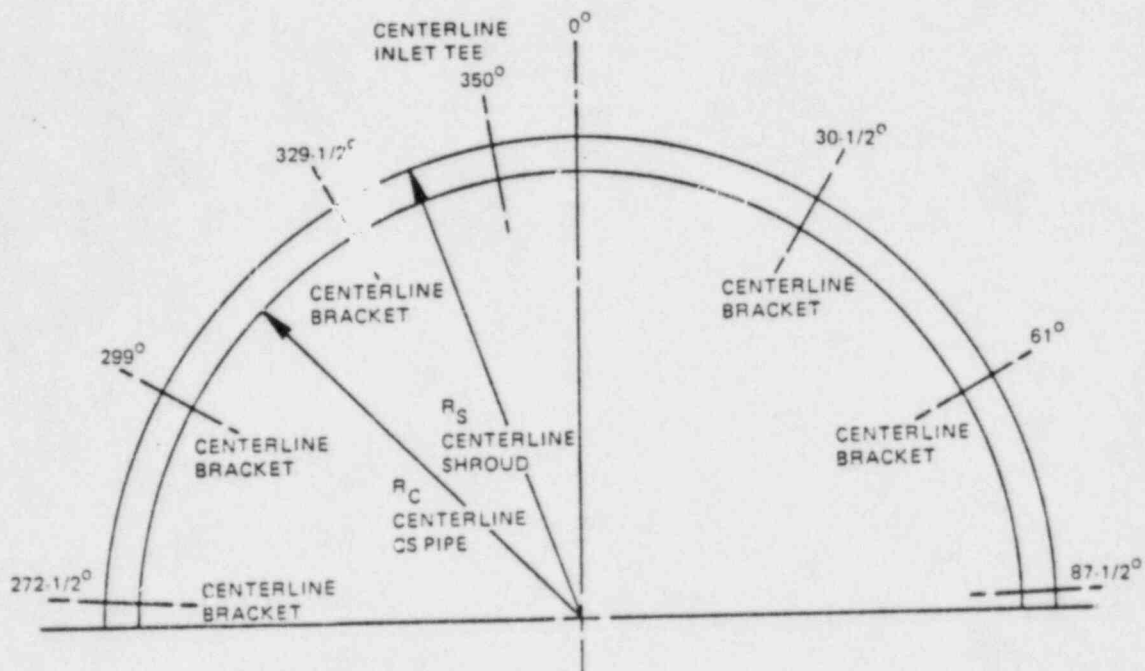
$$V = \frac{W_{\max}}{\rho A} = \frac{11.85 (144)}{62.2 (1.095)} = 25.05 \text{ ft/sec @ exit from HEADER}$$

$$F_y = 50(1.095) + \frac{62.2 (25.05)^2 (1.095)}{32.2 (144)} = \underline{\underline{63.97 \text{ lb}}}$$

$$F_z = \frac{\rho V^2 A}{g} + \cancel{\frac{W}{A}} \quad V = 26.95 \text{ ft/sec @ EXIT FROM NOZZLE}$$

$$F_z = \frac{62.2 (26.95)^2 (1.018)}{32.2 (144)} = \underline{\underline{9.92 \text{ lb}}}$$

A.1.6 Thermal Expansion Mismatch Loads - Intact Sparger



$$R_s = \frac{186\frac{1}{2}}{2} + \frac{1.5}{2} = 94 \text{ in.}$$

$$R_c = \frac{186\frac{1}{2}}{2} - \frac{4.0}{2} = 91.25 \text{ in.}$$

SHROUD TEMPERATURE = 550°F

CS PIPE TEMPERATURE = 200°F

{ See Section A.5-1

$$\therefore \Delta T = 350^\circ\text{F}$$

$$\Delta R = \alpha R \Delta T$$

For 304 STAINLESS STEEL,

$$\alpha = 9.6 \times 10^{-6} \text{ in/in.}^\circ\text{F}$$

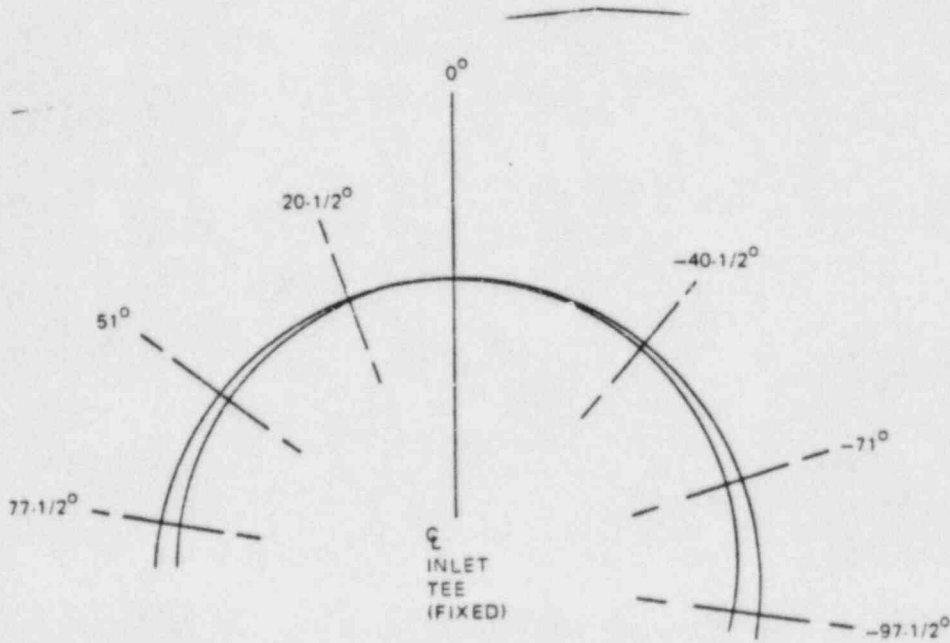
$$R = \frac{186.5}{2} = 93.25 \text{ in. at shroud-to-pipe interface}$$

$$\Delta R_{90^\circ} = 9.6 \times 10^{-6} (93.25) (350^\circ) = 0.313 \text{ in.}$$

(For 90° arc)

FOR SEGMENT:

$$\text{Assume } \Delta R = \Delta R_{90^\circ} (1 - \cos \theta) = 0.313 (1 - \cos \theta)$$



$$\Delta R_{-40\frac{1}{2}^\circ} = 0.313 (1 - \cos 40\frac{1}{2}^\circ) = \underline{0.075 \text{ in.}}$$

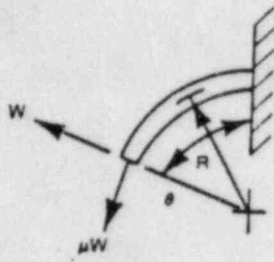
$$\Delta R_{-71^\circ} = 0.313 (1 - \cos 71^\circ) = \underline{0.211 \text{ in.}}$$

$$\Delta R_{-97\frac{1}{2}^\circ} = 0.313 (1 - \cos 97\frac{1}{2}^\circ) = \underline{0.354 \text{ in.}}$$

$$\Delta R_{20\frac{1}{2}^\circ} = 0.313 (1 - \cos 20\frac{1}{2}^\circ) = \underline{0.0198 \text{ in.}}$$

$$\Delta R_{51^\circ} = 0.313 (1 - \cos 51^\circ) = \underline{0.166 \text{ in.}}$$

$$\Delta R_{77\frac{1}{2}^\circ} = 0.313 (1 - \cos 77\frac{1}{2}^\circ) = \underline{0.245 \text{ in.}}$$



Assume the  $\Delta R$  is resisted only by each bracket support in turn:

$$\Delta R = \frac{WR^3}{4EI} (2\theta - \sin 2\theta) - \frac{\mu WR^3}{4EI} (\cos 2\theta - 4 \cos \theta + 3)$$

$$W = \frac{4EILR}{R^3 (2\theta - \sin 2\theta - \mu \cos 2\theta + 4\mu \cos \theta - 3\mu)}$$

$$E = 28 \times 10^6 \text{ lb/in.}^2 \quad R = R_c = 93.25 - 2.0 = 91.25$$

$$I = \frac{\pi}{64} (4.0^4 - 3.548^4) = 4.79 \text{ in.}^4$$

$$\mu = 0.2 \text{ (coefficient of friction)}$$

$$W = \frac{4 (28 \times 10^6) (4.79) \Delta R}{(91.25)^3 (2\theta - \sin 2\theta - 0.2 \cos 2\theta + 0.8 \cos \theta - 0.6)}$$

$$W = \frac{706 \Delta R}{(2\theta - \sin 2\theta - 0.2 \cos 2\theta + 0.8 \cos \theta - 0.6)}$$

$$W_{-40\frac{1}{2}^\circ} = \frac{706 (0.075)}{0.403} = \underline{131 \text{ lb}}$$

$$W_{-71^\circ} = \frac{706 (0.211)}{1.68} = \underline{89 \text{ lb}}$$

$$W_{-97\frac{1}{2}^\circ} = \frac{706 (0.354)}{3.15} = \underline{79 \text{ lb}}$$

$$W_{20\frac{1}{2}^\circ} = \frac{706 (0.0198)}{0.0579} = \underline{241 \text{ lb}}$$

$$W_{51^\circ} = \frac{706 (0.116)}{0.747} = \underline{110 \text{ lb}}$$

$$W_{77\frac{1}{2}^\circ} = \frac{706 (0.245)}{2.04} = \underline{85 \text{ lb}}$$

A.1.7 Thermal Expansion Mismatch Loads - Broken Sparger

1. Assume break in sparger at T-Box during core spray injection.
2. Assume  $\Delta T$  at sparger-to-shroud =  $350^\circ\text{F}$  (maximum - see Section A.1.6).

$$\Delta R = \alpha R \Delta T$$

$$\alpha = 9.6 \times 10^{-6} \text{ in./in.-}^\circ\text{F} \quad (304\text{-SS})$$

$$R = 93.25 \text{ in. at shroud-to-pipe interface}$$

$$\Delta R_{90^\circ} = 9.6 \times 10^{-6} (93.25) (350^\circ) = 0.313 \text{ in.}$$

$$\text{Assume } \Delta R_\theta = \Delta R_{90^\circ} (1 - \cos \theta)$$

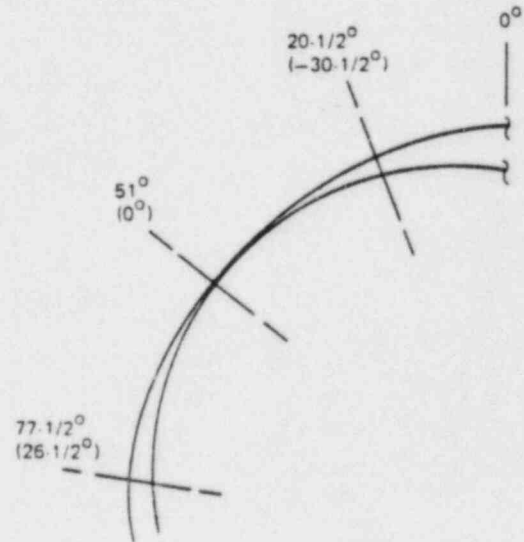
Take the  $51^\circ$  bracket as  $\theta = 0^\circ$

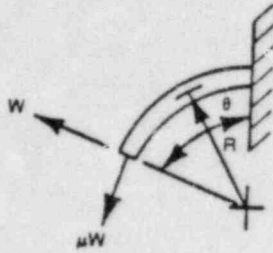
Then:  $20\frac{1}{2}^\circ$  bracket is at  $\theta = 20\frac{1}{2} - 51 = -30\frac{1}{2}^\circ$ .

$77\frac{1}{2}^\circ$  bracket is at  $\theta = 77\frac{1}{2} - 51 = 26\frac{1}{2}^\circ$ .

$$\Delta R_{-30\frac{1}{2}^\circ} = 0.313 (1 - \cos 30\frac{1}{2}^\circ) = 0.0433 \text{ in.}$$

$$\Delta R_{26\frac{1}{2}^\circ} = 0.313 (1 - \cos 26\frac{1}{2}^\circ) = 0.0329 \text{ in.}$$





Assume that the  $51^\circ$  bracket is fixed and that the corresponding  $\Delta R$  is resisted by the brackets to each side of it:

$$\Delta R = \frac{WR^3}{4EI} (2\theta - \sin 2\theta) - \frac{\mu WR^3}{4EI} (\cos 2\theta - 4 \cos \theta + 3)$$

$$W = \frac{4EI\Delta R}{R^3 (2\theta - \sin 2\theta - \mu \cos 2\theta + 4 \mu \cos \theta - 3\mu)}$$

$$E = 28 \times 10^6 \text{ lb/in.}^2 \quad R = R_c = 93.25 - 2.0 = 91.25$$

$$I = \frac{\pi}{64} (4.0^4 - 3.548^4) = 4.79 \text{ in.}^4$$

$$\mu = 0.2 \text{ (coefficient of friction)}$$

$$W = \frac{4 (28 \times 10^6) (4.79) \Delta R}{(91.25)^3 (2\theta - \sin 2\theta - 0.2 \cos 2\theta + 0.8 \cos \theta - 0.6)}$$

$$= \frac{706 \Delta R}{(2\theta - \sin 2\theta - 0.2 \cos 2\theta + 0.8 \cos \theta - 0.6)}$$

$$W_{-30\frac{1}{2}^\circ} = \frac{706 \times 0.0433}{(2\pi \times 30.5/180 - \sin 61^\circ - 0.2 \cos 61^\circ + 0.8 \cos 30.5^\circ - 0.6)}$$

$$= 168 \text{ lb}$$

$$W_{26\frac{1}{2}^\circ} = \frac{706 \times 0.0329}{(2\pi \times 26.5/180 - \sin 53^\circ - 0.2 \cos 53^\circ + 0.8 \cos 26.5^\circ - 0.6)}$$

$$= 190 \text{ lb (maximum)}$$



A.2 FLOW INDUCED VIBRATION - NATURAL FREQUENCY

GE Design Basis requires that the natural frequency  $f_n$  is equal to or greater than three (3) times the vortex shedding frequency.

A.2.1 Flow Induced Vibration

The vortex shedding frequency,  $f_v$ , is given by

$$\frac{f_v D}{V} = 0.21$$

V = velocity past shroud wall = 5 ft/sec (Conservative value - more realistic value is ~3.5 ft/sec)

D = sparger pipe diameter =  $\frac{4.0}{12}$  ft

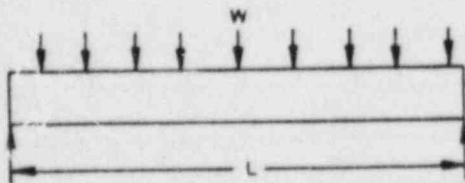
$$f_v = \frac{0.21 (5)}{(4/12)} = \underline{\underline{3.15 \text{ Hz}}}$$

A.2.2 Natural Frequency

The sparger natural frequency is now calculated for four different cases. The first two cases are bounding for the intact sparger. The last two cases are for the broken sparger.

Case 1 - Intact Sparger

Calculate the natural frequency of the sparger by examining the longest segment between support brackets. Assume this section has a uniform load w per unit length, both ends simply supported.



$$f_n = \frac{K_n}{2\pi} \sqrt{\frac{EI}{wL^4}}$$

$$K_n = 9.87$$

$$I = 4.79 \text{ in.}^4$$

$$E = 25.75 \times 10^6 \text{ lb/in.}^2$$

$$L = \frac{40.5}{180} \times \pi \times 91.25 = 64.5 \text{ in. (distance from T-box centerline to the first bracket on longer pipe arm)}$$

$$W = 1.37 \text{ lb/in.}$$

$$f_n = \frac{9.87}{2\pi} \sqrt{\frac{25.75 \times 10^6 (4.79) (32.2) (12)}{1.37 (64.5)^4}} = 70.4 \text{ Hz}$$

$$\text{Ratio} = \frac{f_n}{f_v} = \frac{70.4}{3.15} > 3$$

### Case 2 - Intact Sparger (Missing Bracket)

Calculate the natural frequency of the sparger by examining the longest segment between support brackets ignoring an intermediate support. Values other than L are same as previous case.

$$L = \frac{71}{180} \times \pi \times 91.25 = 113$$

$$f_n = 70.4 \left( \frac{64.5}{113} \right)^2 = 22.9$$

$$\text{Ratio} = \frac{f_n}{f_v} = \frac{22.9}{3.15} > 3$$

### Case 3 - Broken Sparger (Simple Cantilever)

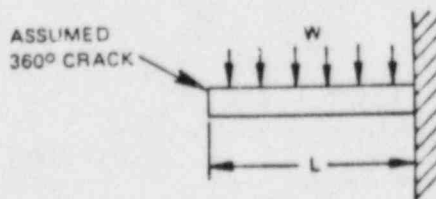
Calculate the natural frequency of the unsupported sparger segment. Assume the segment acts as a cantilever and has a uniform load w (force/unit length). Conservatively assume that the crack is located in the long arm of the sparger.

NOTE: Length of unsupported segment is taken 3" from T-box centerline to account for location of crack.

$$f_n = \frac{k_n}{2\pi} \sqrt{\frac{EI\alpha}{wL^4}}$$

$$k_n = 3.52$$

$$E = 25.75 \times 10^6 \text{ lb/in.}^2$$



$$I = 4.79 \text{ in.}^4$$

$$L_{\text{max}} = [40\frac{1}{2} (\pi/180) \times 91.25] - 3 = 64.5 - 3 = 61.5 \text{ in.}$$

(distance from crack to bracket)

$$w = 1.37 \text{ lb/in. (Section A.1.1)}$$

$$f_n = \frac{3.52}{2\pi} \sqrt{\frac{25.75 \times 10^6 (4.79) (32.2) (12)}{1.37 (61.5)^4}} = 27.6 \text{ Hz}$$

$$\text{Ratio} = \frac{f_n}{f_v} = \frac{27.6}{3.15} > 3$$

Case 4 - Broken Sparger (Include Effect of Two Near Brackets)

Calculate the natural frequency accounting for the effect of the two near brackets. Conservatively assume that the crack is located in the long arm of the sparger.

Rayleigh's Method:

The total kinetic energy of the system is zero at the maximum displacement but is maximum at the static equilibrium point. On the other hand, the total potential energy is maximum at the maximum displacement but is zero at the static equilibrium point. From conservation of energy:

$$(K.E.)_{\text{max}} = (P.E.)_{\text{max}}$$

$$\frac{1}{2} \sum \frac{W y^2 w_n^2}{g} = \frac{1}{2} \sum W y$$

where

W = weight, lb

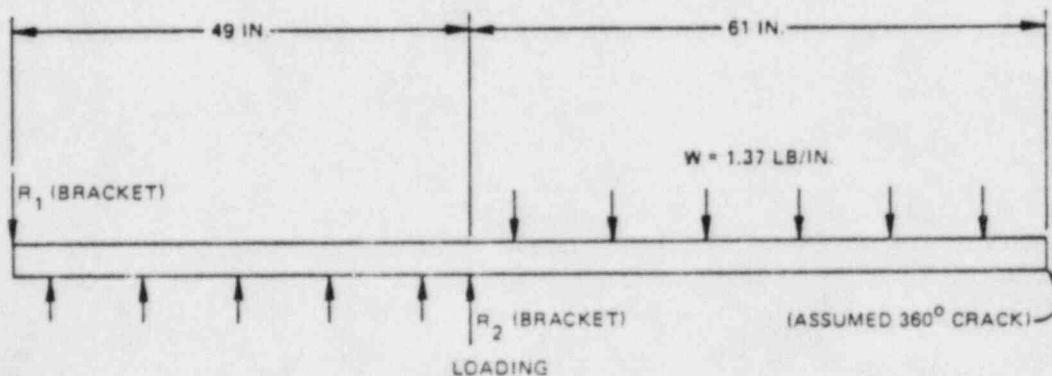
y = deflection, in.

$g$  = gravitational constant = 386 in./sec<sup>2</sup>

$\omega_n$  = natural frequency, radians/sec

The deflection of the member is obtained by successive graphical integrations starting with the shear diagram.

The loading diagram is shown below. The reaction loads are calculated to develop the shear diagram. The slope at the left end ( $R_1$ ) is calculated to initialize the slope ( $dy/dx$ ) diagram.



$$\begin{aligned} \Sigma M_1 = 0 \quad 49 R_2 &= 1.37 (61) (49 + 61/2) - \frac{1.37 (49)^2}{2} \\ R_2 &= 102.0 \text{ lb} \end{aligned}$$

$$\begin{aligned} \Sigma M_2 = \quad 49 R_1 &= \frac{1.37 (49)^2}{2} + \frac{1.37 (61)^2}{2} \\ R_1 &= 85.6 \text{ lb} \end{aligned}$$

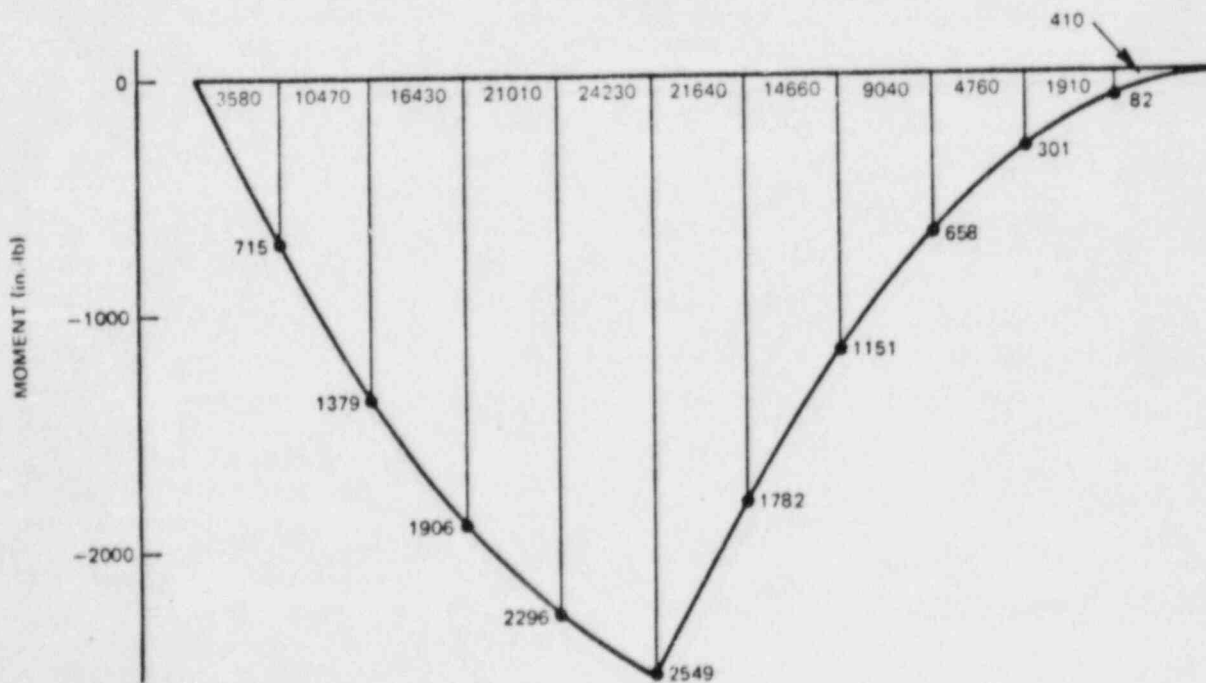
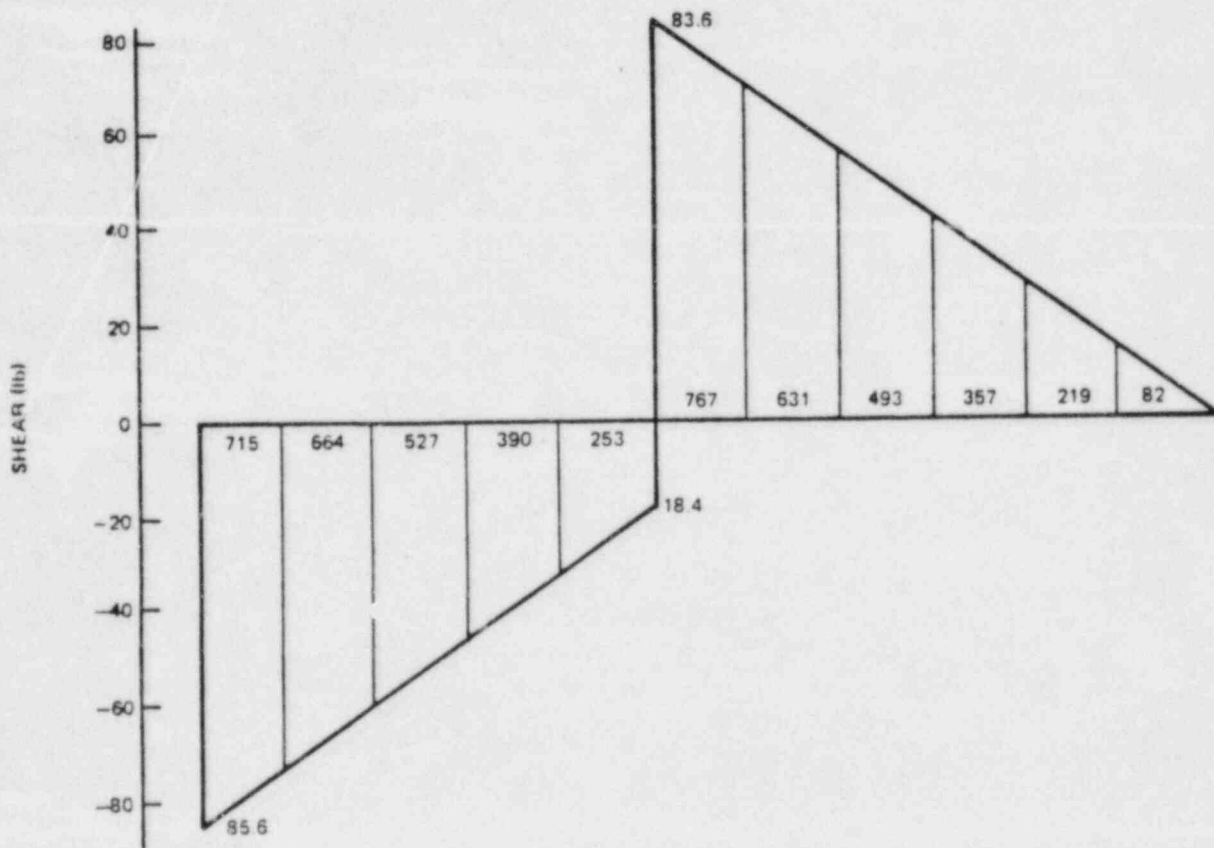
$$85.6 - 1.37 (49) - 102.0 + 1.37 (61) = 0 \quad (\text{Check})$$

Slope at  $R_1$ :

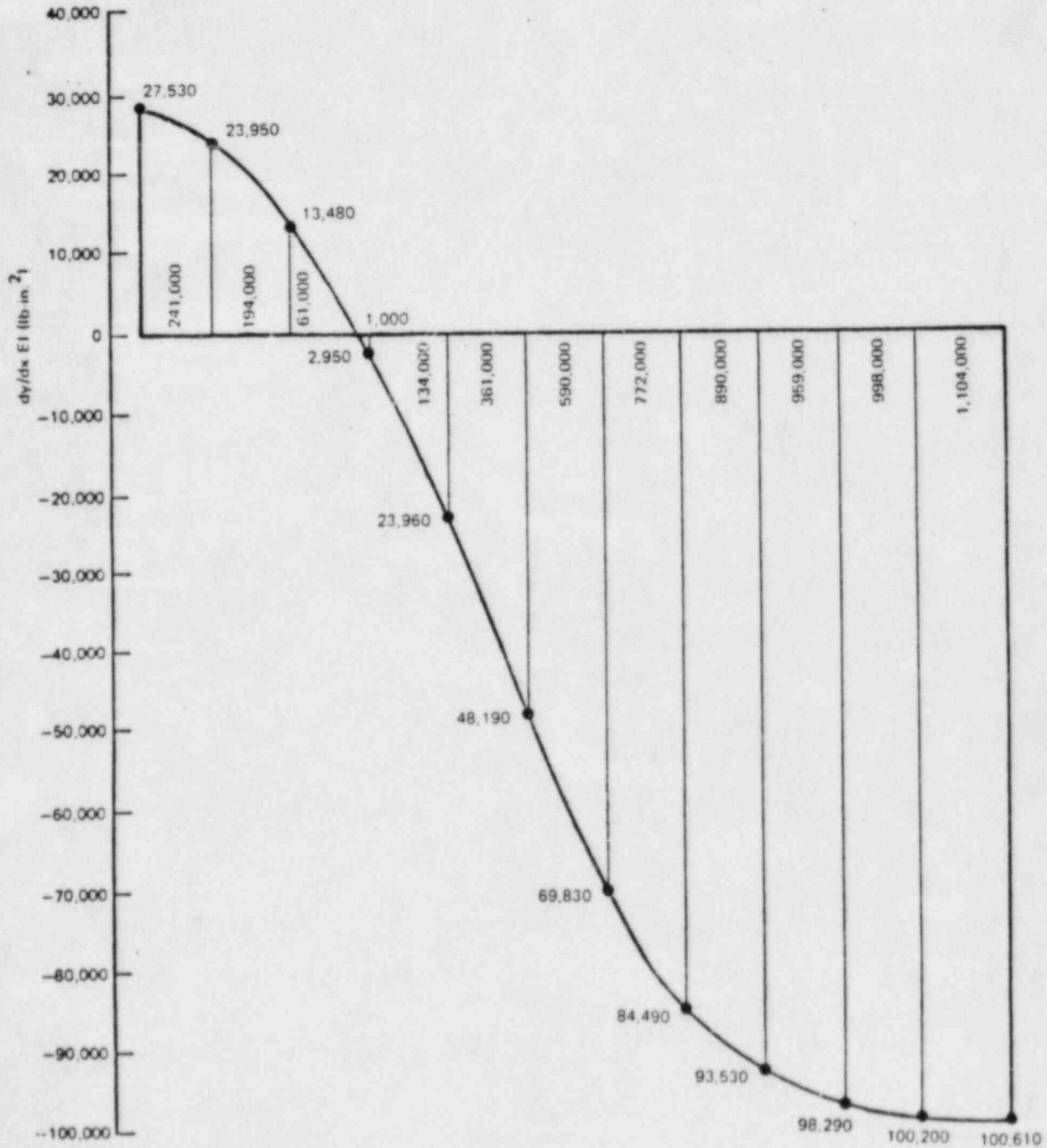
$$\theta_1 = \frac{1}{24} \frac{w l_1^2}{EI} + \frac{1}{6} \frac{M_2 l_2}{EI} \quad M_2 = \frac{1.37 (61)^2}{2} = 2549 \text{ in.-lb}$$

$$\theta EI = \frac{w l_1^3}{24} + \frac{M_2 l_2}{6} = \frac{1.37 (49)^3}{24} + \frac{2549 (49)}{6} = 27530 \text{ lb-in.}^2$$

The shear diagram is now constructed. It is then graphically integrated to construct the moment diagram.



The slope ( $dy/dx$ ) diagram is now constructed by graphical integration of the moment diagram.

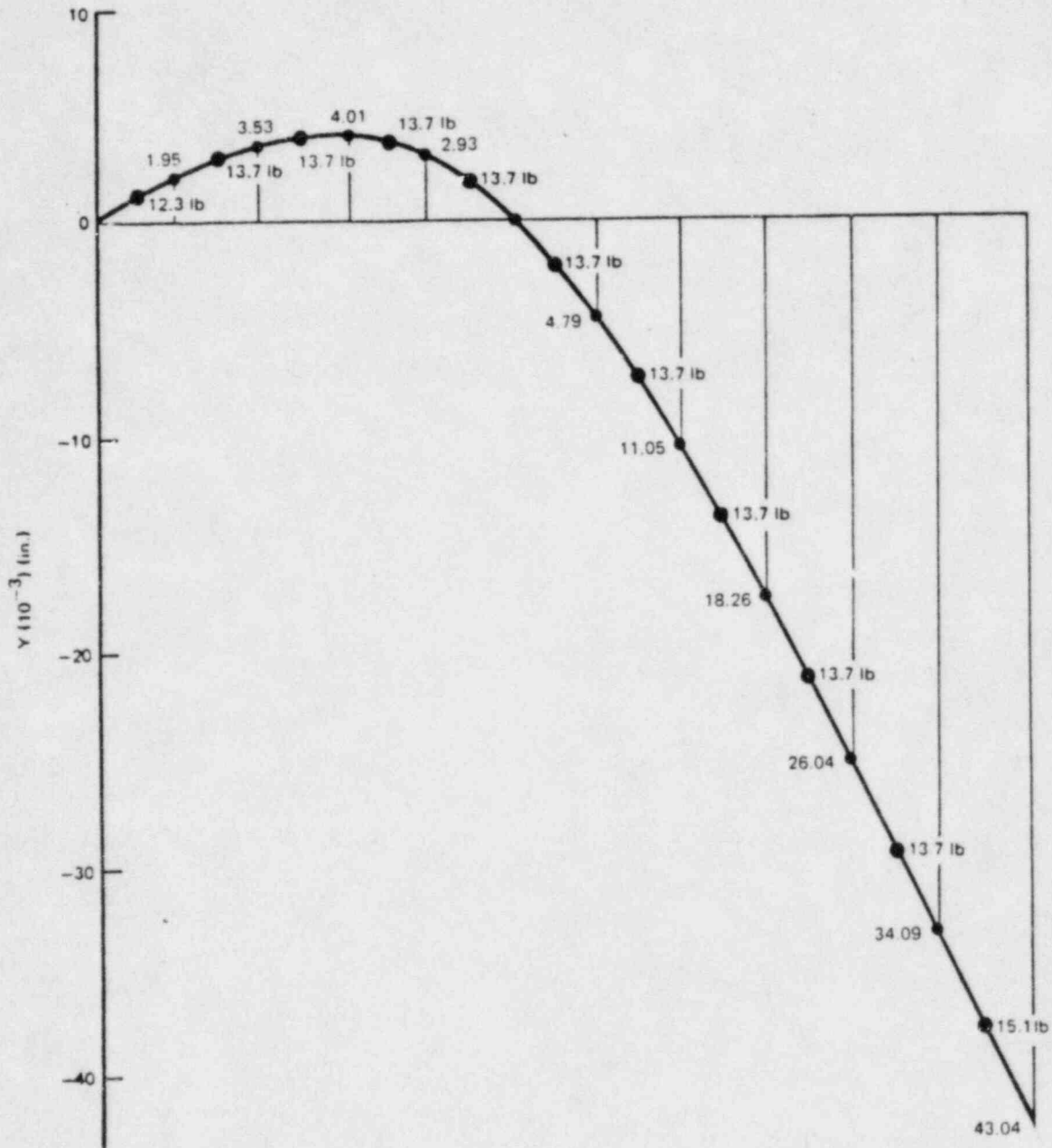


Graphical integration of the slope diagram yields deflections.

	$\frac{(\text{lb-in.}^2)}{yEI \text{ (X1000)}}$	$\frac{(\text{in.})}{y \text{ (10}^{-3}\text{)}}$	Length (in.)
Left End Bracket	0	0	0
	241	1.95	9
	435	3.53	19
	495	4.01	29
	361	2.93	39
Bracket	0	0	49
	-590	-4.79	59
	-1362	-11.05	69
	-2252	-18.26	79
	-3211	-26.04	89
	-4203	-34.09	99
Right End	-5307	-43.04	110

$$EI = 123.3 (10^6) \text{ lb-in.}^2$$

The deflection diagram is now constructed.



The weight of the member is now distributed as shown above. The natural frequency can now be determined.



$$\begin{aligned} \Sigma W y^2 &= [12.3 (1.0)^2 + 13.7 (2.8)^2 + 13.7 (3.8)^2 + \\ &13.7 (3.5)^2 + 13.7 (1.5)^2 + 13.7 (2.4)^2 + \\ &13.7 (7.9)^2 + 13.7 (14.7)^2 + 13.7 (22.7)^2 + \\ &13.7 (30.0)^2 + 15.1 (38.5)^2] (10^{-6}) \\ &= 0.04581 \text{ lb-in.}^2 \end{aligned}$$

$$\begin{aligned} \Sigma W y &= [12.3 (1.0) + 13.7 (2.8) + 13.7 (3.8) + \\ &13.7 (3.5) + 13.7 (1.5) + 13.7 (2.4) + \\ &13.7 (7.9) + 13.7 (14.7) + 13.7 (22.1) + \\ &13.7 (30.0) + 15.1 (38.5)] (10^{-3}) \\ &= 1.809 \text{ lb-in.} \end{aligned}$$

$$w_n^2 = (386) \left( \frac{1.809}{0.0458} \right) = 15240$$

$$w_n = 123.5 \text{ rad/sec}$$

$$f_n = \frac{w_n}{2\pi} = \frac{123.5}{2\pi} = 19.6 \text{ Hz}$$

$$\text{Ratio} = \frac{f_n}{f_v} = \frac{19.6}{3.15} = 6.2 > 3$$

### A.2.3 Conclusions

1. The natural frequency of the intact sparger, even when a bracket is assumed missing, is greater than three (3) times the vortex shedding frequency. Therefore, fatigue resulting from flow-induced vibrations cannot be hypothesized as a cause of cracking. Also, the loads used to calculate stresses for the intact sparger condition (see Section A.3) do not require amplification.

2. The natural frequency of a broken sparger (assumed 360° throughwall crack near the tee-box) is greater than three (3) times the vortex shedding frequency. Therefore, flow-induced vibration under this assumed condition will not be a problem and the loads used to calculate stresses for the assumed broken sparger condition (see Section A.4) do not require amplification.

### A.3 STRESSES FOR UNBROKEN SPARGER

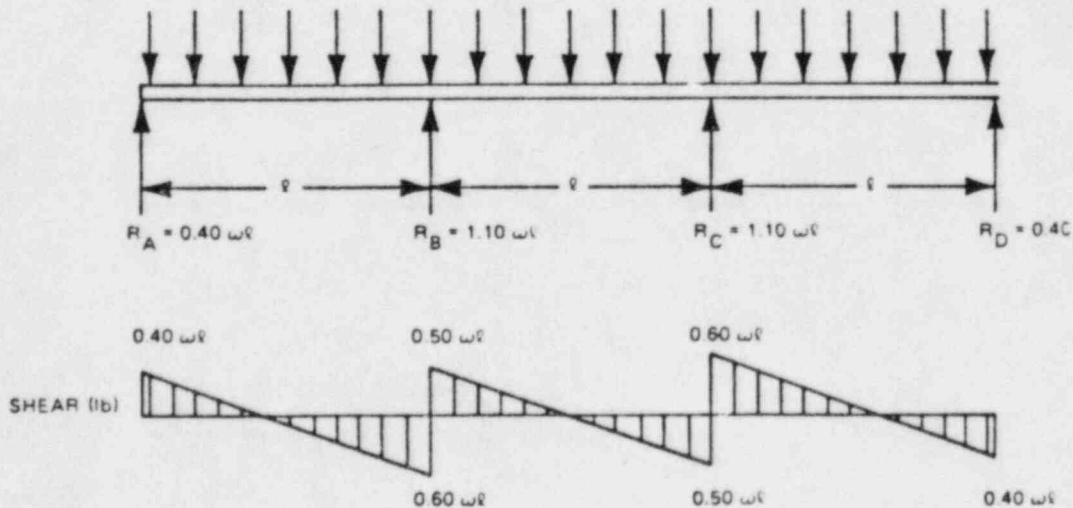
This section contains the calculation of stresses in the intact sparger condition during normal plant operation and during the core spray injection event. During normal plant operation, there is no core spray flow. The sparger  $\Delta P = 0$  and  $\Delta T = 0$ . Impingement loads and weight loads are low and are bounded by the postulated seismic event.

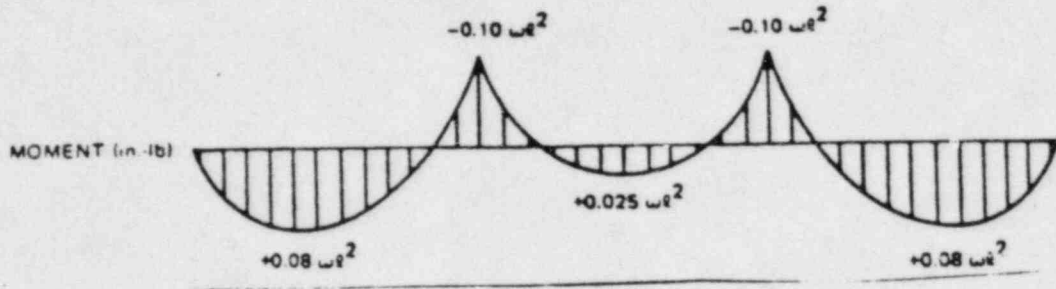
Design loads during core spray injection are the design loads for the sparger. Thermal mismatch between the cold sparger (due to injection) and the hot shroud produce significant loads on the sparger pipe arms and on the brackets. Pressure and thrust loads produce stresses in the pipe arm and nozzles.

#### A.3.1 Pipe Stresses

##### A.3.1.1 Seismic and Impingement

For simplicity assume continuous beam - three equal spans.





$$l = \frac{40.5}{180} \times \pi \times 91.25 = 64.5 \text{ in. (Assume maximum span length for conservatism)}$$

$$w = 2.74 \text{ lb/in. (Seismic)}$$

$$w = 1.0 \text{ lb/in. (Impingement)}$$

{ See Section A.1.3

$$M_{\max} = 0.1 (2.74) (64.5)^2 = 1140 \text{ in.-lb}$$

$$\sigma = \frac{Mc}{I} \quad I = 4.79 \text{ in.}^4 \quad c = \frac{4.0}{2} = 2.0 \text{ in.}$$

$$\sigma_{\max} = \frac{1140 (2.0)}{4.79} = 476 \text{ lb/in.}^2 \text{ (Seismic)}$$

$$\sigma_{\max} = 476 \left(\frac{1.0}{2.74}\right) = 173.7 \text{ lb/in.}^2 \text{ (Impingement)}$$

A.3.1.2 Differential Pressure

$$\Delta P_{\max} = 50.0 \text{ psi}$$

$$R_o = 2.0 \text{ in.}$$

$$R_i = 3.548/2 = 1.774$$

$$t_{\text{nom.}} = 0.226$$

$$t_{\min} = 0.226 - 2 (0.003) \text{ [corrosion allowance]} = 0.220 \text{ in.}$$

• Hoop Stress

$$\sigma = \frac{P R_i}{t} = \frac{50.0 (1.774)}{0.220} = 404 \text{ lb/in.}^2$$

- Axial Stress

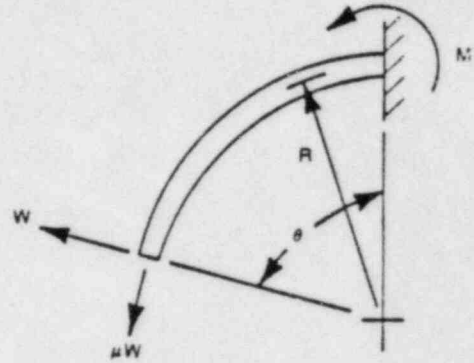
$$\sigma = \frac{P R_i}{2t} = \frac{404}{2} = \underline{202} \text{ lb/in.}^2$$

A.3.1.3 Mismatch Due to Thermal Expansion

$$m = WR \sin \theta - \mu WR (1 - \cos \theta)$$

$$= WR [\sin \theta - \mu (1 - \cos \theta)]$$

Assume  $\mu = 0.2$                        $R = 94.25$   
 (See Section A.1.6)



- $-40\frac{1}{2}^\circ$  Bracket

$$M_{-40\frac{1}{2}^\circ} = 131 (91.25) [\sin 40.5^\circ - 0.2 (1 - \cos 40.5^\circ)]$$

$$= \underline{7191} \text{ in.-lb}$$

- $-71^\circ$  Bracket

$$M_{-71^\circ} = 89 (91.25) [\sin 71^\circ - 0.2 (1 - \cos 71^\circ)]$$

$$= \underline{6583} \text{ in.-lb}$$

- $-97\frac{1}{2}^\circ$  Bracket

$$M_{-97\frac{1}{2}^\circ} = 79 (91.25) [\sin 97\frac{1}{2}^\circ - 0.2 (1 - \cos 97\frac{1}{2}^\circ)]$$

$$= \underline{5517} \text{ in.-lb}$$

- $20\frac{1}{2}^\circ$  Bracket

$$M_{20\frac{1}{2}^\circ} = 241 (91.25) [\sin 20\frac{1}{2}^\circ - 0.2 (1 - \cos 20\frac{1}{2}^\circ)]$$

$$= \underline{7423} \text{ in.-lb (maximum)}$$

- 51° Bracket

$$M_{51^\circ} = 110 (91.25) [\sin 51^\circ - 0.2 (1 - \cos 51^\circ)]$$

$$= \underline{7056} \text{ in.-lb}$$

- 77½° Bracket

$$M_{77\frac{1}{2}^\circ} = 85 (91.25) [\sin 77\frac{1}{2}^\circ - 0.2 (1 - \cos 77\frac{1}{2}^\circ)]$$

$$= \underline{6357} \text{ in.-lb}$$

Sum of Stresses Attributable to Core Spray Injection:

$$\sigma_{\max} = \sigma_{\text{bending}} + \sigma_{\text{bracket friction}} + \sigma_{\Delta P}$$

$$= \frac{Mc}{I} + \frac{uW}{A_p} + \frac{Pr}{2t}$$

$$c = \frac{4.0}{2} = 2 \text{ in.}$$

$$I = 4.79 \text{ in.}^4$$

$$uW = 0.2 (241)$$

$$M = 7423 \text{ in.-lb}$$

$$A_p = 2.68 \text{ in.}^2$$

$$\frac{Pr}{2t} = 202 \text{ lb/in.}^2 \text{ (Section A.3.1.2)}$$

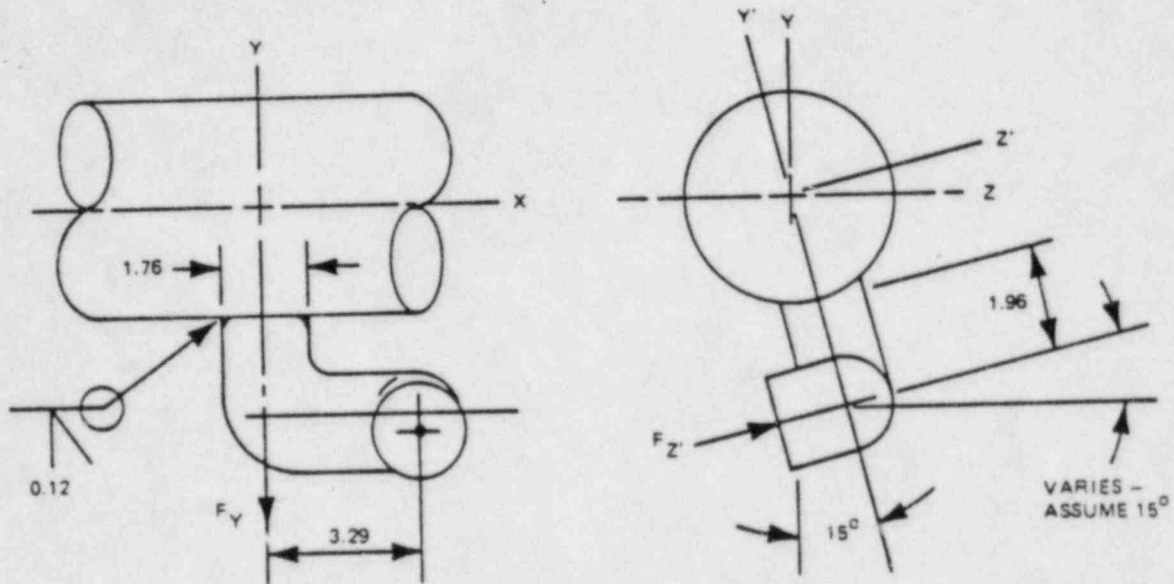
$$\sigma_{\max} = \frac{7423 (2.0)}{4.79} + \frac{0.2 (241)}{2.68} + 202$$

$$= 3099 + 18 + 202$$

$$= \underline{3319} \text{ lb/in.}^2$$

A.3.2 Nozzle Stress

A.3.2.1 Nozzle Thrust



Weld Properties:

$$I = \frac{\pi}{64} (1.76^4 - 1.52^4) = 0.209 \text{ in.}^4$$

$$K = \frac{\pi}{32} (1.76^4 - 1.52^4) = 0.418 \text{ in.}^4$$

$$A = \frac{\pi}{4} (1.76^2 - 1.52^2) = 0.618 \text{ in.}^2$$

$$c = \frac{1.76}{2} = 0.88 \text{ in.}$$

$$t = 0.12 \text{ in.}$$

$$r = \frac{1.76}{2} = 0.88 \text{ in.}$$

$$F_y = 64 \text{ lb} \quad F_{z'} = 9.9 \text{ lb} \quad (\text{Section A.1.5})$$

$$P = 50 \text{ psi} \quad (\text{Section A.1.4})$$

The resulting loads at the weld are:

$$F_{\text{axial}} = F_y = 64 \text{ lb}$$

$$F_{\text{shear}} = F_z = 9.9 \text{ lb}$$

$$T_{\text{torsion}} = 3.29 F_z = 3.29 (9.9) = 32.6 \text{ in.-lb}$$

$$M_{\text{moment}} = 1.96 F_z = 1.96 (9.9) = 19.4 \text{ in.-lb}$$

The stresses are conservatively calculated as:

$$\begin{aligned} \sigma_y &= \pm \frac{M_m c}{I} + \frac{F_a}{A} + \frac{Pr}{2t} \\ &= \pm \frac{19.4 (0.88)}{0.209} + \frac{64}{0.618} + \frac{50 (0.88)}{2 (0.12)} \\ &= \pm 81.7 + 103.6 + 183 \end{aligned}$$

$$\sigma_y = \underline{369} \text{ lb/in.}^2, \quad 205 \text{ lb/in.}^2$$

$$\tau_{xy} = \frac{T_T c}{K} + \alpha \frac{F_s}{A} \quad \alpha = 2 \text{ (thin wall cylinder)}$$

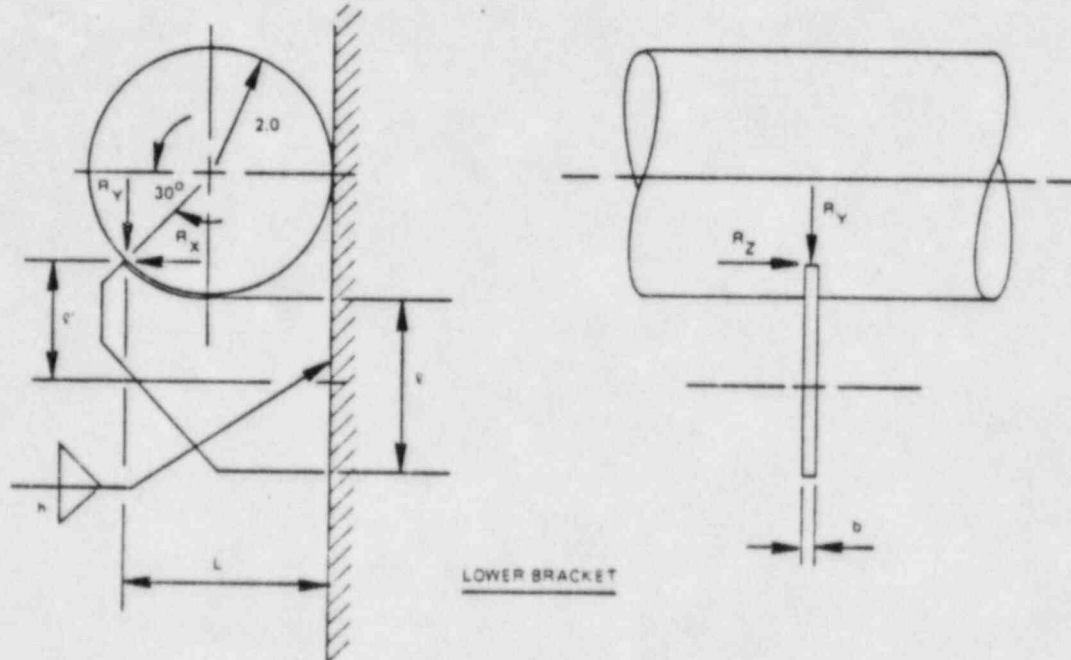
$$= \frac{(32.57)(0.88)}{0.418} + 2 \frac{9.9}{0.618}$$

$$= 60 + 32$$

$$\tau_{xy} = \underline{101} \text{ lb/in.}^2$$

A.3.3 Bracket Stresses

A.3.3.1 Lower Bracket Stresses Due to Thermal Expansion



$$i = 4.0 - 2.0 = 2.0 \text{ in.}$$

$$L = 2.0 (1 + \cos 30^\circ) = 3.73 \text{ in.}$$

$$i' = \frac{2.0}{2} + (1 - \sin 30^\circ) (2.0) = 2.0 \text{ in.}$$

$$b = 0.5 \text{ in.}$$

$$h = 0.25 \text{ in.}$$

$$R_x = 241 \text{ lb (Section A.1.6)}$$

$$R_z = \mu R_x = 0.2 (241) = 48.2 \text{ lb}$$

$$R_y = 0$$



Maximum shear stress in the fillet weld is

$$\tau = \frac{\sqrt{2}}{2} \frac{R_x + R_z}{hl} + \frac{\sqrt{2}}{2} \frac{M}{(b+h)(l \cdot h)h}$$

where

$$M = l' R_z$$

$$\tau = \frac{\sqrt{2}}{2} \frac{(241 + 48.2)}{0.25(2.0)} + \frac{\sqrt{2}}{2} \frac{(2.0) 48.2}{(0.5 + 0.25)(2.0)(0.25)}$$

$$\tau = 409 + 208 = \underline{\underline{617}} \text{ lb/in.}^2$$

Maximum normal stress in weld is:

$$\sigma_{\max} = \frac{\sqrt{2}}{2} \frac{R_x}{hl} = \frac{R_z}{hl(b+h)} \sqrt{2L^2 + \frac{(b+h)^2}{2}} + \frac{3\sqrt{2}M}{hl^2}$$

where

$$M = l' R_x$$

$$\sigma_{\max} = \frac{\sqrt{2}}{2} \frac{(241)}{0.25(2.0)} + \frac{3\sqrt{2}(2.0)(241)}{0.25(2.0)^2}$$

$$- \frac{48.2}{0.25(2.0)(0.5 + 0.25)} \sqrt{2(3.73)^2 + \frac{(0.5 + 0.25)^2}{2}}$$

$$\sigma_{\max} = 341 + 2045 + 681.4 = \underline{\underline{3067}} \text{ lb/in.}^2$$

Maximum normal stress in plate is ...

$$\sigma_{\max} = \frac{R_x}{A} + \frac{t \cdot R_x C_{xy}}{I_{xy}} + \frac{L R_z C_{zx}}{I_{zx}}$$

$$A = 0.5 (2.0) = 1.0 \text{ in.}^2$$

$$I_{xy} = \frac{b^3}{12} = \frac{0.5 (2.0)^3}{12} = 0.333 \text{ in.}^4$$

$$C_{xy} = \frac{2.0}{2} = 1.0 \text{ in.}$$

$$I_{zx} = \frac{t b^3}{12} = \frac{2.0 (0.5)^3}{12} = 0.02083 \text{ in.}^4$$

$$C_{zx} = \frac{0.5}{2} = 0.25 \text{ in.}$$

$$\sigma_{\max} = \frac{241}{1.0} + \frac{(2.0) (241) (1.0)}{0.3333} + \frac{3.73 (48.2) (0.25)}{0.02083}$$

$$= 241 + 1446 + 2158$$

$$\sigma_{\max} = \underline{\underline{3845}} \text{ lb/in.}^2$$

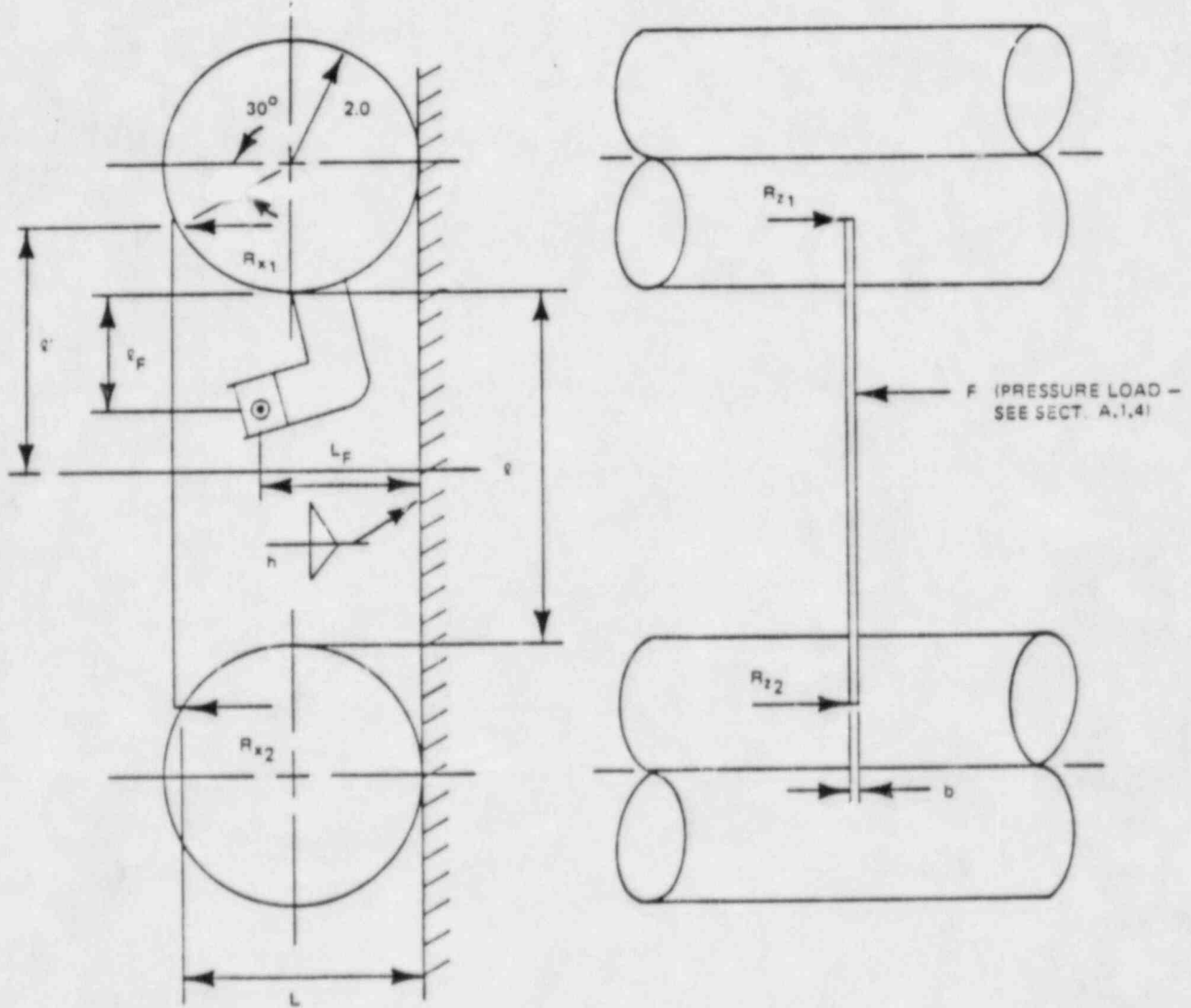
Maximum shear stress in plate

$$\tau = \frac{R_x + R_z}{b t} + \frac{t \cdot R_z (3t + 1.8b)}{t^2 b^2}$$

$$= \frac{241.0 + 48.2}{0.5 (2.0)} + \frac{(2.0) (48.2) (3 \times 2.0 + 1.8 \times 0.5)}{(2.0)^2 (0.5)^2}$$

$$\tau = 289.2 + 665 = \underline{\underline{954}} \text{ lb/in.}^2$$

A.3.3.2 Middle Bracket Stresses Due to Thermal Expansion



$$r = 10.25 - 2(2.0) = 6.25 \text{ in. } b = 0.5 \text{ in.}$$

$$r_F = \frac{6.25}{2} + (1 - \sin 30^\circ)(2.0) = 4.13 \text{ in. } h = 0.25 \text{ in.}$$

$$L = (1 + \cos 30^\circ)(2.0) = 3.73 \text{ in.}$$

$$r_F = (2.0 + 1.96) \cos 15^\circ + (1.50 + 1.18) \sin 15^\circ - 2.0$$

$$l_F = 2.52$$

$$L_F = 2.0 - (2.0 + 1.96) \sin 15^\circ + (1.50 + 1.18/2) \cos 15^\circ$$

$$L_F = 2.99 \text{ in.}$$

(NOTE:  $l_F$ ,  $L_F$  used in Section A.4.3.3)

Assume

$$R_{x1} = R_{x2} = 241 \text{ lb} \quad (\text{Section A.1.5})$$

$$R_{z1} = R_{z2} = 0.2 (241) = 48.2$$

Shear Stress

$$\tau_{AVG} = \frac{\sqrt{2}}{2} \left( \frac{R_{z1} + R_{z2}}{hi} \right) = \frac{\sqrt{2}}{2} \frac{96.4}{(0.25)(6.25)}$$

$$\tau_{AVG} = \underline{\underline{44 \text{ lb/in.}^2}} \text{ (weld)}$$

$$i_{AVG} = \frac{(R_{z1} + R_{z2})}{bi} = \frac{96.4}{0.5(6.25)}$$

$$i_{AVG} = \underline{\underline{31 \text{ lb/in.}^2}} \text{ (Bracket)}$$

Normal Stress

$$\sigma = \frac{\sqrt{2}}{2} \frac{R_{x1} + R_{x2}}{hi} \pm \frac{R_{z1} + R_{z2}}{hi(b+h)} \sqrt{2L^2 + \frac{(b+h)^2}{2}}$$

$$\sigma = \frac{\sqrt{2}}{2} \frac{241 (2)}{0.25 (6.25)} \pm \frac{2 (48.2)}{0.25 (6.25) (0.5 + 0.25)} \times$$

$$\sqrt{2 (3.73)^2 + \frac{(0.5 + 0.25)^2}{2}}$$

$$= 218.1 \pm 436$$

$$\sigma = \underline{654} \text{ lb/in.}^2, \quad -218 \text{ lb/in.}^2 \quad (\text{WELD})$$

$$\sigma = \frac{R_{x_1} + R_{x_2}}{b_i} \pm \frac{(L - h) (R_{z_1} + R_{z_2}) C}{I}$$

$$c = 0.25 \text{ in.} \quad I = 0.0651 \text{ in.}^4$$

$$\sigma = \frac{2 (241)}{0.5 (6.25)} \pm \frac{(3.73 - 0.25) (96.4) (0.25)}{0.0651}$$

$$= 154 \pm 1288$$

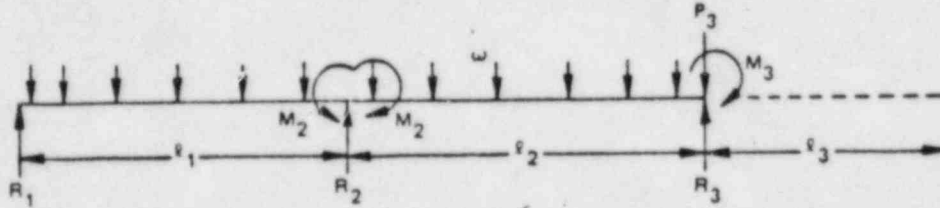
$$\sigma = \underline{1442} \text{ lb/in.}^2, \quad -1134 \text{ lb/in.}^2 \quad (\text{BRACKET})$$

#### A.4 STRESSES FOR BROKEN SPARGER

This section contains the calculation of stresses during normal plant operation and during the core spray injection event. The analysis conservatively assumes a 360° throughwall crack in the longer pipe arm at the T-box and ignores the effect of a clamp (or assumes no clamp is installed). The analysis includes all the loading conditions identified in Section A.3. In addition, the stresses in the middle bracket due to the pressure load are calculated. (A nozzle will contact the middle bracket in order to axially restrain the broken sparger arm when it is pressurized). Stresses in both the middle bracket and the lower bracket (assumes lower sparger cracks) are calculated in order to bound the condition.

A.4.1 Pipe Stress Due to Seismic Load

Assume uniformly loaded beam with three supports, end moment  $M_3$  and force  $P_3$  and the 3rd support.



using theorem of three moments...

$$\frac{M_1 l_1}{I_1} + 2 M_2 \left( \frac{l_1}{I_1} + \frac{l_2}{I_2} \right) + \frac{M_3 l_2}{I_2} = \frac{w_1 l_1^3}{4I_1} + \frac{w_2 l_2^3}{4I_2}$$

$$M_1 = 0 \quad I_1 = I_2 \quad w_1 = w_2$$

$$2M_2 \left( \frac{l_1 + l_2}{I} \right) + \frac{M_3 l_2}{I} = \frac{w (l_1^3 + l_2^3)}{4I}$$

$$M_2 = \frac{\frac{w}{4} (l_1^3 + l_2^3) - M_3 l_2}{2 (l_1 + l_2)}$$

$M_3$  is caused by the cantilevered section of pipe between the support bracket and the break

$$M_3 = \frac{w l_3^2}{2}$$

Likewise,

$P_3$  is caused by the cantilevered section

$$P_3 = w l_3$$

For Seismic

$$\omega = 2.74 \text{ lb/in. (see Section A.1.3)}$$

$$l_1 = 26\frac{1}{2} \times \left[ \frac{\pi}{180} \times 91.25 \right] = 42.2 \text{ in.}$$

$$l_2 = 30\frac{1}{2} \times \left[ \frac{\pi}{180} \times 91.25 \right] = 48.6 \text{ in.}$$

$$l_3 = 40\frac{1}{2} \times \left[ \frac{\pi}{180} \times 91.25 \right] = 64.5 \text{ in.}$$

$$P_3 = 2.74 (64.5) = \underline{\underline{177 \text{ lb}}}$$

$$M_3 = \frac{2.74(64.5)^2}{2} = \underline{\underline{5700 \text{ in-lb}}}$$

$$M_2 = \frac{\frac{2.74}{4} (42.2^3 - 48.6^3) - 5700 (48.6)}{2 (42.2 + 48.6)}$$

$$= \underline{\underline{-809 \text{ in-lb}}}$$

$$\sigma = \frac{Mc}{I} \quad I = 4.79 \text{ in.}^4 \quad c = \frac{4.0}{2} = 2.0 \text{ in.}$$

$$\sigma_{\max} = \frac{5700 (2.0)}{4.79} = \underline{\underline{2380 \text{ lb/in.}^2}}$$

$$\tau_{\max} = 2 \frac{F}{A} = 2 \frac{201}{2.68} = \underline{\underline{150 \text{ lb/in.}^2}}$$

For impingement

$$\omega_1 = |-1.0| = 1.0 \text{ lb/in. (see Section A.1.3)}$$

$$F_3 = 177 (1.0/2.74) = \underline{\underline{65 \text{ lb.}}}$$

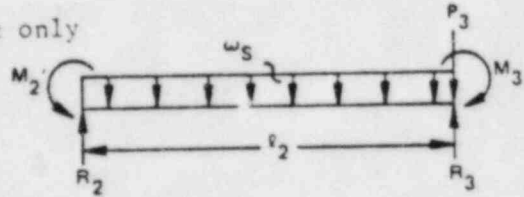
$$M_3 = 5700 (1.0/2.74) = \underline{\underline{2080 \text{ in-lb.}}}$$

$$M_2 = -809 (1.0/2.74) = \underline{-295 \text{ in.-lb.}}$$

$$\sigma_{\text{max}} = 2080 (2.0/4.79) = \underline{868 \text{ lb/in.}^2}$$

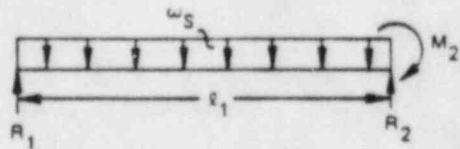
o Determine reaction loads for seismic only

$$\Sigma M_2 = 0 \text{ For segment 2:}$$



$$\begin{aligned} R_3 &= P_3 + \frac{w_s l_2}{2} + \frac{M_s}{l_2} - \frac{M_2}{l_2} \\ &= 177 + \frac{2.74 (48.6)}{2} + \frac{5700}{48.6} - \frac{(-809)}{48.6} \\ &= \underline{377.5 \text{ lb}} \end{aligned}$$

$$\Sigma M_2 = 0 \text{ For Segment 1:}$$



$$\begin{aligned} R_1 &= \frac{w_s l_1}{2} - \frac{M_2}{l_1} \\ &= \frac{2.74 (42.2)}{2} - \frac{(-809)}{42.2} \\ &= \underline{77.0 \text{ lb}} \end{aligned}$$



$$\Sigma M_1 = 0 \text{ For Segment 1, } \Sigma M_3 = 0 \text{ For Segment 2:}$$

$$R_2 = \frac{\omega_s \ell_1}{2} + \frac{M_2}{\ell_1} + \frac{\omega_s \ell_2}{2} + \frac{M_2}{\ell_2} - \frac{M_3}{\ell_2}$$

$$= \frac{(2.74)(42.2)}{2} + \frac{(-809)}{42.2} + \frac{(2.74)(48.6)}{2} + \frac{(-809)}{48.6} - \frac{5700}{48.6}$$

$$= \underline{-28.7 \text{ lb}}$$

$$R_1 + R_2 + R_3 = \underline{426}$$

$$(2.74)(\ell_1 + \ell_2 + \ell_3) = \underline{\underline{426}}$$

} CHECK

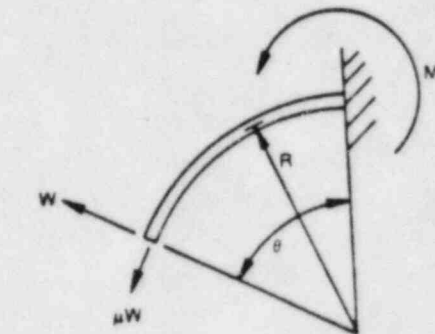
## A.4.1.1 Mismatch Due to Thermal Expansion

$$\begin{aligned}
 M &= WR \sin \theta - \mu WR (1 - \cos \theta) \\
 &= WR (\sin \theta - \mu (1 - \cos \theta))
 \end{aligned}$$

Assume

$$\mu = 0.2 \quad R = 91.25$$

(See Section A.1.7)

 $\mu$  = coef, of friction

$$\begin{aligned}
 M_{-30.5^\circ} &= 168 (91.25) (\sin 30.5^\circ - 0.2 (1 - \cos 30.5^\circ)) \\
 &= \underline{7356} \text{ in.-lb.}
 \end{aligned}$$

$$\begin{aligned}
 M_{26.5^\circ} &= 190 (91.25) (\sin 26.5^\circ - 0.2 (1 - \cos 26.5^\circ)) \\
 &= \underline{7372} \text{ in.-lb (maximum)}
 \end{aligned}$$

$$\sigma_{\max} = \sigma_{\text{BENDING}} + \sigma_{\text{BRACKET FRICTION}} + \frac{Pr}{2t}$$

$$= \frac{Mc}{I} + \frac{\mu W}{A_p} + \frac{Pr}{2t}$$

$$c = 4.0/2 = 2.0 \text{ in.}, \quad I = 4.79 \text{ in.}^2$$

$$\mu W = 0.2 (190), \quad A_p = 2.68 \text{ in.}^2$$

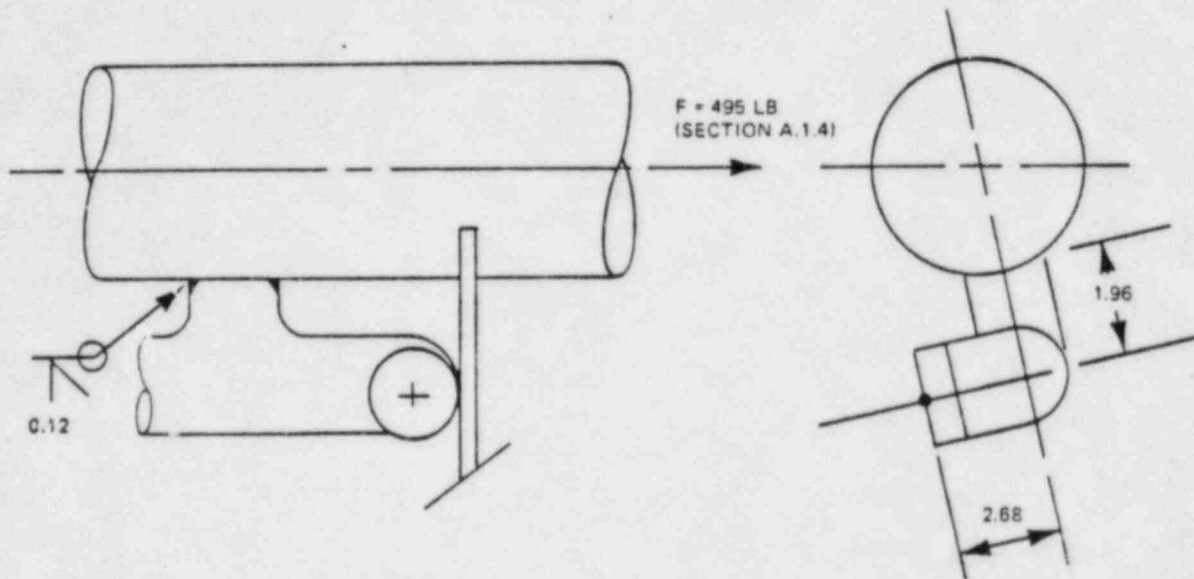
$$\frac{Pr}{2t} = 202 \text{ lb/in.}^2 \quad (\text{Section A.3.1.2 - BOUNDING VALUE})$$

$$\sigma_{\max} = \frac{7372 (2.0)}{4.79} + \frac{0.2 (190)}{2.68} + 202$$

$$= \underline{\underline{3316}} \text{ lb/in.}^2$$

A.4.2 Nozzle Stresses Due to Pressure Load

Assume 360° break, nozzle loaded by bracket.



The resulting loads at the weld are.

$$F_{\text{SHEAR}} = F = 495 \text{ lb}$$

$$T_{\text{TORSION}} = 2.68 F = 2.68 (495) = 1327 \text{ in.-lb.}$$

$$M_{\text{MOMENT}} = 1.96 F = 1.96 (495) = 970 \text{ in.-lb}$$

The stresses are conservatively calculated as...

$$\begin{aligned} \sigma_y &= \pm \frac{M_m c}{I} + \frac{Pr}{2t} \\ &= \pm \frac{970 (0.88)}{0.209} + \frac{50 (0.88)}{2 (0.12)} \\ &= \pm 4084 + 183 \end{aligned}$$

P = 50 psig (see Section A.1.4)  
For Weld Properties, see  
Section A.3.2.1

$$\sigma_y = -3901 \text{ lb/in.}^2, \quad \underline{\underline{4267 \text{ lb/in.}^2}}$$

$$\tau_{xy} = \frac{T_T c}{k} + a \frac{F_s}{A} \quad a = 2.0$$

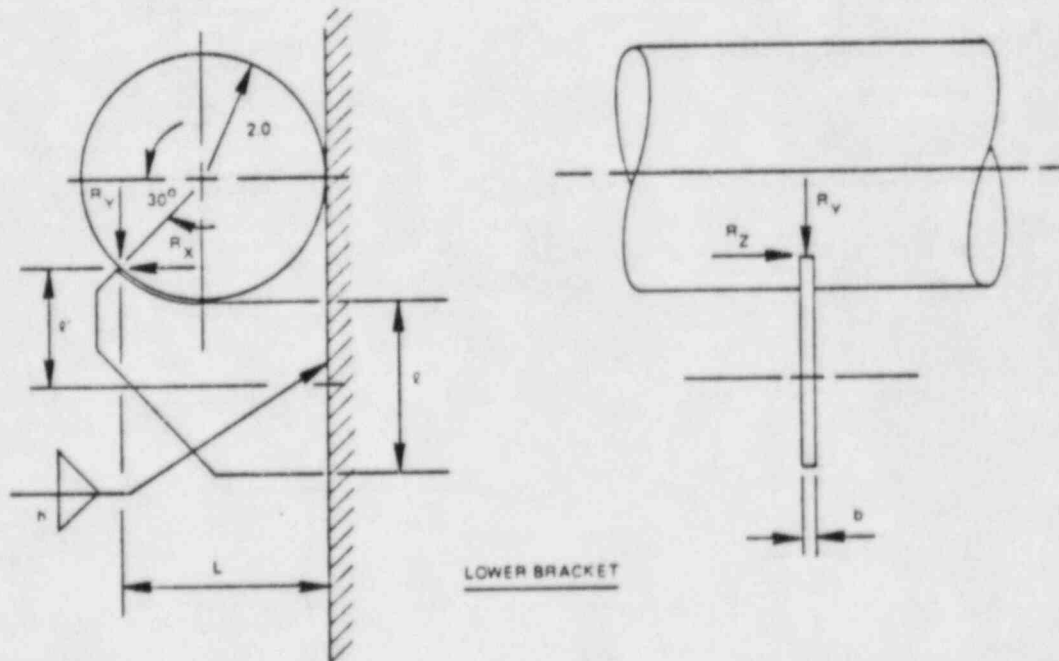
$$= \frac{1327 (0.88)}{0.418} + 2 \frac{495}{0.618}$$

$$= 2794 + 1602$$

$$\tau_{xy} = \underline{\underline{4396 \text{ lb/in.}^2}}$$

### A.4.3 Bracket Stresses

#### A.4.3.1 Lower Bracket Stress Due to Seismic Loading



$$e = 4.0 - 2.0 = 2.0 \text{ in.} \quad L = 2.0 (1 + \cos 30^\circ) = 3.73 \text{ in.}$$

$$e' = \frac{2.0}{2} + (1 - \sin 30^\circ) (2.0) = 2.0 \text{ in.}$$

$$b = 0.5 \text{ in.} \quad h = 0.25 \text{ in.}$$

$$R_y = 377.5 \text{ lb} \quad R_x = 0 \quad R_z = 0$$

(Section A.1.3)

(Note conservatism - uses highest bracket load at weakest bracket)

The stress in the fillet weld is ...

$$\tau_{AVG} = \frac{\sqrt{2}}{2} \frac{R_y}{h l} = \frac{\sqrt{2}}{2} \frac{(377.5)}{0.25 (2.0)} = \underline{\underline{534}} \text{ lb/in.}^2$$

$$\begin{aligned} C_{BENDING} &= \frac{3 \sqrt{2} M}{h l^2} = \frac{3 \sqrt{2} L R_y}{h l^2} \\ &= \frac{3 \sqrt{2} (3.73) (377.5)}{(0.25) (2)^2} = \underline{\underline{5974}} \text{ lb/in.}^2 \end{aligned}$$

## A.4.3.2 Lower Bracket Stress Due to Thermal Expansion

$$R_x = 190 \text{ lb} \quad R_z = \mu R_x = 0.2 (190) = 38 \text{ lb}$$

(Section A.1.7)  $R_y = 0$

Maximum shear stress in the fillet weld is...

$$\tau = \frac{\sqrt{2}}{2} \frac{R_x + R_z}{h} + \frac{\sqrt{2}}{2} \frac{M}{(b+h) (l-h) (h)}$$

where

$$M = l \cdot R_z$$

$$\tau = \frac{\sqrt{2}}{2} \frac{190 + 38}{0.25 (2.0)} + \frac{\sqrt{2}}{2} \frac{(2.0) 38}{(0.5 + 0.25) (2.0 - 0.25) (0.25)}$$

$$\tau = 322.4 + 163.8 = \underline{\underline{486}} \text{ lb/in.}^2$$

Maximum normal stress in weld is ...

$$\sigma_{\max} = \frac{\sqrt{2} R_x}{2 h l} + \frac{R_z}{h l (b+h)} \sqrt{2L^2 + \frac{(b+h)^2}{2}} + \frac{3 \sqrt{2} M}{h l^2}$$

where

$$M = l R_x$$

$$\sigma_{\max} = \frac{\sqrt{2}}{2} \frac{(190)}{0.25 (2.0)} + \frac{3 \sqrt{2} (2.0) (190)}{0.25 (2.0)^2}$$

$$+ \frac{52.8}{0.25 (2.0) (0.5 + 0.25)} \sqrt{2 (3.73)^2 + \frac{(0.5 + 0.25)^2}{2}}$$

$$\sigma_{\max} = 268.7 + 1612.2 + 746.5 = \underline{\underline{3360}} \text{ lb/in.}^2$$

Maximum normal stress in plate is...

$$\sigma_{\max} = \frac{R_x}{A} + \frac{l R_x C_{xy}}{I_{xy}} + \frac{L R_z C_{zx}}{I_{zx}}$$

$$A = 0.5 (2.0) = 1.0 \text{ in.}^2$$

$$I_{xy} = \frac{b l^3}{12} = \frac{0.5 (2.0)^3}{12} = 0.333 \text{ in.}^4$$

$$C_{xy} = \frac{2.0}{2} = 1.0 \text{ in.}$$

$$I_{zx} = \frac{\ell b^3}{12} = \frac{(2.0)(0.5)^3}{12} = 0.02083$$

$$C_{zx} = \frac{0.5}{2} = 0.25$$

$$\begin{aligned} \sigma_{\max} &= \frac{190}{1.0} + \frac{(2.0)(190)(1.0)}{0.3333} + \frac{3.73(38)(0.25)}{0.02083} \\ &= 190.0 + 1140.0 + 1701.1 \end{aligned}$$

$$\sigma_{\max} = \underline{\underline{3031}} \text{ lb/in.}^2$$

Maximum Shear Stress in Plate

$$\begin{aligned} \tau &= \frac{R_x + R_z}{b\ell} + \frac{\ell R_z (3\ell + 1.8b)}{\ell^2 b^2} \\ &= \frac{190 + 38}{0.5(2.0)} + \frac{(2.0)(38)(3 \times 2.0 + 1.8 \times 0.5)}{(2.0)^2 (0.5)^2} \\ &= 228 + 524 = \underline{\underline{752}} \text{ lb/in.}^2 \end{aligned}$$

#### A.4.3.3 Middle Bracket Stress Due to Pressure Load

(Refer to Figure, Section A.3.3.2)

$$F = 495 \text{ lb} \quad (\text{Section A.1.4})$$

Shear Stress (Neglect Torsion - Small)

$$\tau_{\text{AVG}} = \frac{\sqrt{2}}{2} \frac{F}{ht} = \frac{\sqrt{2}}{2} \frac{(495)}{0.25(6.25)} = \underline{\underline{224}} \text{ lb/in.}^2 \quad (\text{WELD})$$

$$\tau_{AVG} = \frac{F}{bl} = \frac{495}{0.5 (6.25)} = \underline{158} \text{ lb/in.}^2 \quad (\text{BRACKET})$$

Stress Due to Bending

$$\begin{aligned} \sigma_{max} &= \frac{F}{hl(b+h)} \sqrt{2L_F^2 \frac{(b+h)^2}{2}} \\ &= \frac{495}{0.25 (6.25) (0.5 + 0.25)} \sqrt{2 (2.99)^2 + \frac{(0.5 + 0.25)^2}{2}} \end{aligned}$$

$$\sigma_{max} = \underline{1800} \text{ lb/in.}^2 \quad (\text{WELD})$$

$$\sigma_{max} = \frac{Mc}{I} \quad c = \frac{0.5}{2} = 0.25 \text{ in.}$$

$$I = \frac{lb^3}{12} = \frac{6.25 (0.5)^3}{12} = 0.0651 \text{ in.}^4$$

$$M = (L_F - h) F$$

$$\sigma_{max} = \frac{(2.99 - 0.25) (495) (0.25)}{0.0651} = \underline{5210} \text{ lb/in.}^2 \quad (\text{BRACKET})$$

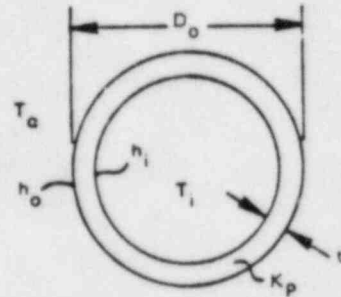
#### A.5 CORE SPRAY SPARGER TEMPERATURE CALCULATIONS

This section contains heat transfer calculations to determine the maximum (bounding) temperature differential between the pipe arm and the shroud.



A.5.1 Temperature Difference - Bracket to Pipe

$$\left. \begin{aligned} h_i &= 5145 \text{ Btu/hr-ft}^2\text{-}^\circ\text{F} \\ h_o &= 390 \text{ Btu/hr-ft}^2\text{-}^\circ\text{F} \\ k &= 10 \text{ Btu/hr-ft-}^\circ\text{F} \end{aligned} \right\} \text{(Section A.5.2)}$$



$$D_o = 4.0 \text{ in.} \quad t = 0.226 \text{ in.} \quad D_i = 3.548 \text{ in.}$$

$$T_i = \text{water in sparger} = 80^\circ\text{F}$$

$$T_o = \text{water outside} = 550^\circ\text{F}$$

$$A_i = \pi \left( \frac{3.548}{12} \right) (1) = 0.9289 \text{ ft}^2 \text{ (1 ft long section)}$$

$$A_o = \pi \left( \frac{4.80}{12} \right) (1) = 1.0472 \text{ ft}^2 \text{ (1 ft long section)}$$

$$A_p = \pi \left( \frac{4.0 + 3.548}{2 (12)} \right) (1) = 0.9880 \text{ ft}^2 \text{ (1 ft long section)}$$

The thermal resistance, R is

$$\frac{1}{R} = \frac{1}{\frac{1}{A_i h_i} + \frac{1}{A_o h_o} + \frac{t}{A_p k}}$$

$$Q = \frac{T_o - T_i}{\frac{1}{A_i h_i} + \frac{1}{A_o h_o} + \frac{1}{A_p k}}$$

$$\Delta T_{\text{FILM OUTSIDE}} = Q \frac{1}{A_o h_o} = \frac{\frac{1}{A_o h_o} (T_o - T_1)}{\frac{1}{A_i h_i} + \frac{1}{A_o h_o} + \frac{t}{A_p k}}$$

$$\Delta T_{\text{FILM INSIDE}} = \frac{\frac{1}{A_i h_i} (T_o - T_1)}{\frac{1}{A_i h_i} + \frac{1}{A_o h_o} + \frac{t}{A_p k}}$$

$$x = \frac{1}{A_i h_i} + \frac{1}{A_o h_o} + \frac{t}{A_p k}$$

$$x = \frac{1}{(0.9289) 5145} + \frac{1}{(1.0472) 390} + \frac{0.226/12}{0.9880 (10)}$$

$$x = 0.000209 + 0.002449 + 0.001906 = 0.004564$$

$$\Delta T_{\text{FILM OUTSIDE}} = \frac{0.002449 (550-80)}{0.004564} = 252^\circ\text{F}$$

$$\text{Outside metal temp} = 550 - 252^\circ = 298^\circ\text{F}$$

$$\Delta T_{\text{FILM INSIDE}} = \frac{0.000209 (550-80)}{0.004564} = 21.5^\circ\text{F}$$

$$\text{Inside metal temp} = 80 + 21.5 = 101.5^\circ\text{F}$$

$$\text{Average sparger (pipe) temperature} = \frac{298 + 101.5}{2} = 200^\circ\text{F}$$

$$\Delta T_{\text{SHROUD TO PIPE}} = 550 - 200 = \underline{\underline{350^\circ\text{F}}}$$

In practice, the core spray pumping system cannot inject into the reactor until the pressure reaches about 300 psia where  $T_{SAT} = 417^{\circ}F$ . In this case, the  $\Delta T_{BRACKET TO PIPE}$  is less than  $337^{\circ}F$  ( $417-80$ )\*. Thus the above calculation bounds the inadvertent injection case. It also bounds the case of core spray operation during LOCA for the same reason.

Conservatism in the calculation are:

1. Bounding for reason described above
2. Assumes steady state conditions ( $Q_o = Q_p = Q_i$ )
3. Neglects heat conduction to clamp from pipe.
4. Assumes runout flow.

#### A.5.2 Heat Transfer Coefficients

A. Inside sparger arm (near tee box)

Assume AVG film temperature =  $90^{\circ}F$  (Check:  $(101.5+80)/2 = 91^{\circ}$ )

$$D_o = 3.548/12 \text{ ft} + A_{FLOW} = \frac{\pi}{4} (3.548/12)^2 = 0.0687 \text{ ft}^2$$

$$\rho = 62.1 \text{ lb/ft}^3 \quad Q_{RO} = 6000 \text{ gpm (Section A.5.3)}$$

$$v = 0.833 (10^{-5}) \text{ ft}^2/\text{sec}$$

$$w_{TOTAL} = 6000 \text{ gpm (1 min/60 sec) (ft}^3/7.48 \text{ gal) (62.1 lb/ft}^3)$$

$$= 830 \text{ lb/sec}$$

\* $\Delta T_{FILM INSIDE}$  and  $\Delta T_{PIPE}$  are ignored.

$$\dot{w}_{\text{Long Side Arm}} = 830 (100/360) = 231 \text{ lb/sec}$$

$$V = \frac{\dot{w}}{A_p} = \frac{231}{0.0687 (62.1)} = 54.1 \text{ ft/sec}$$

$$Nu = 0.023 Re^{0.8} Pr^{1/3}$$

$$Re = \frac{3.548}{12} \left( \frac{54.1}{0.833 (10^5)} \right) = 1.92 \times 10^6$$

$$Pr = 5.20 @ 90^\circ\text{F}$$

$$Nu = 0.023 (1.92 \times 10^6)^{0.8} (5.20)^{1/3} = 4237$$

$$\frac{hD}{k} = Nu$$

where:

$$D = \frac{3.548}{12} \text{ ft}$$

$$k = 0.359 \text{ Btu/hr-ft-}^\circ\text{F @ } 90^\circ\text{F}$$

$$\therefore h_1 = \frac{4237 (0.359)}{\frac{3.548}{12}} = \frac{5145 \text{ Btu/hr-ft}^2\text{-}^\circ\text{F}}{12}$$

B. Outside of Sparger Arm

Assume Average Velocity is 2 ft/sec

Assume Average Film Coef. Temperature =  $425^\circ\text{F}$  (Check:  $(550+298)/2 = 424^\circ\text{F}$ )

Assume Heat Transfer is like a cylinder in Cross Flow

$$\nu = 0.166 \times 10^{-5} \text{ ft}^2/\text{sec} @ 425^\circ\text{F}$$

$$k = 0.374 \text{ Btu/ft-hr-}^\circ\text{F}$$

$$Pr = 0.927$$

$$\frac{h_o D_o}{k} = [0.35 + 0.56 (Re)^{0.5}] Pr^{0.31}$$

$$D_o = \frac{4}{12} \text{ ft}$$

$$Re = \frac{2(4)}{12(0.166)(10^{-5})} = 4.02 \times 10^5$$

$$h_o = \frac{0.374}{(4/12)} [0.35 + 0.56 (4.02 \times 10^5)^{0.5}] 0.927^{0.31}$$

$$\therefore h_o = 390 \text{ Btu/hr-ft}^2\text{-}^\circ\text{F}$$

#### A.5.3 Pump Head/Runout

$$\text{Rated Flow} = Q_R = 4625 \text{ gpm} @ 128 \text{ psia}$$

$$\text{Shut-off Head} = 380 \text{ psia}$$

$$P = P_{SH} - CQ^2$$

$$128 = 380 - C(4625)^2$$

$$C = \frac{380-128}{(4625)^2} = 1.178 \times 10^{-5}$$

$$@ P = 14.7,$$

$$Q_{RO} = \sqrt{\frac{P_{SH} - P}{1.178 (10^{-5})}} = 5570 \text{ gpm}$$

For conservatism, assume runout flow to be 6000 gpm

#### A.6 REFERENCES

Roark, R. J., "Formulas for Stress and Strain", McGraw Hill, Fourth Edition, 1965.

Hopkins, R. B., "Design Analysis of Shafts and Beams", McGraw Hill.

"Machinery's Handbook", The Industrial Press, 16th Edition, 1959.

Blevins, R.D., "Flow-Induced Vibration", Van Nostrand Reinhold Co., 1977.

Kreith, "Principles of Heat Transfer", International, 1969.

Welty, et. al., "Fundamentals of Momentum, Heat and Mass Transfer", John Wiley, 1969.

Shields, C. M., Wade, G. E., "Core Spray Distribution Report No. 16, 218 Standard Plant", NEDE 13006-3.

GE Drawing 730E854, "Shroud".

Appendix B  
FLOW VELOCITY CALCULATIONS

This appendix describes the calculations for the flow velocities supporting statements in Subsections 3.4.2.1 and 3.4.2.2 of the text.

### B.1 FLOW VELOCITY IN BYPASS REGION

Assumptions:

1. The plant is operating at rated power (2436 Mwt) and flow  $78.5 \times 10^6$  lb/hr.
2. The bypass flow fraction is 12% ( $9.29 \times 10^6$  lb/hr).
3. The water in the bypass regions is saturated.
4. There is no downflow in the bypass region. This assumption is discussed later.

There are two parallel flow paths in the bypass region--one is between the fuel channels, and the other is between the core shroud and the outermost fuel assemblies. The flow areas for these paths are shown schematically in Figure B-1. The simple analysis that follows will give an estimate of the relative flow velocity in the neighborhood of the spray sparger.

Path 1 is between the core shroud and the outermost fuel channels. The flow area along path 1 changes from  $A_1$ , between the bottom and top of the active fuel, to  $A_5$  at the top guide to  $A_6$  immediately above the top guide:

$$A_1 = 3758 \text{ in.}^2,$$

$$A_5 = 1189 \text{ in.}^2,$$

$$A_6 = 7157 \text{ in.}^2$$

Path 2 is between the fuel channels. The flow area along path 2 changes from  $A_2$  to  $A_3$  at the top guide to  $A_4$  above the fuel channels:

$$A_2 = 3118 \text{ in.}^2,$$

$$A_3 = 1486 \text{ in.}^2,$$

$$A_4 = 20160 \text{ in.}^2$$

From the geometry and the flow areas, the loss coefficient  $K$  for path 1 is approximately 1.0 and for path 2 is approximately 1.1. Therefore, for an equal pressure drop:

$$\frac{K_1 W_1^2}{A_5^2} = \frac{K_2 W_2^2}{A_3^2}$$

$$\frac{(1.0)W_1^2}{1189} = \frac{(1.1)W_2^2}{1486}$$

$$W_1 = 0.94 W_2$$

But

$$W_1 + W_2 = 9.29 \times 10^6$$

Therefore,

$$W_1 = 4.8 \times 10^6 \text{ lb/hr}$$



The velocity in the bypass region between the core spray sparger and the fuel assemblies is then:

$$V = W_1 / \rho A_5 = 4.8 \times 10^6 / [3600 \times 45.8 \times (1189/144)] = 3.5 \text{ ft/sec.}$$

The fluid in this region is primarily saturated liquid.

The upward fluid velocity in the periphery of the core bypass region was conservatively estimated at 3.5 ft/sec. The maximum sized piece that can be lifted from this vicinity in the upper plenum is approximately 0.4 inch in length (Reference B-1).

## B.2 FLOW VELOCITY AT TOP SURFACE OF CORE PLATE

$$V = (W_{\text{Total Bypass}}) / \rho A$$

Since

$$W_{\text{Total Bypass}} = 9.29 \times 10^6 \text{ lb/hr}$$

$$A = \pi/4 (D^2 - Nd^2)$$

$$D = \text{inside diameter of shroud} = 174.5 \text{ in.}$$

$$N = \text{number of control rod guide tubes} = 137$$

$$d = \text{outside diameter of control rod guide tube} = 10.75 \text{ in.}$$

$$\rho = \text{density} = 45.8 \text{ lb/ft}^3$$

Then

$$V = (9.29 \times 10^6) / [3600 \times 45.8 \times \pi (174.5^2 - 137 (10.75)^2) / (4 \times 144)]$$

$$V = 0.71 \text{ ft/sec}$$

From Reference B-1, a core spray nozzle cannot be lifted with this velocity and therefore the nozzle will remain at the bottom of the bypass.

### B.3 FLOW VELOCITY AT THE TOP OF THE FUEL ASSEMBLY HANDLES

$$W_{\text{Total}} = 78.5 \times 10^6 - 9.29 \times 10^6 = 69.21 \times 10^6 \text{ lb/hr}$$

$$A = na$$

$$n = \text{number of fuel assemblies} = 560$$

$$a = \text{area associated with each fuel assembly} \sim (6)^2 = 36 \text{ in.}^2$$

The nominal single phase velocity is:

$$V = (W_{\text{Total}}) / \rho A$$

Then

$$V = (69.21 \times 10^6) / (3600 \times 45.8 (560 \times 36/144)) = 3.00 \text{ ft/sec.}$$

At this location, the fluid is a mixture of steam and water. Therefore, to estimate the lifting force due to the mixture, a two-phase friction multiplier is used:

$$\phi^2_m = 1 + x (\rho_f / \rho_g - 1)$$

$$x = \text{quality} = \frac{\text{mass flow rate of steam}}{\text{total mass flow rate}}$$

$$x = 10.5 \times 10^6 / (78.5 \times 10^6) = 0.134$$

with,

$$\rho_f = 45.8 \text{ lb/ft}^3$$

$$\rho_g = 2.35 \text{ lb/ft}^3$$

$$\phi^2 = 1 + 0.134 ((45.8/2.35) - 1) = 3.48$$

The total lifting force on a section of core spray pipe per unit length is

$$F = C_D A \rho_f \phi^2 v^2 / (2g)$$

where

$$C_D = \text{drag coefficient} = 1.2$$

$$A = \text{area } (4.0 \text{ in.} \times 1 \text{ (ft/ft)}) / 12 \text{ (in./ft)} = 0.333 \text{ ft}^2/\text{ft}$$

Then the maximum weight that can be lifted is:

$$F = 1.2 \times 0.333 \times 62.8 \times 3.48 \times (3.00)^2 / (2 \times 32.2) = 8.9 \text{ lb/ft}$$

The buoyant weight of the sparger segment is about 15 lb/ft. Therefore, the sparger pipe segment will not be lifted by the upward velocity lifting force.

#### B.4 REFERENCE

- B-1. "Consequences of a Postulated Flow Blockage Incident in a Boiling Water Reactor," General Electric Company, October 1977 (NEDO-10174, Rev. 1).

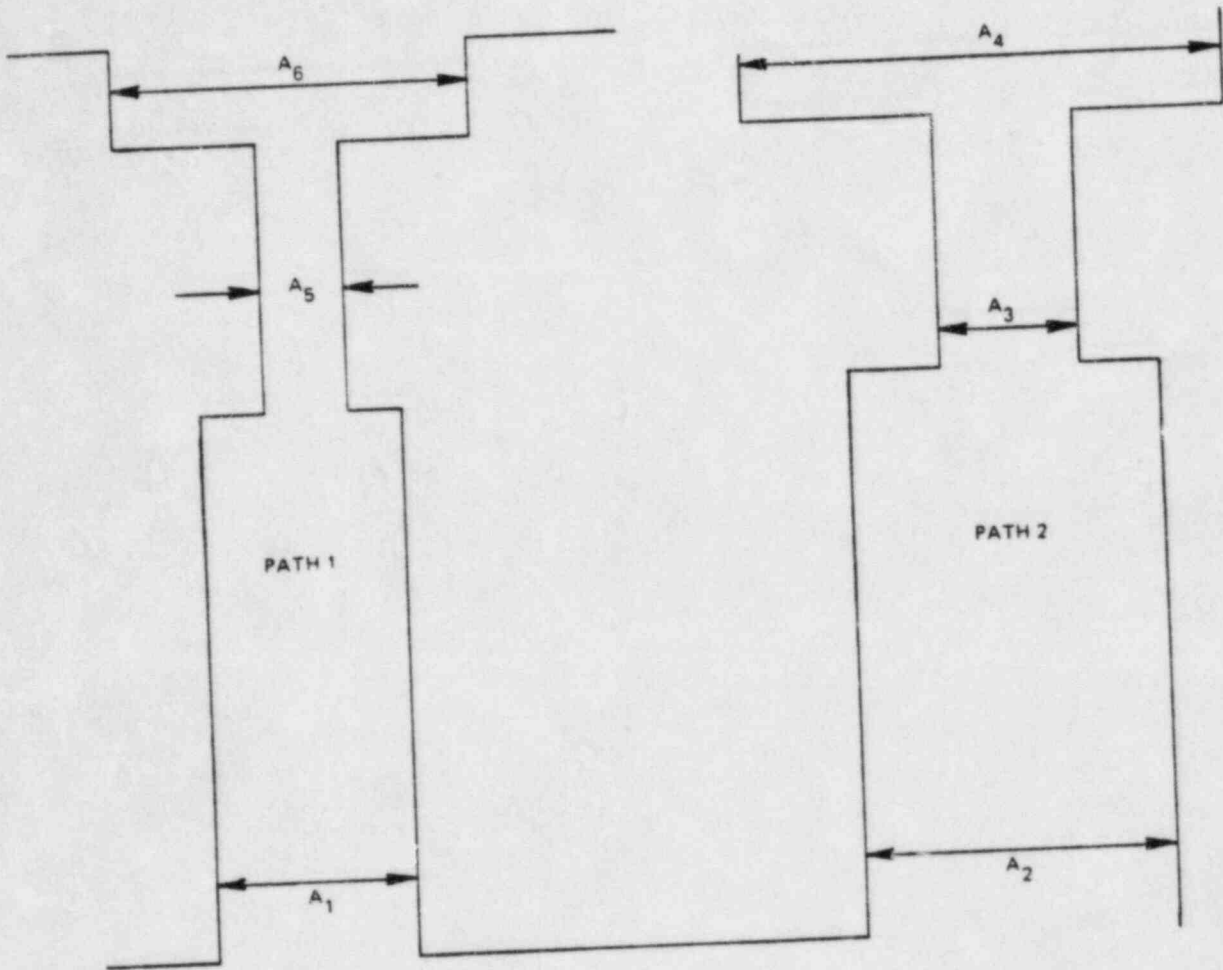


Figure B-1. Flow Paths